THE ASTROPHYSICAL JOURNAL SUPPLEMENT SERIES, 91:1–78, 1994 March

THE LYMAN-ALPHA FOREST NEAR 34 QUASI-STELLAR OBJECTS WITH $z > 2.6$

JILL BECHTOLD
Steward Observatory, University of Arizona, Tucson, AZ 85721
Received 1992 May 14; accepted 1993 July 30

ABSTRACT

Moderate-resolution spectra of 34 high-redshift QSOs were obtained at the Multiple Mirror Telescope and Palomar 5 m Telescope in order to study the properties of the Lyα forest absorption lines with $z_{\rm abs} \approx z_{\rm em}$. For $z_{\rm abs} \ll z_{\rm em}$, the evolution of the number of lines per unit redshift, dN/dz, is well described by the form $(1+z)^\gamma$, with $\gamma = 1.89 \pm 0.28$ for lines with rest equivalent width greater than 0.32 Å. For lines stronger than 0.16 Å, $\gamma = 1.32 \pm 0.24$. These results imply slower evolution in the mean free path for absorption for the clouds than previously thought. When this sample is combined with *HST* results for low redshift (Bahcall et al. 1993), a single γ is an acceptable fit to the data, with $\gamma = 1.26 \pm 0.13$ for $z_{\rm abs} = 0$–4.1, although an inflection at $z \approx 1.5$ may be present. In the high-redshift sample, there is a significant trend of decreasing γ with decreasing equivalent width limit, or, alternatively, a change in equivalent width distribution with redshift. There is no significant curvature in the $\log(dN/dz)$ versus $\log(1+z)$ relation for the strong lines, but some steepening of γ at $z \approx 2.5$ for the weak ones. While these findings for the weak lines are highly significant in a statistical sense, they may result from some subtle line-blending problem, rather than a real physical process.

The lines with $z_{\rm abs} \approx z_{\rm em}$ are significantly depleted. The strength of the deficit of lines depends weakly on QSO Lyman limit luminosity, but not redshift. The strength of the deficit also depends on the rest equivalent width of the lines, with weak lines showing a relatively weaker effect. These findings support previous suggestions that the "proximity effect" results from enhanced photoionization by the QSO's EUV radiation, rather than some property of the QSO or intergalactic medium which evolves with redshift. The simple photoionization model of Bajtlik, Duncan, & Ostriker describes the data well. If the ionizing background at the Lyman limit, J_ν, is assumed to be constant with redshift for $1.6 < z < 4.1$, and writing $J_\nu = J_{-21} \times 10^{-21}$ ergs cm^{-2} s^{-1} Hz^{-1} sr^{-1}, then $J_{-21} \approx 3$. This value is formally consistent with previous results, although about a factor of 3 larger. Hence, the factor by which QSOs fail to provide the EUV background at high redshifts (at least in this simple picture), is also increased. If the redshift dependence of J_ν is parameterized as $J_\nu \propto (1+z)^j$, then j is *not* well constrained owing to the small redshift interval sampled, and acceptable fits are obtained for $-7 < j < 4$. Additions to the simple model and the resulting uncertainties in these estimates of J_ν are discussed. One serious uncertainty is the neutral fraction of the clouds. If the clouds are nearly neutral, then J_ν must be implausibly low, $J_{-21} \approx 0.01$, in order to account for the proximity effect observed in this sample. In addition, if the systemic redshifts of the QSOs are systematically underestimated, then J_{-21} may be up to a factor of $\sim$3 smaller. Given these uncertainties, the J_{-21} at $z \approx 3$ derived from the proximity effect is in reasonable agreement with the expected contribution of luminous QSOs.

Subject heading: quasars: absorption lines

1. INTRODUCTION

Several workers have shown evidence for a systematic deficit of Lyα forest lines with absorption redshift, $z_{\rm abs}$, near the QSO emission-line redshift, $z_{\rm em}$, suggesting that the quasar itself decreases the observed number density of clouds in its immediate environment (Weymann, Carswell, & Smith 1981; Murdoch et al. 1986; Tytler 1987; Carswell et al. 1987; Bechtold 1987; Bajtlik, Duncan, & Ostriker, 1988, hereafter BDO; Lu, Wolfe, & Turnshek 1991, hereafter LWT). This so-called "inverse" or "proximity" effect has ramifications beyond the study of the Lyα forest per se. In many models for the Lyα forest clouds, the absorbers are intervening pregalactic or protogalactic gas clouds, photoionized by the integrated ultraviolet radiation field of QSOs. It has been suggested that the "proximity effect" results from the clouds being more ionized than average due to the ionizing photons from the QSOs in whose spectra they are being observed. Quantitatively, in this picture, the data available to date suggested a value for the ambient integrated background which is in sharp disagreement with the predicted background from QSOs, given estimates for the quasar luminosity function (Carswell et al. 1987; BDO). Thus, the "proximity effect" may have important implications for the evolution of the quasar luminosity function, and the contribution of other sources, such as young galaxies, to the integrated ultraviolet radiation field at early epochs (Bechtold et al. 1987; Miralde-Escude & Ostriker 1990; Songaila, Cowie, & Lilly 1990; Meiksin & Madau 1993; Cen & Ostriker 1993).

At the inception of this project, these results were based on a sample of only 19 QSOs (BDO, their Table 1). This sample had several shortcomings. First, the spectra were quite inhomogeneous, having been obtained and analyzed by several different groups, and show a wide range of signal-to-noise and resolution. Second, there were only four QSOs in the sample with $z_{\rm em} > 3$, the redshifts at which the value of the integrated UV background derived from modeling of the proximity effect differs most significantly from the value predicted from the QSO luminosity function (although see Madau 1992). These four were also the most luminous QSOs in the sample, and the ones that showed the most marked "proximity" effect.

Moreover, all of the objects in the BDO sample with $z_{em} > 3$ were radio loud, having been discovered in radio surveys. Other investigations have shown that the environments of radio-loud QSOs differ from those of radio-quiet QSOs. Anderson et al. (1987) found an excess of C IV absorbers with $z_{abs} \approx z_{em}$ for a sample of radio-loud QSOs, which is not seen for radio-quiet objects (Young et al. 1982b). Yee & Green (1987) showed that radio-loud QSOs live in richer cluster environments than radio-quiet QSOs. Thus, one might expect to see an *excess* of Lyα lines near z_{em}, or at least a dilution of the "proximity" effect in radio-loud objects versus radio-quiet objects, at a fixed continuum luminosity and redshift.

Thus, given the correlations between redshift, continuum EUV luminosity, and radio power in the original sample of 19 QSOs, it was not clear whether or not photoionization was responsible for the "proximity" effect at $z > 3$. It could have been that the "proximity effect" was present in the radio-loud objects only, perhaps resulting from the same environmental influences which cause the high radio power, and has little to do directly with photoionization by the QSO. Alternatively, the data were consistent with the "proximity effect" being fundamentally a function of redshift, since the QSOs at $z_{em} > 3$ had statistically the strongest deficits.

Subsequently, LWT investigated the proximity effect in a somewhat larger sample of 38 QSO spectra, including eight additional objects with $z_{em} > 3$. They found that the proximity effect was not correlated with radio properties, or redshift. Contrary to BDO, they found no correlation of the strength of the proximity effect with Lyman limit luminosity, which is qualitatively expected in the photoionization picture. A quantitative fit to the data, however, was consistent with the BDO photoionization model, with a mean Lyman limit background intensity $J_\nu \approx 10^{-21}$ ergs cm^{-2} s^{-1} Hz^{-1} sr^{-1} at $z \approx 3$.

The purpose of this investigation was to disentangle the correlations between redshift, optical/UV continuum luminosity, and radio power, by observing a new sample of high-redshift QSOs. These include optically selected, and so presumably mostly radio quiet, very luminous QSOs, as well as relatively low luminosity QSOs with $z_{em} > 3$. This last group of objects are too faint ($V > 19$) to study the Lyα forest in the continuum and so have been neglected in previous absorption-line studies. However, since the region of interest is in the strong Lyα emission line where they are effectively brighter ($V \approx 17$–18) it was straightforward to obtain moderate-resolution spectra of the region relevant to the proximity effect. While ideally one would like very high resolution echelle spectra to fully resolve the line profiles and search for weak lines, it will not be feasible for several years to obtain such spectra for this large a number of objects with a significant range in intrinsic properties.

In the course of this work, a sizable sample of Lyα forest lines with $z_{abs} \ll z_{em}$ was also obtained. In order to consider the statistics of the lines near z_{em} in a consistent way, I rederived the standard parameters describing the evolution of the number density of clouds far from the QSOs. The results were surprising, in that they imply somewhat slower evolution in cloud properties than found by LWT or BDO. Also, the sample presented here is now large enough to investigate other issues, such as the dependence of the evolutionary parameters on equivalent width and redshift. Although the theoretical models still have enough free parameters to allow almost any evolution in the context of very different physical situations, in principle the statistics of the clouds given here offer some constraints. Moreover, in light of the recent *HST* observations of Lyα clouds at $z \approx 0$, it seemed timely to reexamine the evolutionary parameters for the ground-based data at high redshift.

In § 2, the new observations are presented, and analysis described. In § 3, the statistics of the lines with $z_{abs} \ll z_{em}$ are presented. In § 4, the statistics of the lines with $z_{abs} \approx z_{em}$ are presented, including a discussion of limits on J_ν derived from the photoionization model. Section 5 summarizes the main results.

2. OBSERVATIONS AND ANALYSIS

2.1. *Absorption-Line Spectroscopy*

Moderate-resolution spectra of 34 QSOs are presented in Figure 1. The QSOs are listed in Table 1, along with their names as reported in Hewitt & Burbidge (1987, 1989), emission-line redshift, date the observations were made, and exposure times. The redshifts were taken from Sargent, Boksenberg, & Steidel (1988) for the QSOs listed there, except for Q0029+073, Q0114−089, and Q0334−204 for which the reported redshift predicted a substantially different wavelength for the peak of Lyα emission than observed here. In those cases, and in cases were Sargent et al. (1988) did not observe the QSO, redshifts were derived from the observed Lyα emission line shown in Figure 1.

Several different instrumental set-ups were used for various practical reasons. However, the data all have similar spectral resolution ($c\Delta\lambda/\lambda \approx 75$ km s^{-1} FWHM), so that the resulting line sample is relatively homogeneous. Each set-up is described in turn below.

The Palomar 5 m Telescope and Double Spectrograph (Oke & Gunn 1982) were used in three configurations. In 1987 May, the 2D-FRUTTI Photon Counter was used in the blue side of the spectrograph with the 1200 l mm^{-1} grating in second order and a 1″ slit. The resulting spectral resolution is 70 km s^{-1} (FWHM). The spectra were flat-fielded using a long quartz comparison lamp exposure obtained during the day, and the considerable s-distortion of the image tube chain was mapped with a quartz lamp exposure through an aperture plate with six circular holes. Iron-argon lamp spectra were taken every half hour during the night to calibrate the pixel-to-wavelength transformation. In 1988 February the TI-CCD No. 432 was used in the blue side of the spectrograph with the 1200 l mm^{-1} grating in second order, and a 2″ slit. The resulting resolution is 75 km s^{-1} (FWHM). The TI-CCD No. 167 was used in the red side with the 1200 l mm^{-1} grating in first order, with resulting spectral resolution of 100 km s^{-1}. Both sides were flattened with dome flats, and bias frames were obtained and subtracted in the usual way. Iron-argon and helium-neon-argon lamp exposures were taken every hour during the night to calibrate the pixel-to-wavelength transformation. Standard stars Ross 34 and G138-31 were observed in order to identify telluric absorption features. Finally, in 1988 July the same TI-

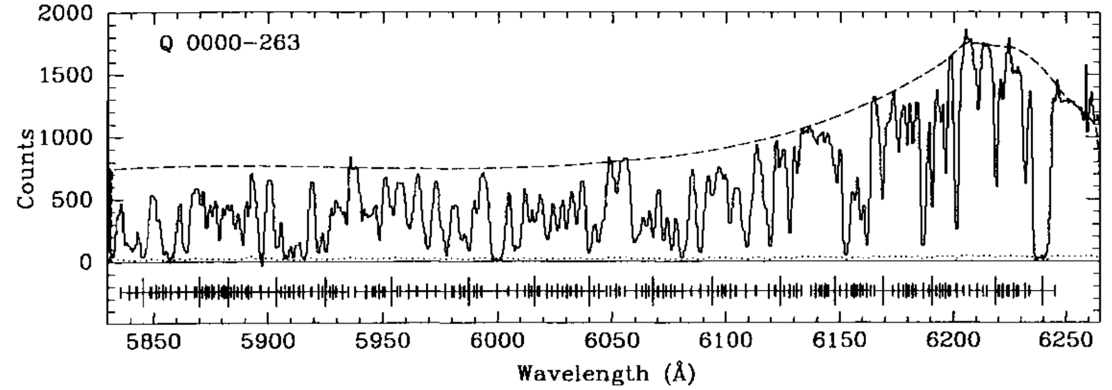

FIG. 1*a*

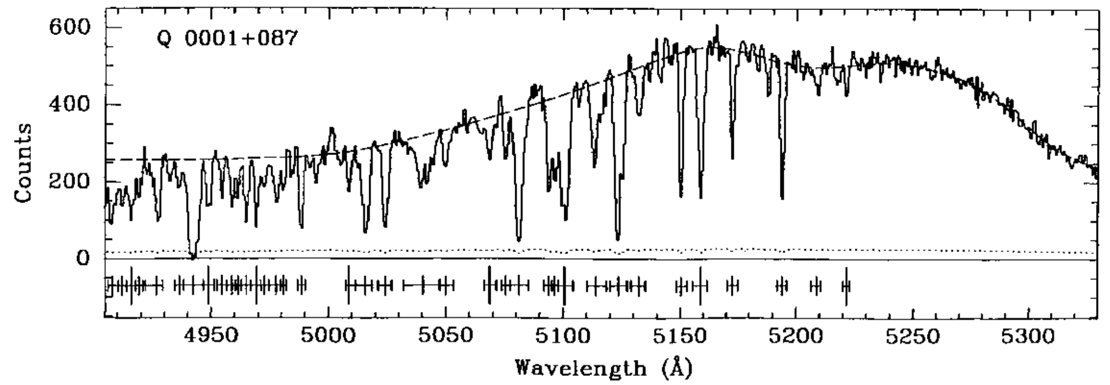

FIG. 1*b*

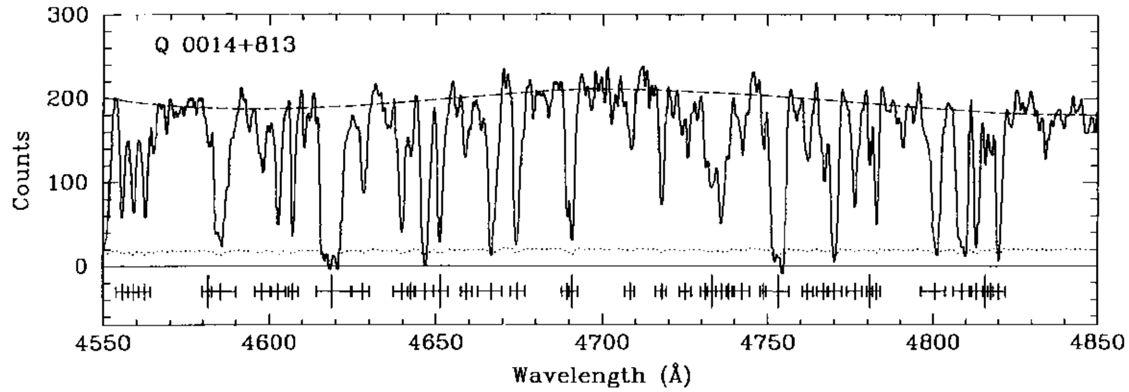

FIG. 1*c*

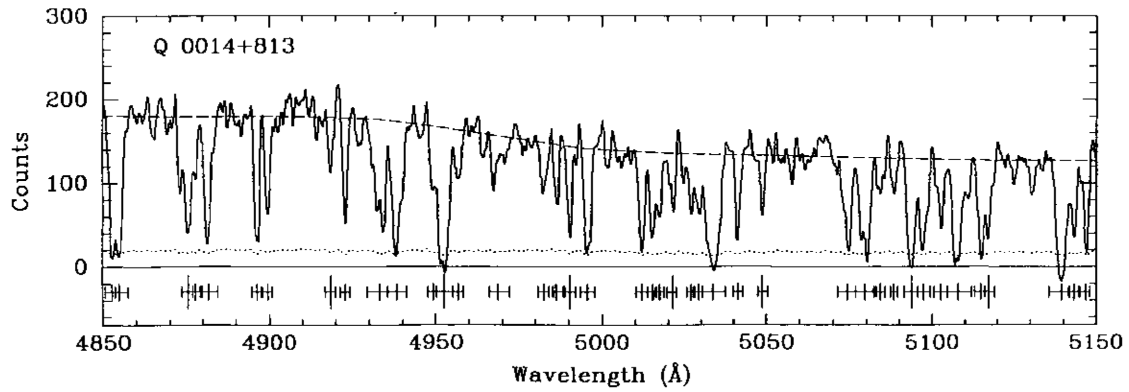

FIG. 1*c—Continued*

FIG. 1.—Spectra of 34 QSOs obtained at the MMT and Palomar 5 m Telescope. *Dashed line* indicates continuum fit; *dotted line* indicates 1 σ errors. Significant lines listed in Table 2 are indicated by vertical bars below each spectrum. Spectra obtained with the MMT Reticon or Palomar 2D-FRUITTI have been smoothed with a Gaussian filter with FWHM of 2 pixels; CCD data has not been smoothed, but has had cosmic rays removed using standard algorithms.

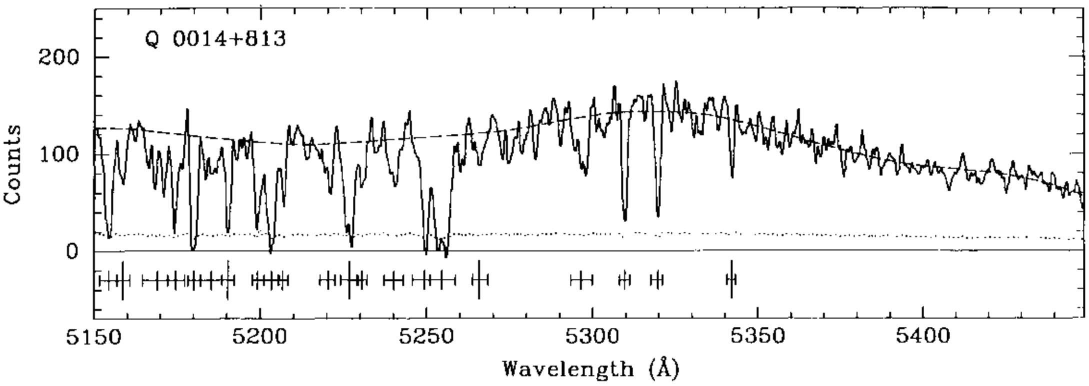

FIG. 1*c*—*Continued*

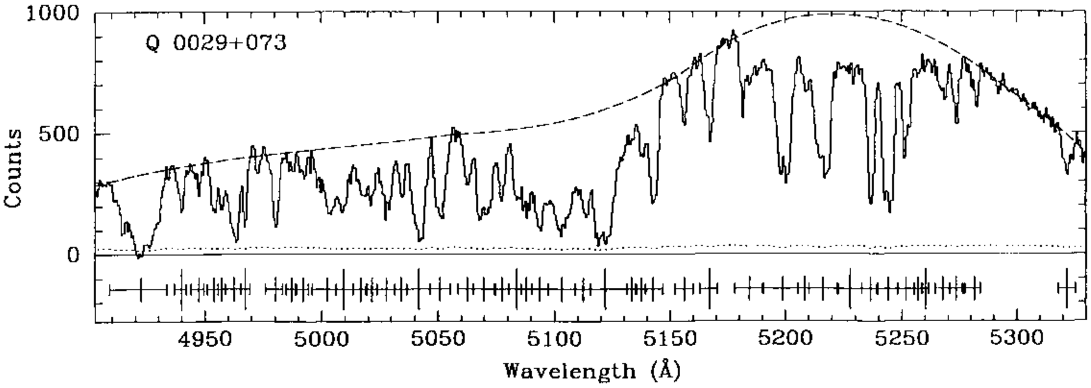

FIG. 1*d*

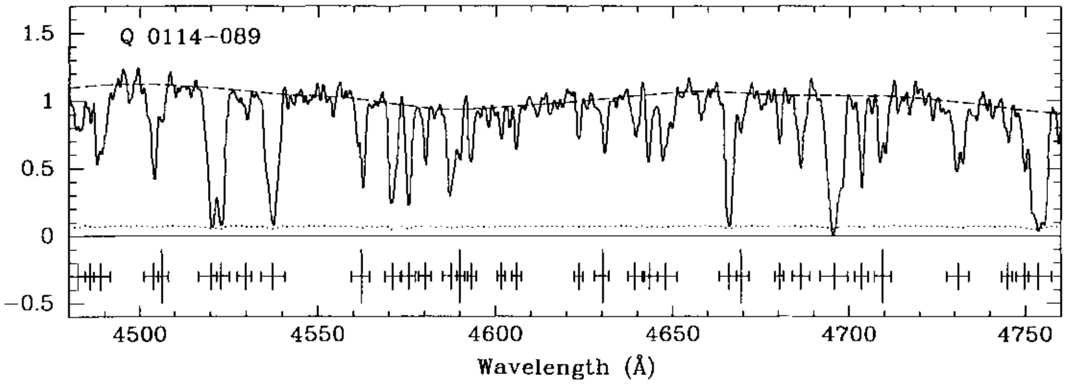

FIG. 1*e*

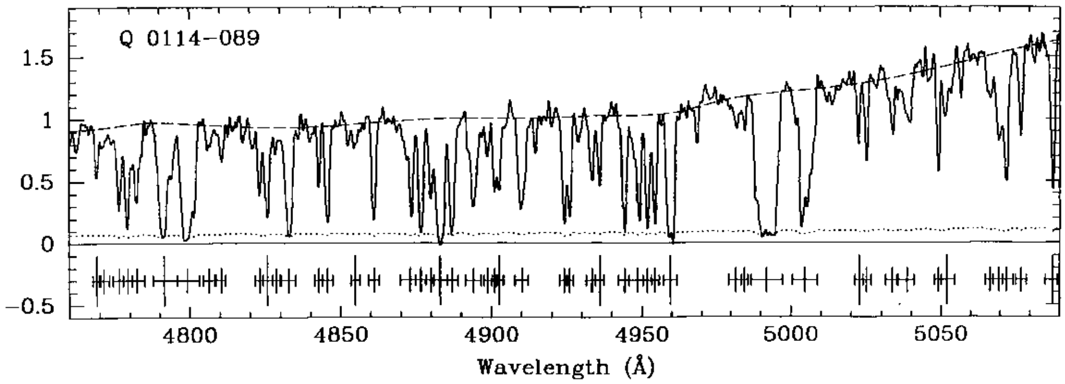

FIG. 1*e*—*Continued*

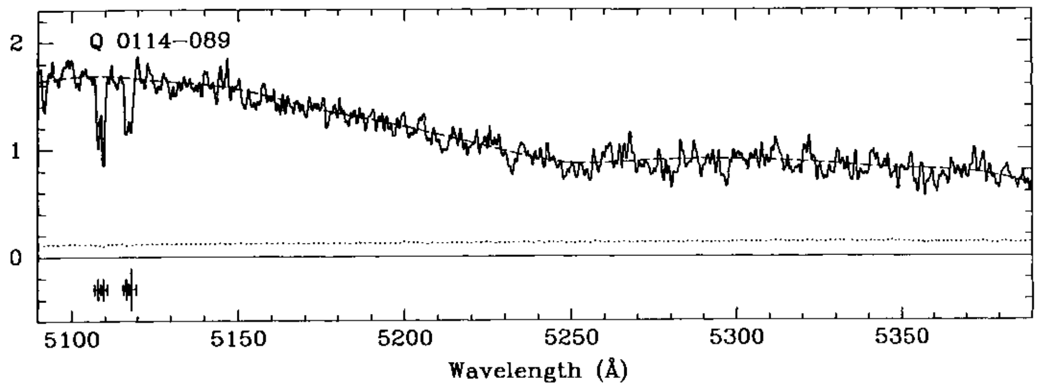

FIG. 1e—*Continued*

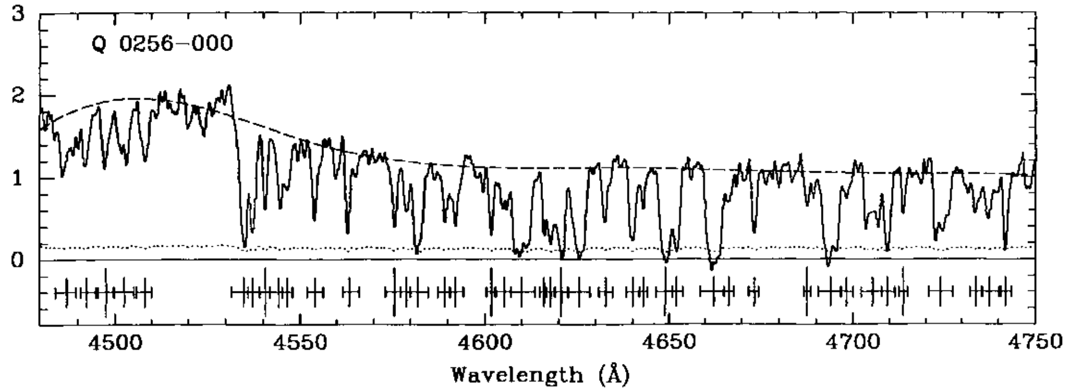

FIG. 1*f*

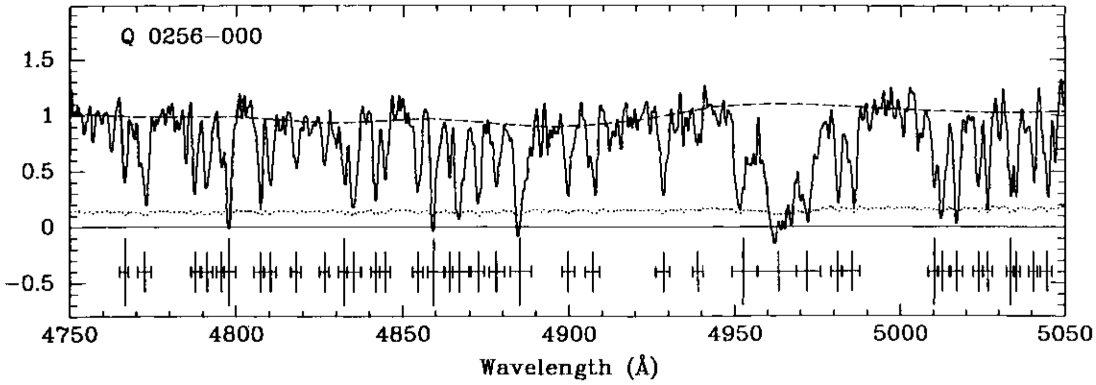

FIG. 1*f*—*Continued*

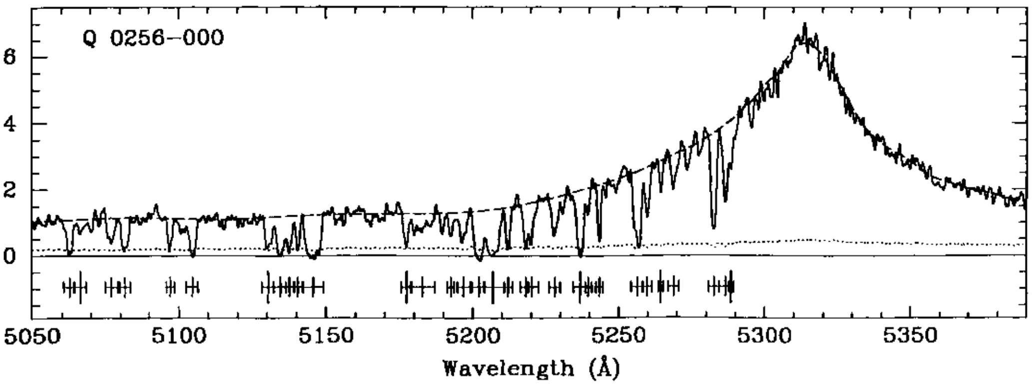

FIG. 1*f*—*Continued*

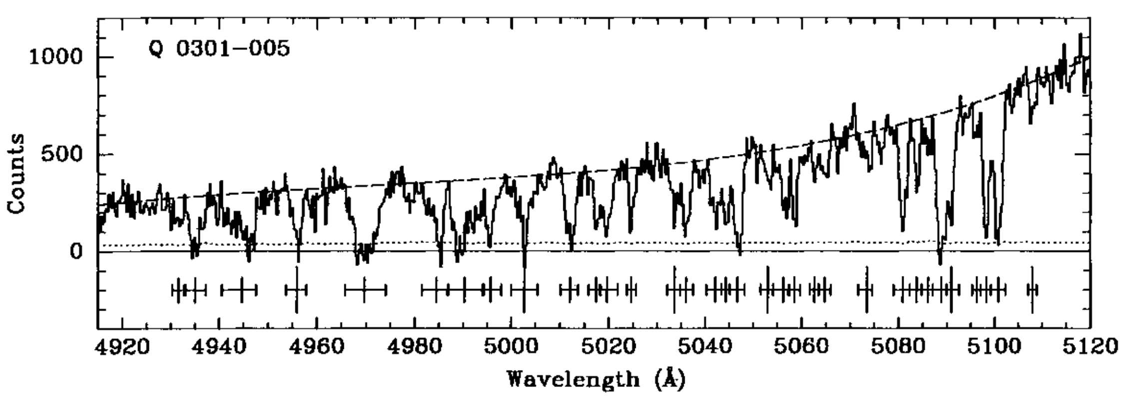

FIG. 1*g*

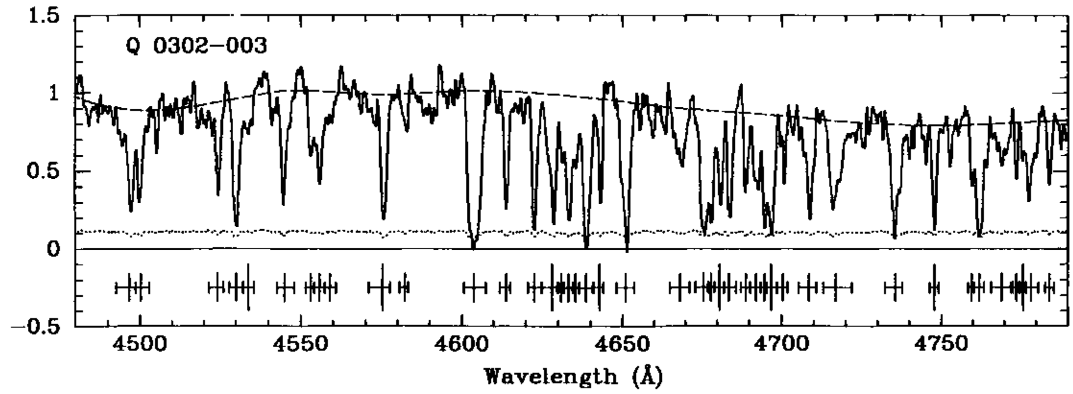

FIG. 1*h*

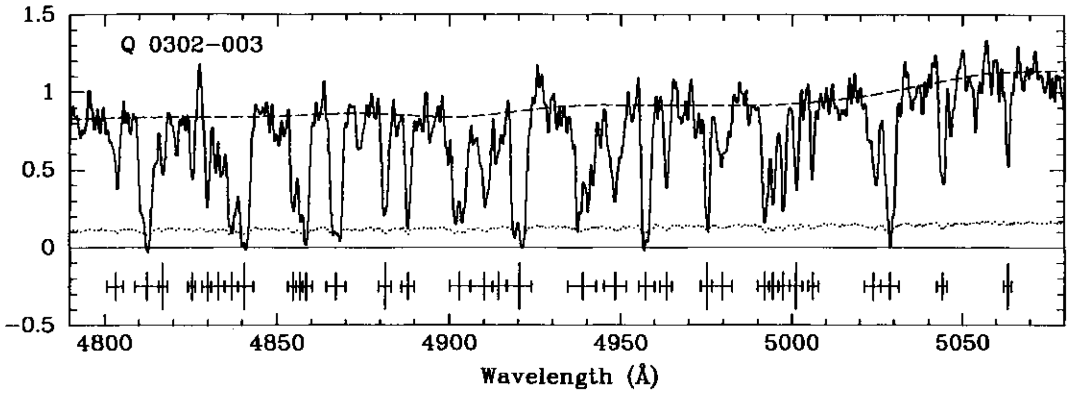

FIG. 1*h—Continued*

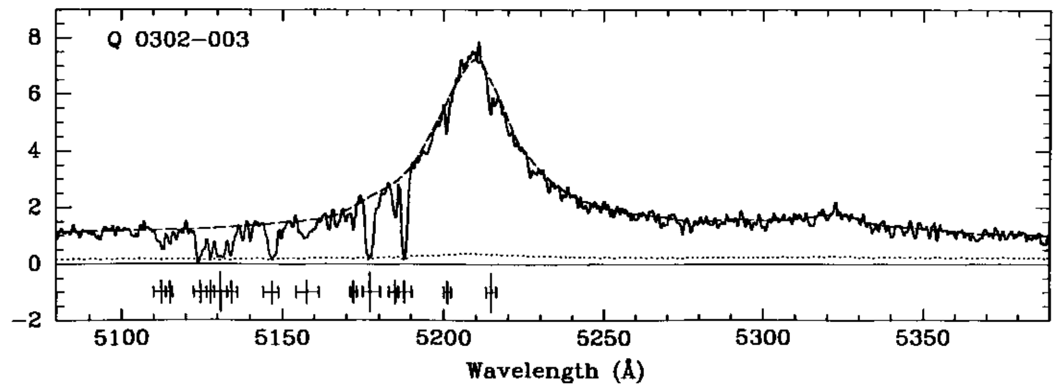

FIG. 1*h—Continued*

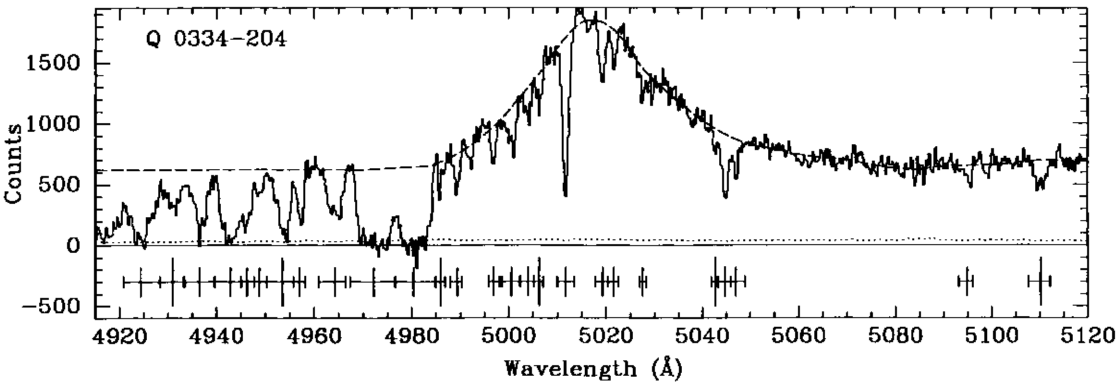

FIG. 1*i*

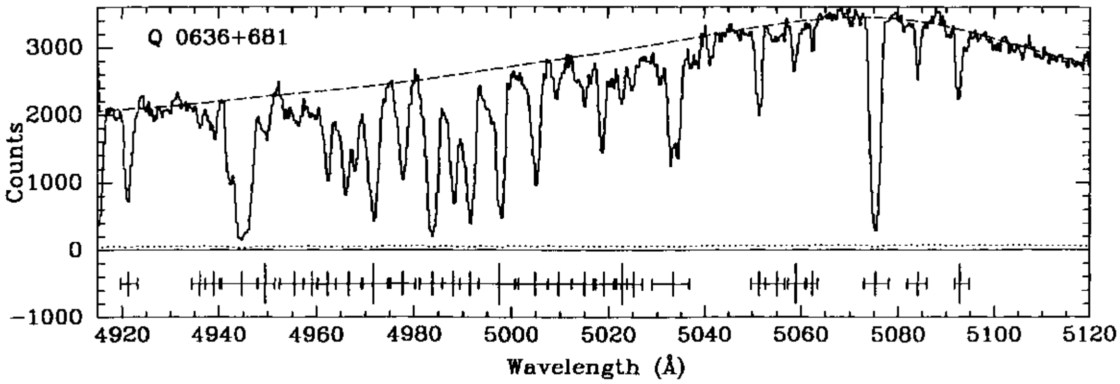

FIG. 1*j*

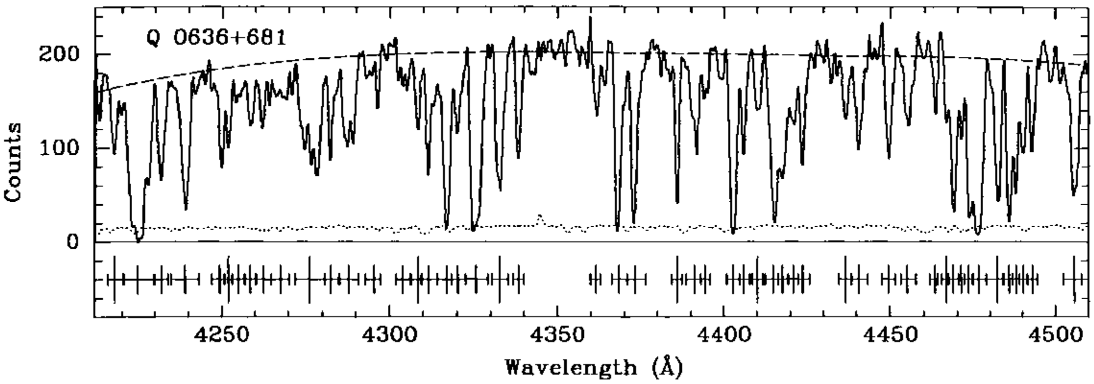

FIG. 1*k*

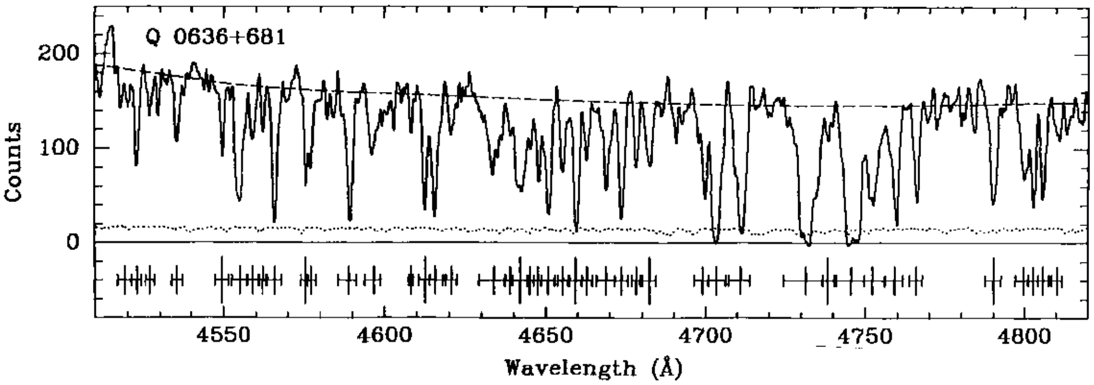

FIG. 1*k*—*Continued*

1994ApJS...91....1B

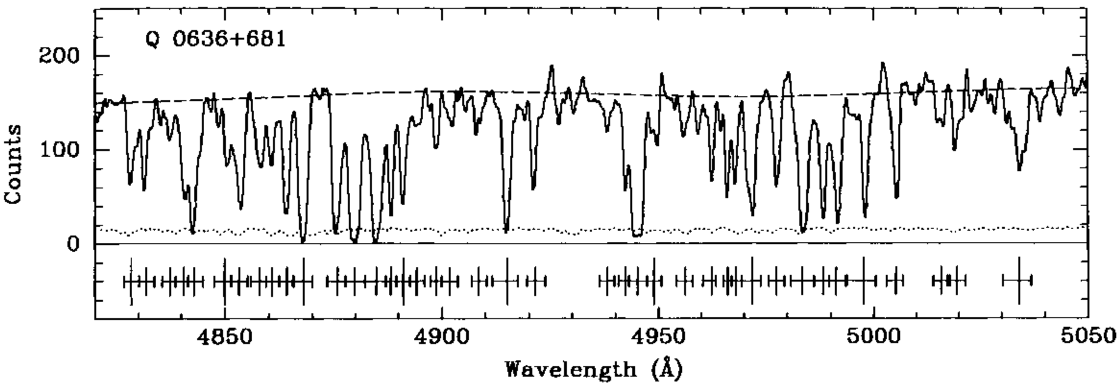

FIG. 1*k*—*Continued*

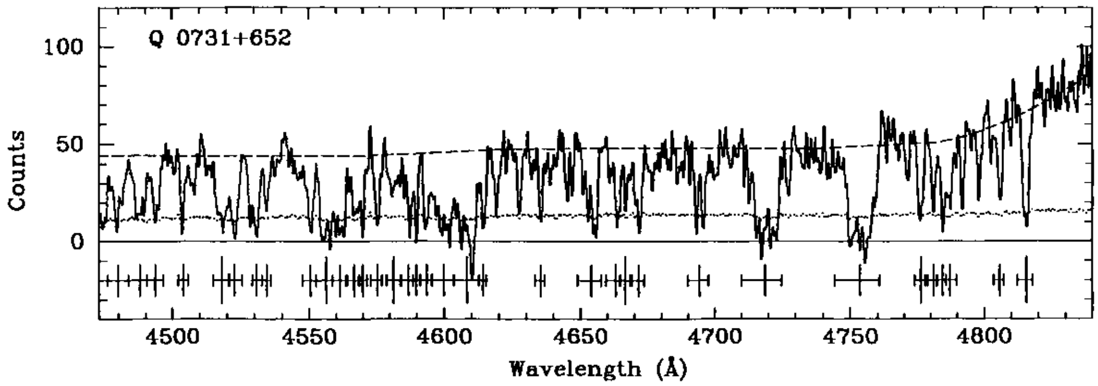

FIG. 1*l*

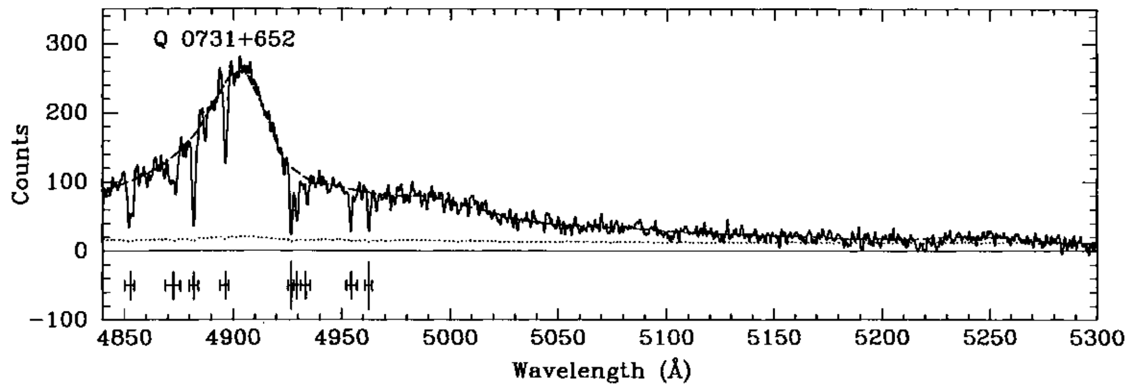

FIG. 1*l*—*Continued*

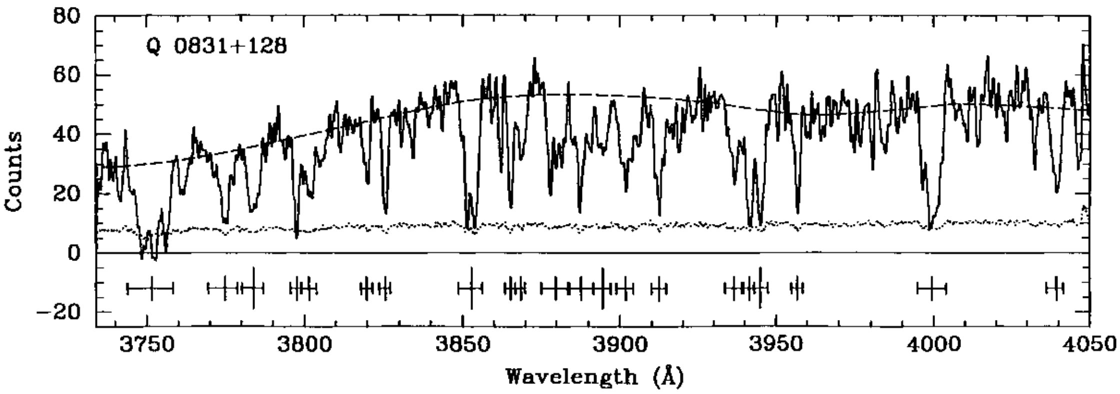

FIG. 1*m*

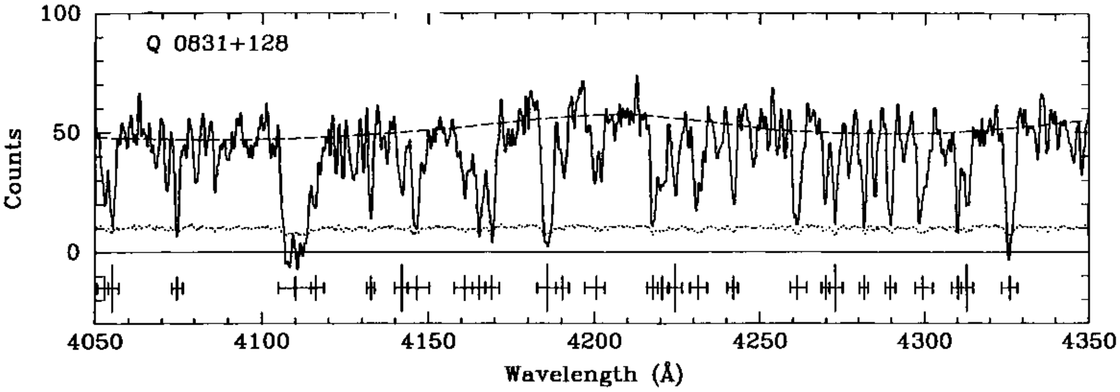

FIG. 1*m*—*Continued*

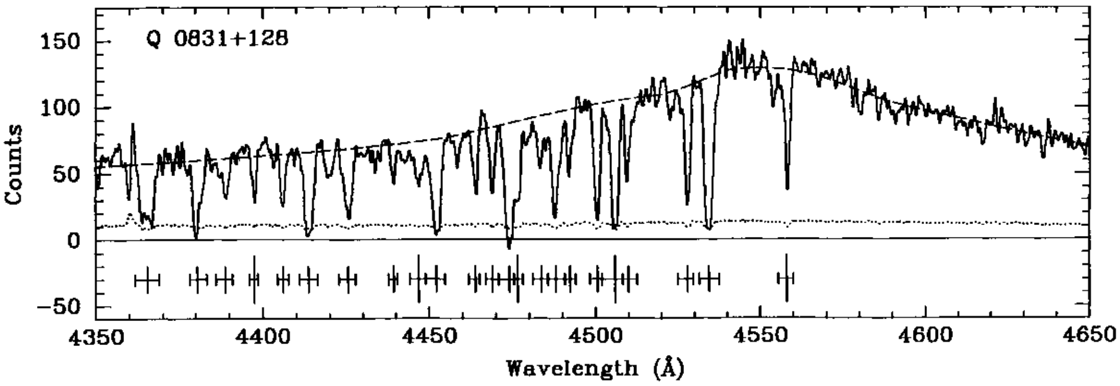

FIG. 1*m*—*Continued*

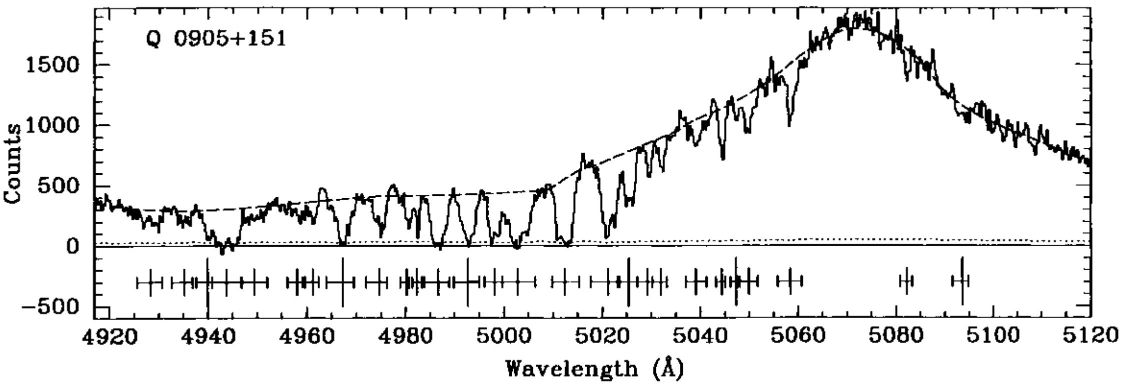

FIG. 1*n*

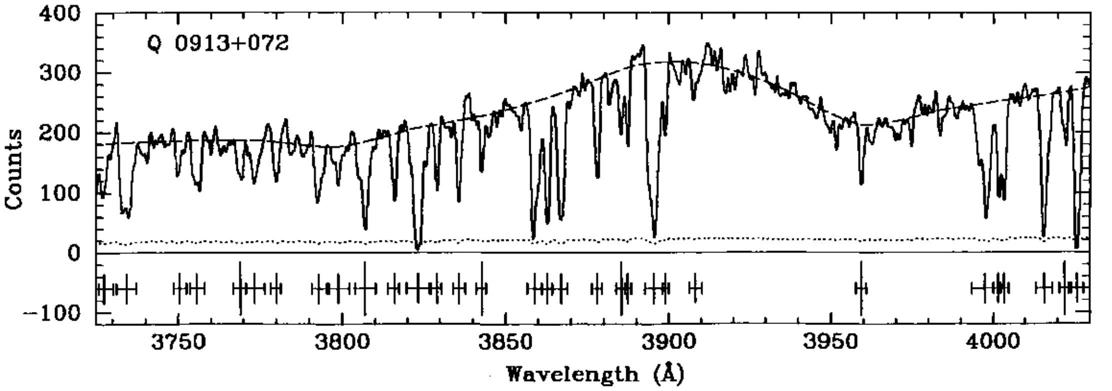

FIG. 1*o*

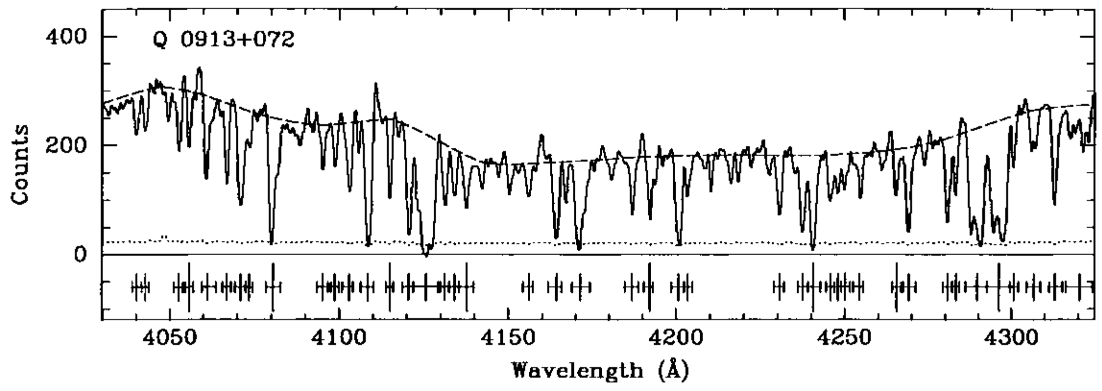

FIG. 1*o*—*Continued*

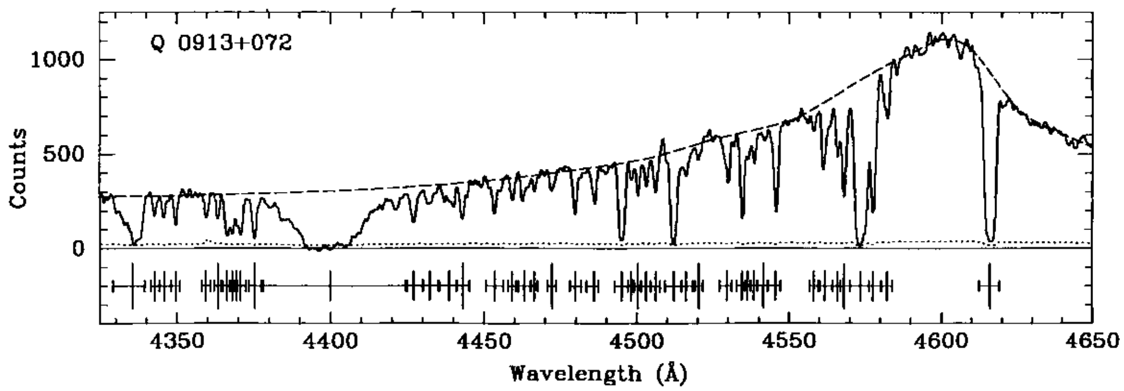

FIG. 1*o*—*Continued*

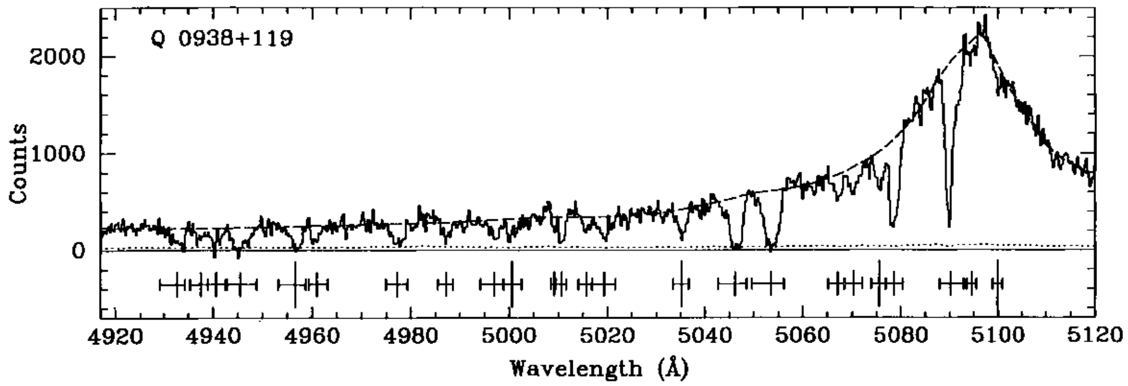

FIG. 1*p*

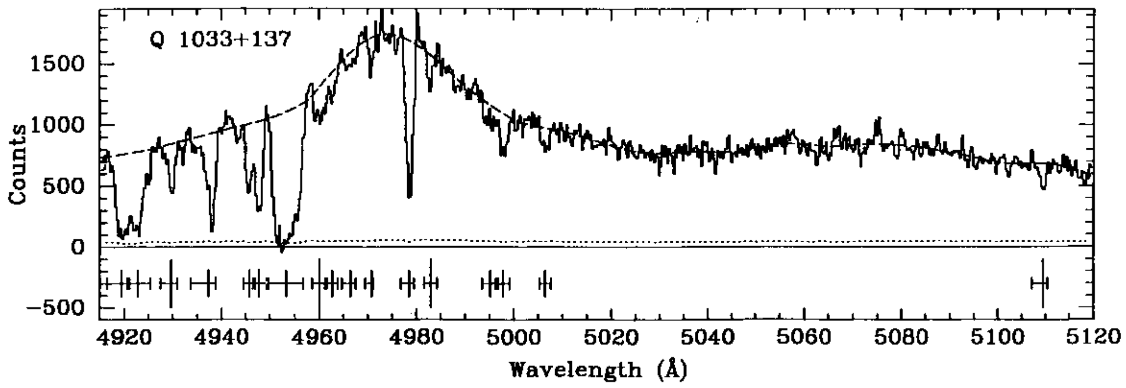

FIG. 1*q*

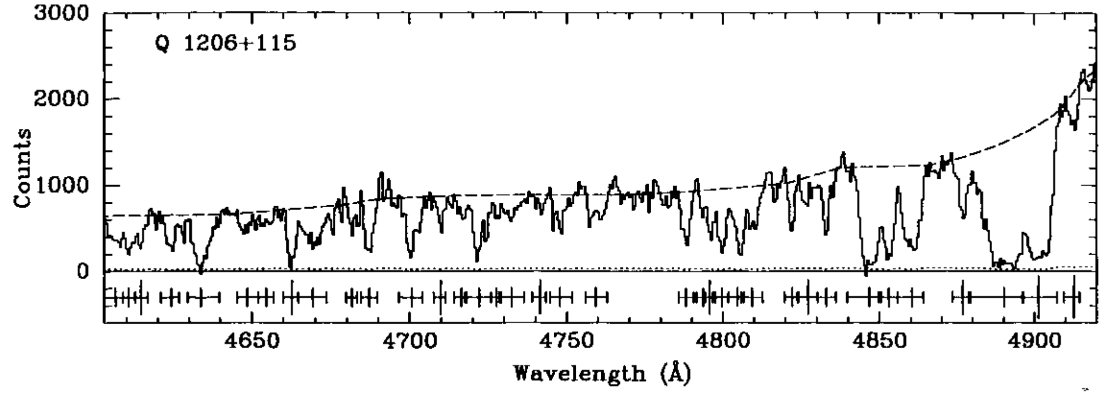

FIG. 1*r*

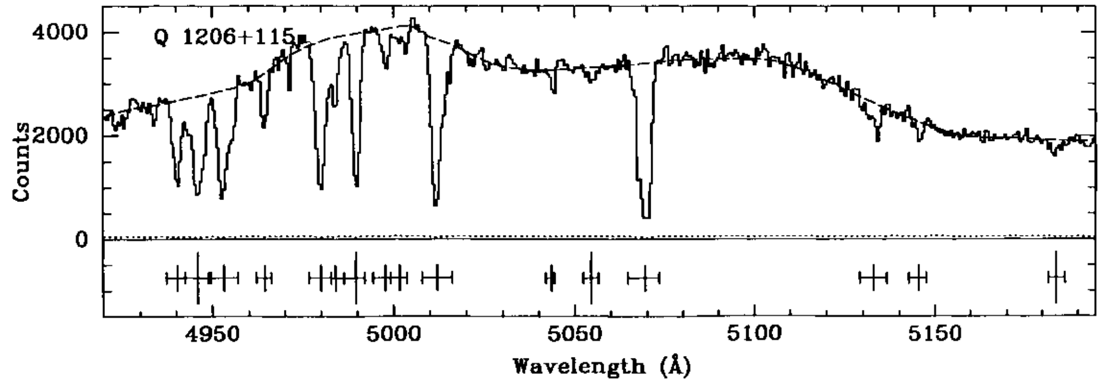

FIG. 1*r*—*Continued*

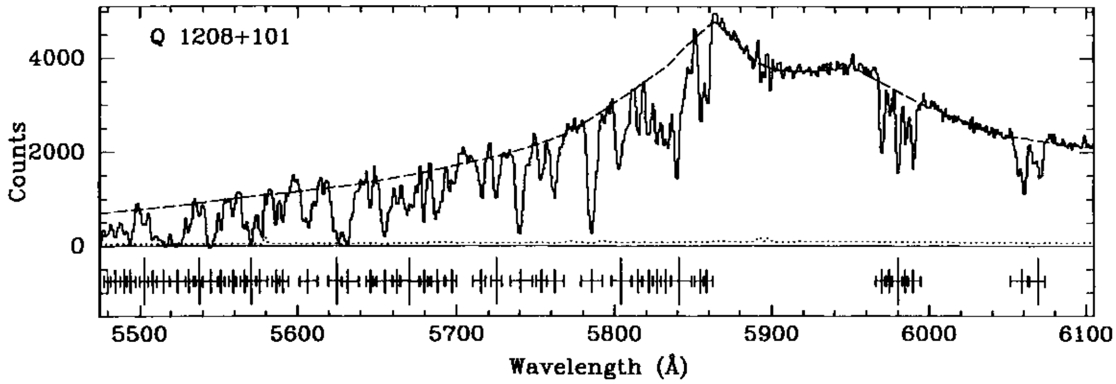

FIG. 1*s*

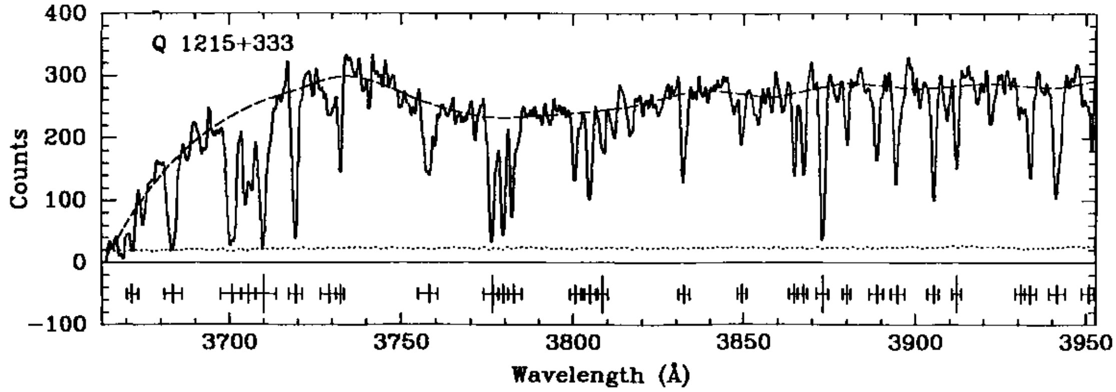

FIG. 1*t*

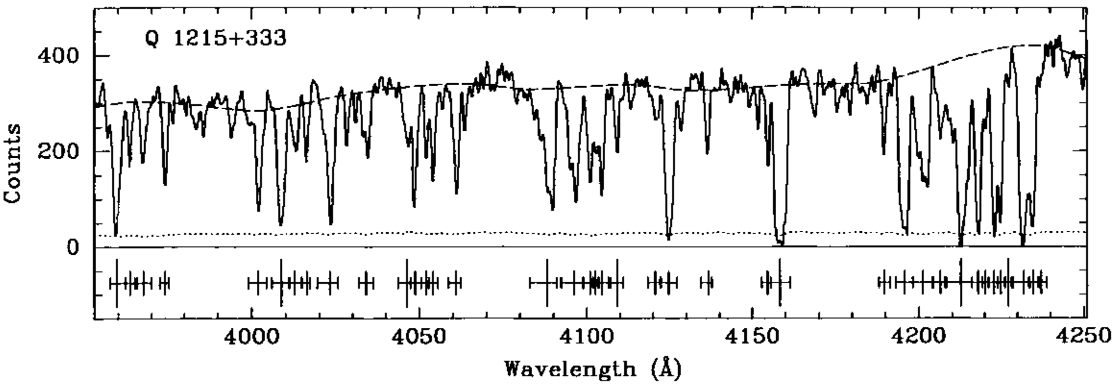

FIG. 1*t*—*Continued*

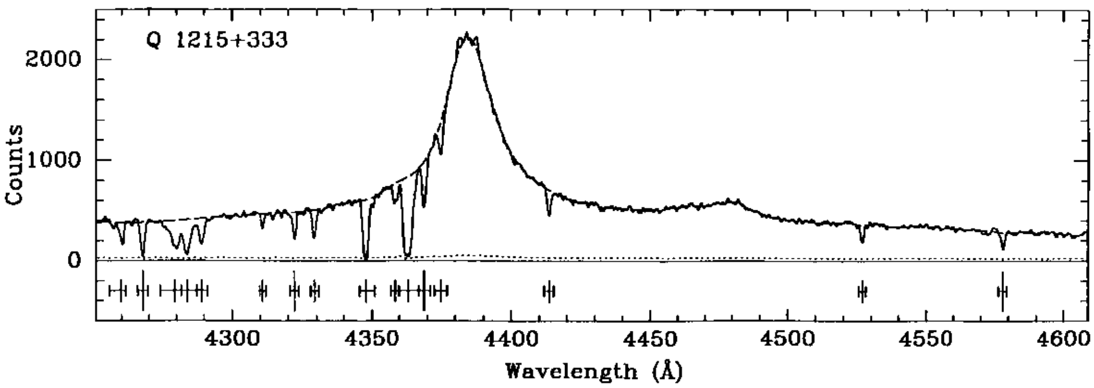

FIG. 1*t*—*Continued*

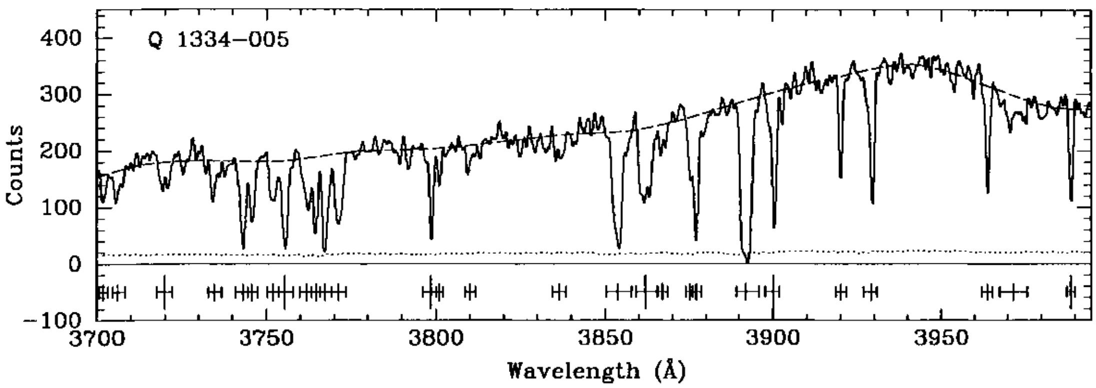

FIG. 1*u*

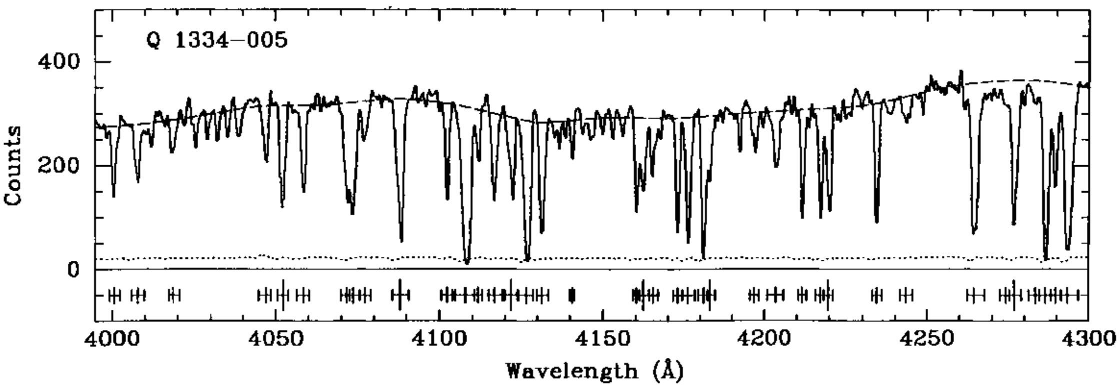

FIG. 1*u*—*Continued*

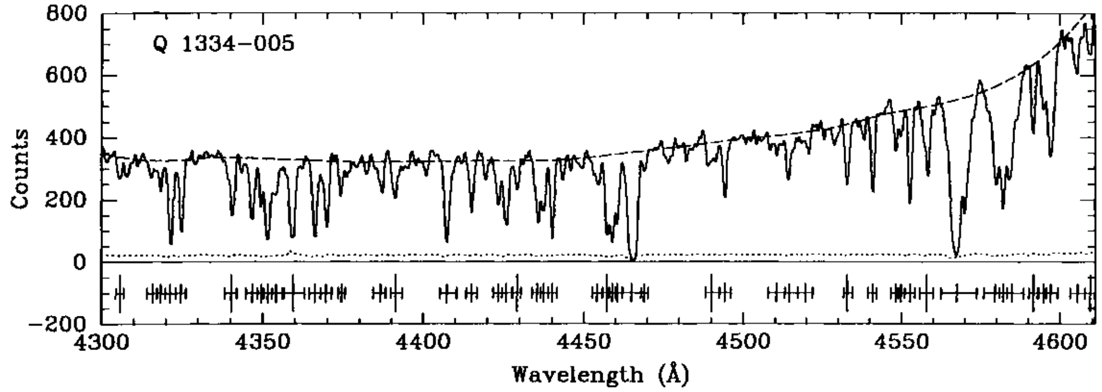

FIG. 1*u*—*Continued*

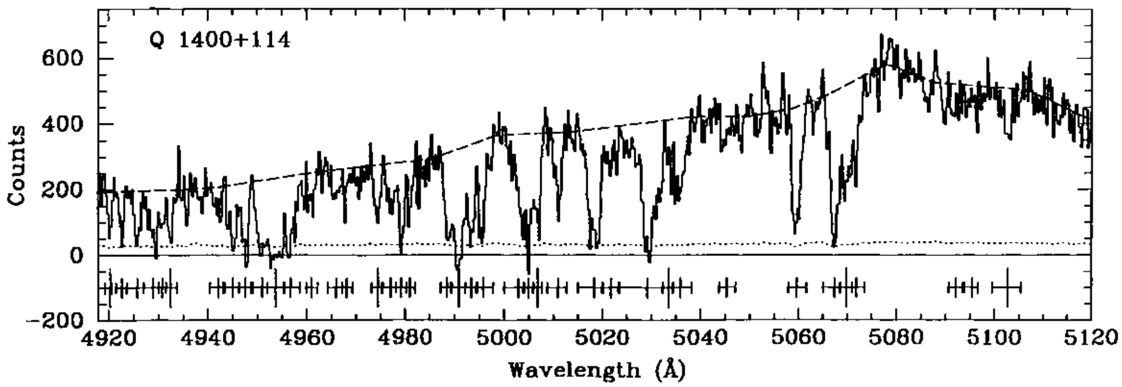

FIG. 1*v*

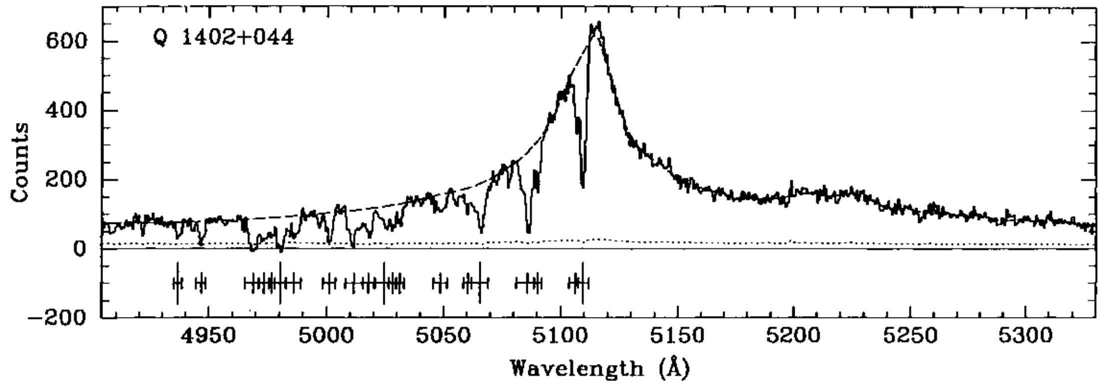

FIG. 1*w*

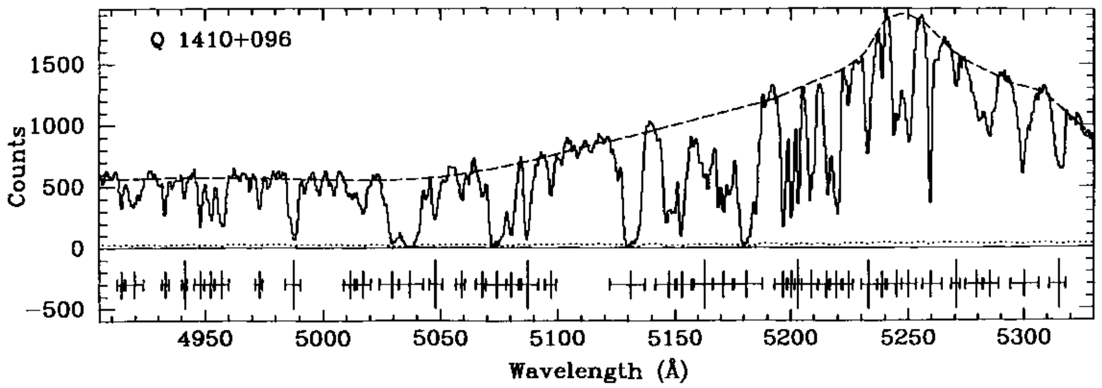

FIG. 1*x*

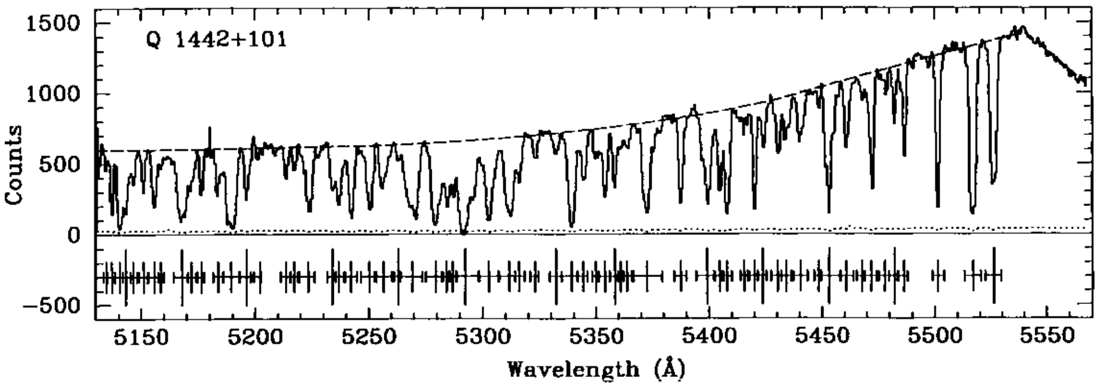

FIG. 1*y*

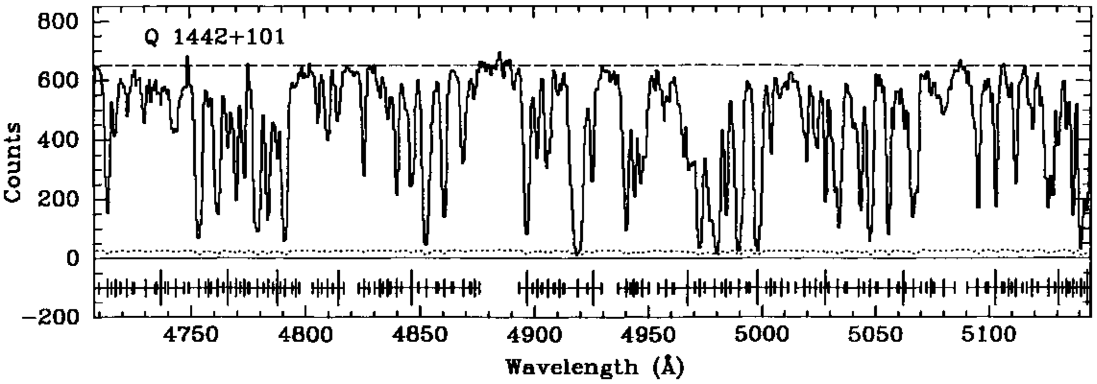

FIG. 1*z*

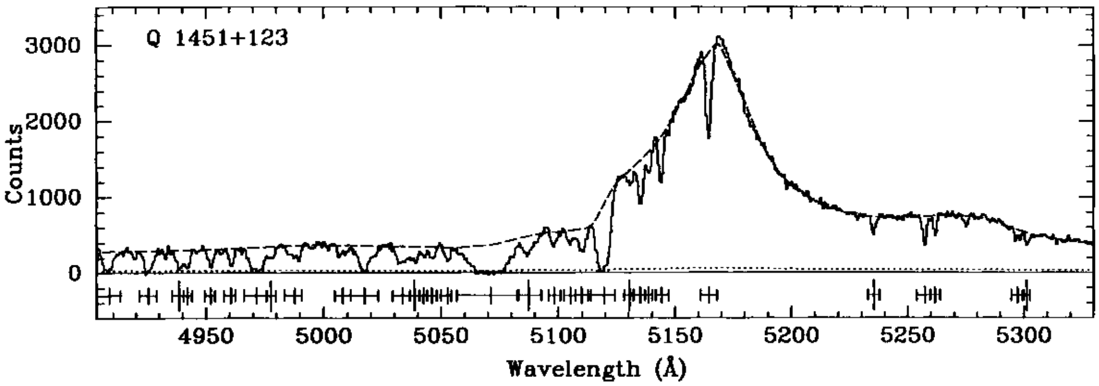

FIG. 1*aa*

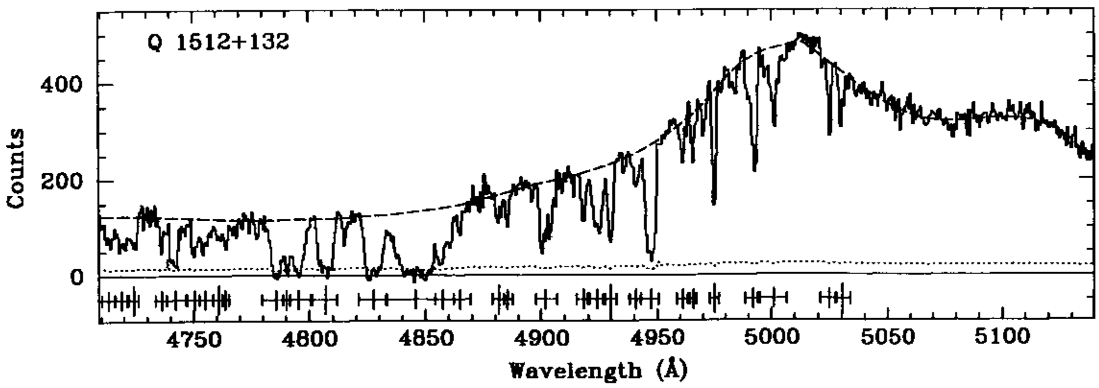

FIG. 1*bb*

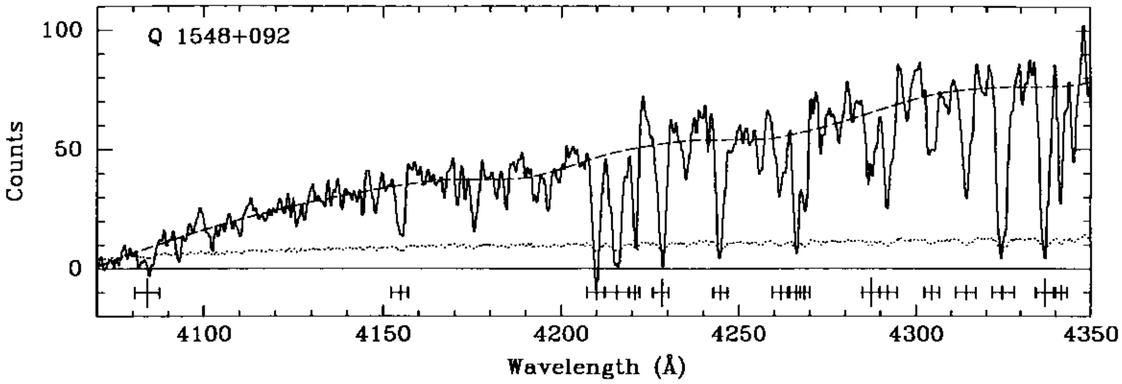

FIG. 1*cc*

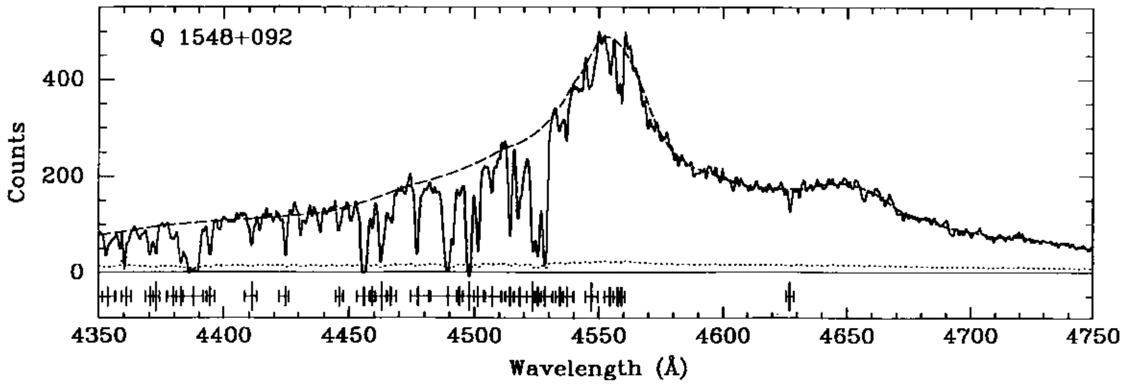

FIG. 1*cc*—*Continued*

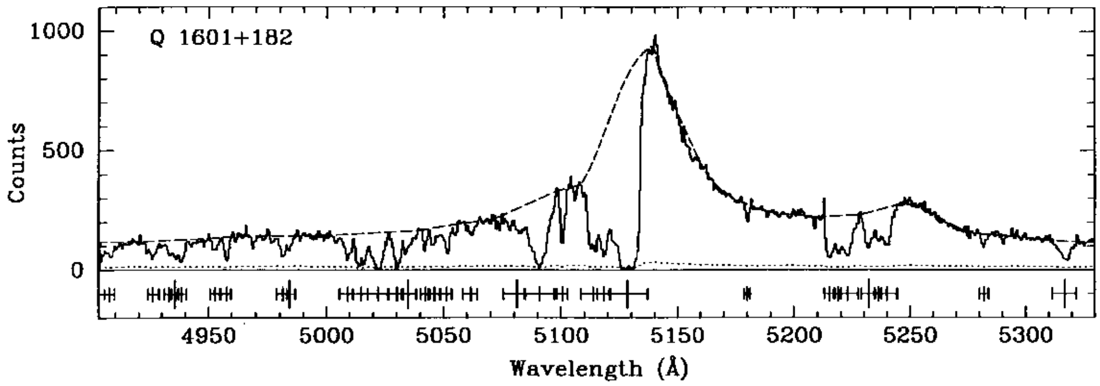

FIG. 1*dd*

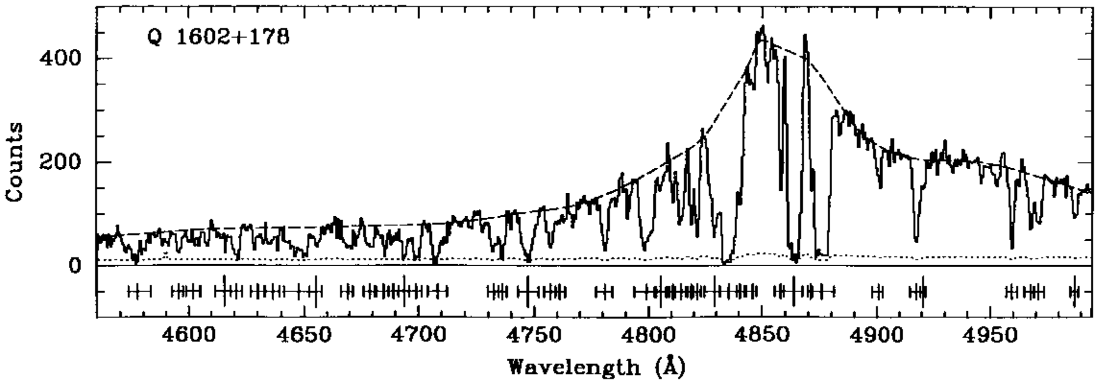

FIG. 1*ee*

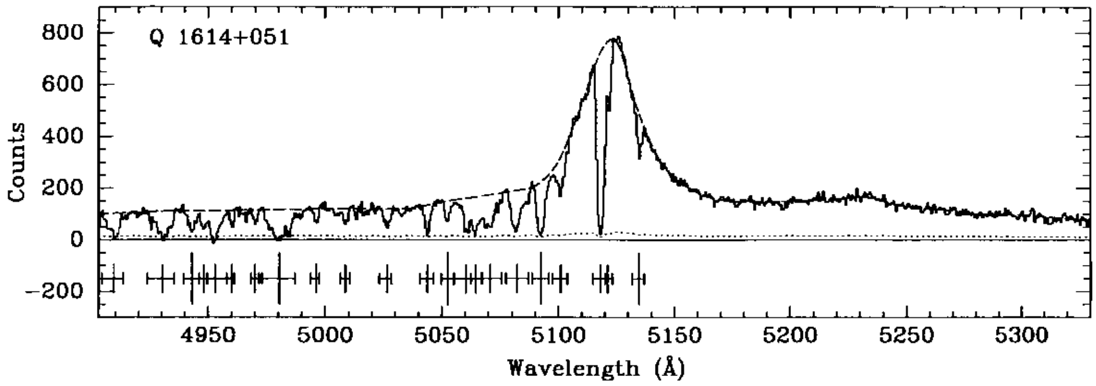

FIG. 1*ff*

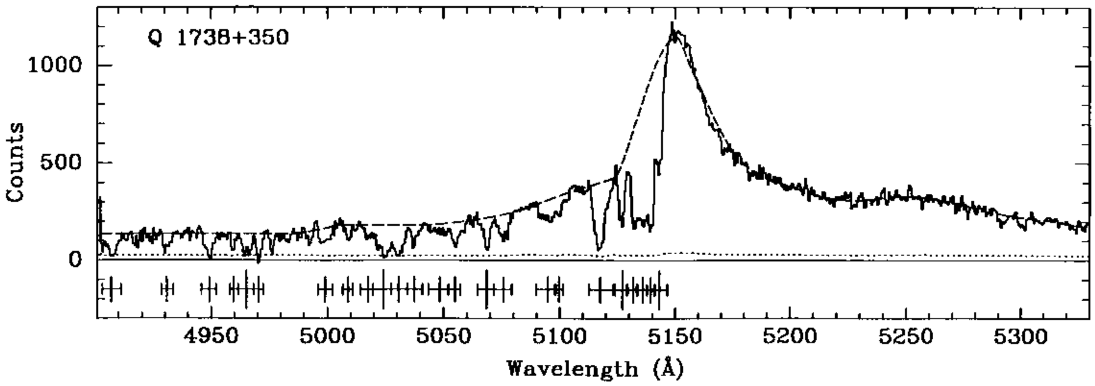

FIG. 1*gg*

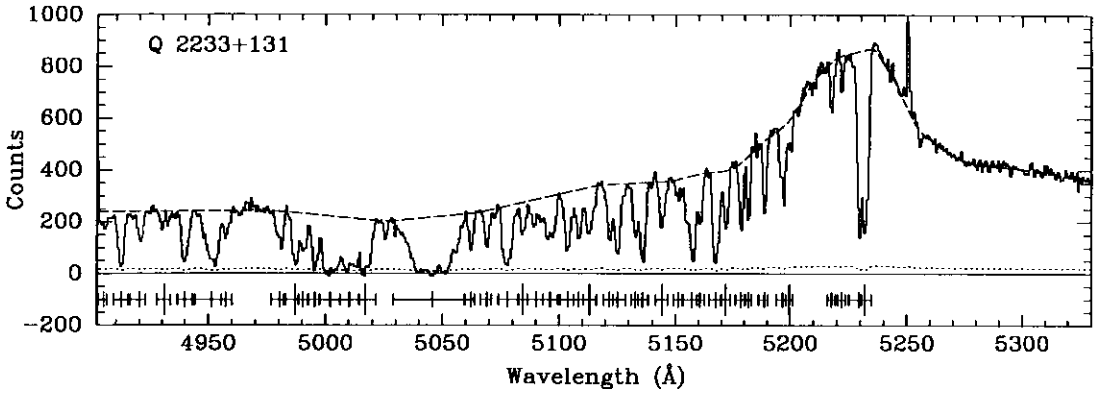

FIG. 1*hh*

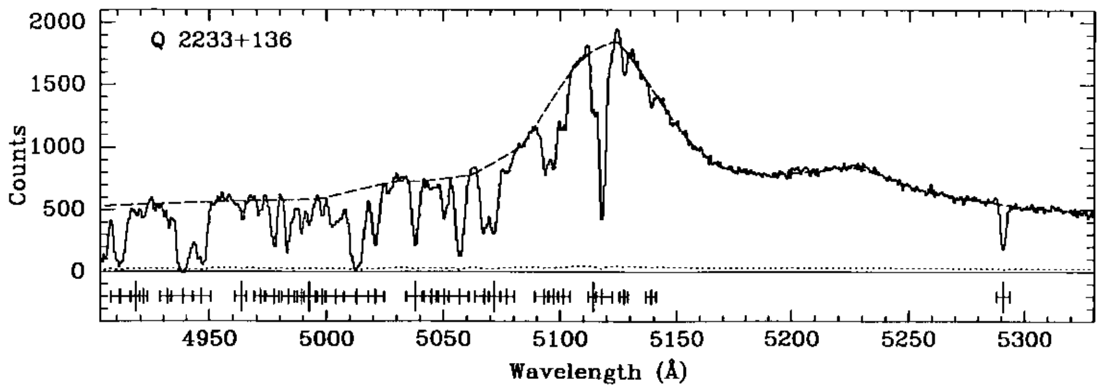

FIG. 1*ii*

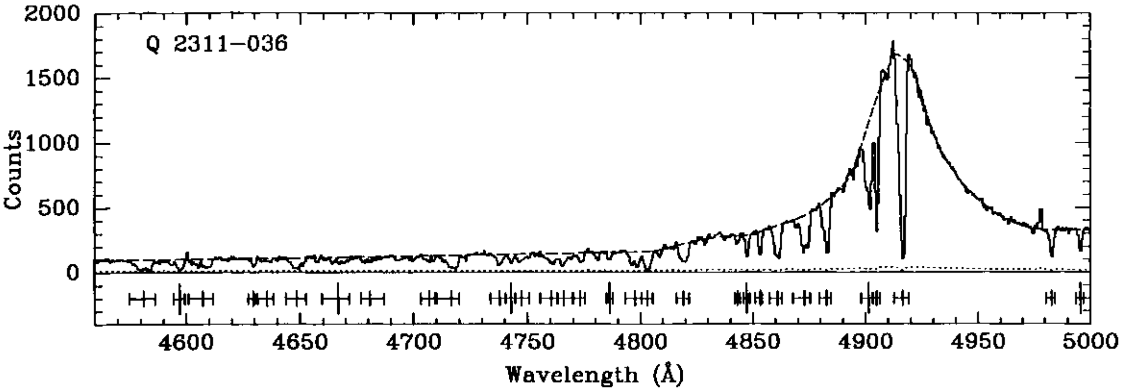

FIG. 1*jj*

TABLE 1
LOG OF OBSERVATIONS

QSO	Alternate Name	Z_{em}	V[a]	Set-Up[b]	Date	Exposure (seconds)
0000-263	Hazard	4.111	17.5	1	12Jul88	7236
0001+087	Hazard	3.243	19.3	1	12Jul88	3000
0014+813	S5	3.384	16.5	2	8Jan89	9600
0029+073	Hazard	3.294	18.4	1	11Jul88	2396
0114-089	UM 670	3.205	17.4	2	22Dec88	7200
0256-000		3.374	18.7	2	22Dec88	3600
0301-005		3.223	18.5	3	10Feb88	5400
0302-003		3.286	18.4	2	22Dec88	3600
0334-204	UM 683	3.126	19.1	3	11Feb88	5400
0636+680	S4	3.174	19.0	3	10Feb88	7200
				2	8Jan89	3600
0731+653	W1	3.033	18.5	2	23Dec88	9000
0831+128	Hazard	2.739	17.8	2	23Dec88	2820
0905+151	Hazard	3.173	19.4	3	11Feb88	7200
0913+072	Hazard	2.784	17.1	2	21Dec88	13200
0938+119		3.192	19.0	3	11Feb88	10800
1033+137	UT	3.092	18.0	3	10Feb88	7200
1206+119	Hazard	3.108	17.9	4	12Apr89	23200
1208+101	Hazard	3.822	17.5	5	11Feb88	7600
1215+33	B2	2.606	17.5	2	6Apr87	12000
1334-005	UM 590	2.842	17.5	2	6Apr87	6600
1400+114	Hazard	3.177	18.9	3	10Feb88	4500
1402+044	Parkes	3.206	18.5	1	12Jul88	2400
1410+096	Hazard	3.313	18.8	1	12Jul88	3600
1442+101	OQ 172	3.554	17.8	1	13Jul88	3000
1451+123	Hazard	3.251	18.6	1	11Jul88	5700
1512+132	Hazard	3.120	19.5	1	13Jul88	3000
1548+092	Hazard	2.748	17.5	6	21May87	10800
1601+182	Cl 1	3.227	19.5	1	12Jul88	3700
1602+178	Cl 4	2.989	19.5	1	13Jul88	3000
1614+051	Parkes	3.216	19.5	1	12Jul88	3000
1738+350		3.239	20.5	1	11Jul88	9600
2233+131		3.295	18.8	1	12Jul88	3000
2233+136		3.209	20.0	1	11Jul88	3600
2311-036	UM 659	3.041	19.9	1	13Jul88	3000

[a] Apparent V magnitude, as listed in Hewitt & Burbidge 1987, 1989.
[b] Instrument set-up: (1) P200, TI-CCD No. 432, 1200 l m^{-1} first order, 1″ slit; resolution ≈ 75 km s^{-1}. (2) MMT, Big Blue Reticon, 832 l mm^{-1} second order, Image Stacker; resolution ≈ 65 km s^{-1}. (3) P200, TI-CCD No. 432, 1200 l m^{-1} second order, 2″ slit; resolution ≈ 75 km s^{-1}. (4) MMT, Red Channel, Echellette Grating, TI-CCD, 1.″25 slit; resolution ≈ 90 km s^{-1}. (5) P200, TI-CCD No. 167, 1200 l m^{-1} first order, 2″ slit; resolution ≈ 100 km s^{-1}. (6) P200, 2D-FRUTTI Photon Counter, 1200 l mm^{-1} second order, 1″ slit; resolution ≈ 70 km s^{-1}.

CCDs were used, with 1200 l mm^{-1} gratings being used in both red and blue sides in first order. Calibration was carried out in the same way as in 1988 February with the stars BD 330−2642 and Feige 110 being used for telluric comparisons.

Spectra were obtained at the Multiple Mirror Telescope (MMT) with two instruments. The MMT Blue spectrograph was used with the 832 l mm^{-1} grating in second order, Image Stacker, "Big Blue" Image Tube, and Photon-Counting Reticon (Latham 1982; Chaffee & Latham 1982). A solid $CuSO_4$ filter was placed in the beam for order blocking, when appropriate. Instrumental pixel-to-pixel fluctuations were divided out using long quartz lamp exposures obtained during the day. During the night, the exposure was stopped every 20 minutes and an exposure of a helium-neon-argon-mercury-cadmium lamp was obtained for wavelength calibration. Standard star exposures of EG 193, G60−54, or EG 248 were taken to look for telluric absorption or residual instrumental features. The resulting spectral resolution is $\sim$65 km s^{-1}.

The MMT Red Spectrograph was used in cross-dispersed mode with the "echellette" grating in orders 11 to 24, using a prism cross-disperser, a TI-CCD and a $1'' \times 10''$ slit (Schmidt et al. 1989). Biases and dome flats obtained during the day were used for calibration, and during the night exposures of a helium-neon-argon lamp were made every 50 minutes. Separate exposures of the same object were rebinned to a common wavelength scale with 35 km s^{-1} $pixel^{-1}$, the instrumental shape of each order was removed using a smooth spline fit to a standard star, and then the orders were spliced together resulting in one continuous spectrum from 4400 Å to 9800 Å. Further discussion of the metal lines seen in the spectrum of Q1206+119 (Figure 1*r*) redward of emission Lyα will be presented elsewhere. The resulting spectral resolution in the region shown in Figure 1*r* is $\sim$90 km s^{-1}.

All data were reduced in the standard way using BARF on a VMS Vax, IRS on a Data General MV 10000, IRAF on SUN workstations, or personally written software for an IBM PC with a Definicon accelerator board. The resolution was determined from reducing the comparison lamp exposures in the same way as the data and measuring the FWHM of all strong but not saturated lines. In all cases, an independent measure of the signal-to-noise was maintained by propagating the variance based on the total number of counts before sky subtraction, and the level of subtracted sky. These were compared to the rms obtained around a continuum fit in regions of the spectra which appeared to be absorption free, when this was practical, to check for noise due to fixed pattern problems, etc. The 1 σ error for each pixel is plotted as a dotted line in Figure 1.

The continuum was fitted iteratively in the following way. A low-order polynomial was fitted to each spectrum, or, for the longer spectra, a separate polynomial was fitted to several portions of each spectrum. Pixels which deviated below the fit by more than 2 σ, as estimated from the variance, were flagged; then a polynomial was fit to the unflagged pixels. The process was repeated 4 or 5 times until convergence was obtained, i.e., until the number of unflagged pixels above the fit was about equal to the number of pixels below the fit and the reduced chi-squared of all unflagged pixels was near 1. Then a cubic spline was fit to the unflagged pixels to obtain the final fit shown by the dashed line in Figure 1. In several cases, difficult regions of the spectrum were removed from the fitting procedure by hand: for example, in the regions around damped Lyα lines. Also, the spline fits were often poor in the 50 or so pixels around the Lyα emission line, which sometimes is very "pointy." In these cases, linear continua were drawn "by hand" to join smoothly onto the spline fits, in order to be sure that the number of absorption lines near z_{em} is determined as accurately as possible.

Significant lines were found by measuring the equivalent width in a bin equal to 2.46 times the number of pixels of the FWHM of the comparison lines, and its error (after Young, Sargent, & Boksenberg 1982a). All such bins where the equivalent width was significant at greater than or equal to 5 σ were flagged. Resolved lines, or blended complexes of lines were thus flagged as several contiguous "significant" resolution elements. The equivalent width of each feature was then measured by specifying start and stop wavelengths for each feature by hand. Alternative approaches to this method were explored using parts of this data set; the results are reported elsewhere (Dobrzycki & Bechtold 1994; Frye et al. 1993). The equivalent widths and their errors (computed from photon statistics only) are listed in Table 2, and the start and stop wavelengths are indicated below each line in Figure 1. The central wavelength of each line given in Table 2 is the centroid, weighted by the depth of each pixel in the line profile below the continuum. All reported wavelengths are vacuum and have been corrected to the heliocentric frame.

Metal-line redshift systems were searched for in several ways. For the Palomar data obtained in the blue side of the Double Spectrograph, the red side was set to cover the corresponding region near the C IV λ1550 emission line at comparable resolution. Thus, QSOs with associated C IV complexes were identified. The literature was searched to identify well-established metal-line redshifts. These included all grade A and B systems listed in the compilation of York et al. (1991), as well as others identified in unpublished spectra obtained by the author. Other candidate redshift systems were found by identifying the lines redward of Lyα emission in the spectra shown here. In addition, any line blueward of Lyα emission appearing in our spectra, or the spectra shown in Wolfe et al. (1986) or Lanzetta et al. (1991), which has rest equivalent width greater than 1.5 Å (assuming an identification of Lyα) was tested as a candidate redshift system.

For each metal-line system redshift, the corresponding lines of the strongest transitions listed in Morton, York, & Jenkins (1988; their Table 4) were then searched for. Identifications which are clearly secure are listed in Table 2, in column (4). For these, the observed wavelength centroid was within 50 km s^{-1} of the predicted position of the line. Less certain identifications are listed in column (5). These include cases where a metal-line transition is predicted to be coincident with the line, but is probably contributing less than half the equivalent width, based on observations of other transitions of the same species, and the f-values listed in Morton, York, & Jenkins (1988). They also include cases were the reality of the redshift system is questionable, because of implausible doublet ratios or because the identification is based on only two or three lines. If Lyα should have been detected but does not appear, the redshift system was not considered real, and none of its lines were included in Table 2, even if it was given a grade of A or B

TABLE 2

LINE LISTS

No.	λ_{obs}	W_λ (Å)	Identification	Possible I.D.
		Q 0000-263		
1	6239.52	8.311 ± 0.043	Lyα λ1215 z =4.124	
2	6231.74	1.698 ± 0.034		
3	6226.60	0.251 ± 0.032		
4	6221.87	0.545 ± 0.031		
5	6218.78	1.371 ± 0.035	Si II λ1260 z =3.9353	
6	6210.65	0.726 ± 0.042		
7	6201.34	2.184 ± 0.037		
8	6196.49	0.906 ± 0.026		
9	6194.05	0.630 ± 0.029		
10	6190.66	1.434 ± 0.027	Si II λ1260 z =4.124	
11	6186.70	3.130 ± 0.032		Si II λ1526 z =3.053
12	6181.92	0.711 ± 0.029		
13	6179.29	0.586 ± 0.031		
14	6175.73	0.877 ± 0.040		
15	6168.97	1.904 ± 0.055		
16	6161.79	2.594 ± 0.027		
17	6159.06	1.450 ± 0.021		N I λ1200 z =4.124
18	6156.20	1.249 ± 0.023	Si IV λ1402 z =3.3897	
19	6152.74	3.750 ± 0.028		
20	6147.79	1.665 ± 0.050		
21	6143.26	0.345 ± 0.037		
22	6139.19	0.383 ± 0.045		
23	6131.25	0.659 ± 0.040		
24	6127.88	2.099 ± 0.039		
25	6123.87	0.516 ± 0.042	Si II λ1193 z =4.124	
26	6118.82	3.911 ± 0.055	Si IV λ1396 z =3.3897	
27	6108.85	4.989 ± 0.054		Si II λ1190 z =4.124
28	6102.11	2.117 ± 0.042		
29	6098.31	0.627 ± 0.039		
30	6093.98	1.423 ± 0.047		
31	6088.53	4.056 ± 0.051		
32	6080.77	5.204 ± 0.044		
33	6075.83	2.898 ± 0.032		
34	6072.35	2.062 ± 0.034		
35	6067.73	2.250 ± 0.039		
36	6064.60	1.700 ± 0.032		
37	6060.44	4.084 ± 0.058		
38	6051.61	0.737 ± 0.051		
39	6044.33	3.739 ± 0.048		
40	6039.89	3.137 ± 0.044		
41	6034.29	2.031 ± 0.053		
42	6030.07	1.694 ± 0.040		
43	6026.07	2.549 ± 0.049		
44	6021.37	3.127 ± 0.049		
45	6016.18	1.457 ± 0.036		
46	6013.66	1.311 ± 0.038		
47	6008.37	4.840 ± 0.058		
48	5999.79	7.531 ± 0.066	Lyα z =3.9353	
49	5990.83	1.132 ± 0.046		
50	5987.31	2.826 ± 0.037		
51	5983.45	2.585 ± 0.045		
52	5977.01	4.345 ± 0.060		
53	5969.15	4.023 ± 0.068		
54	5961.17	2.676 ± 0.063		
55	5953.72	1.751 ± 0.065	Si III λ1206 z =3.9353	
56	5948.26	1.895 ± 0.042		
57	5942.57	2.978 ± 0.069		
58	5932.24	2.548 ± 0.060		
59	5928.07	1.263 ± 0.041		

TABLE 2—*Continued*

No.	λ_{obs}	W_λ (Å)	Identification	Possible I.D.
60	5925.04	2.614 ± 0.035		
61	5921.83	2.831 ± 0.043		N I λ1200 z =3.9353
62	5915.42	3.918 ± 0.052		
63	5911.26	3.810 ± 0.034		
64	5907.47	3.312 ± 0.034		
65	5903.71	2.665 ± 0.049		
66	5896.62	4.099 ± 0.076		
67	5891.28	0.795 ± 0.057		
68	5888.42	2.433 ± 0.047	Si II λ1193 z =3.9353	
69	5885.38	1.505 ± 0.037		
70	5882.77	0.965 ± 0.035		
71	5880.84	0.808 ± 0.029		
72	5878.60	1.911 ± 0.039		
73	5875.61	1.023 ± 0.036		
74	5872.96	1.257 ± 0.040	Si II λ1190 z =3.9353	
75	5870.05	0.879 ± 0.048		
76	5864.04	4.481 ± 0.058	C II* λ1335 z =3.3897	
77	5857.58	4.746 ± 0.038	C II λ1334 z =3.3897	
78	5853.94	2.526 ± 0.034		
79	5850.85	1.153 ± 0.040		
80	5845.29	4.461 ± 0.041		
81	5839.31	4.947 ± 0.049		
			Q 0001+087	
1	5221.25	0.240 ± 0.060	Si II λ1304 z =3.0079	
2	5208.70	0.309 ± 0.075	O I λ1302 z =2.9996	
3	5193.86	1.339 ± 0.066		
4	5172.48	0.958 ± 0.071		
5	5158.71	2.096 ± 0.078		
6	5150.26	1.378 ± 0.065		
7	5132.07	0.824 ± 0.086		
8	5123.56	3.404 ± 0.080		
9	5113.89	1.864 ± 0.106		
10	5100.56	3.246 ± 0.082		
11	5096.35	1.250 ± 0.056		
12	5093.81	1.181 ± 0.065		
13	5081.19	3.552 ± 0.097		
14	5075.46	0.706 ± 0.080		
15	5068.54	0.821 ± 0.094		
16	5049.98	0.839 ± 0.111	Si II λ1260 z =3.0070	
17	5040.37	3.052 ± 0.180	Si II λ1260 z =2.9996	
18	5024.34	2.053 ± 0.113		
19	5015.76	2.785 ± 0.123		
20	5008.92	0.680 ± 0.109		
21	4988.48	1.491 ± 0.091		
22	4980.90	0.600 ± 0.080	N V λ1242 z =3.0070	
23	4977.80	1.231 ± 0.120		
24	4972.77	0.742 ± 0.107		
25	4969.45	1.307 ± 0.110	N V λ1242 z =2.9996	
26	4964.96	1.363 ± 0.109	N V λ1238 z =3.0070 Fe II λ2384 z =1.084	
27	4961.38	0.535 ± 0.079		
28	4959.03	0.937 ± 0.103		
29	4954.59	0.610 ± 0.116	N V λ1238 z =2.9996	
30	4948.99	1.380 ± 0.117	Fe II λ2372 z =1.084	
31	4942.50	5.399 ± 0.126		
32	4936.41	0.690 ± 0.106		
33	4926.51	1.929 ± 0.140		

TABLE 2—*Continued*

No.	λ_{obs}	W_λ (Å)	Identification	Possible I.D.
34	4919.09	0.747 ± 0.087		
35	4915.87	1.695 ± 0.097		
36	4911.84	1.198 ± 0.092		
37	4908.09	1.931 ± 0.094		
			Q 0014+813	
1	5342.13	0.608 ± 0.095		
2	5319.77	1.212 ± 0.110		
3	5309.59	1.335 ± 0.097		
4	5296.54	1.533 ± 0.156	Si IV λ1393 z =2.8004	
5	5265.81	0.771 ± 0.151		
6	5254.50	5.485 ± 0.169	Lyα z =3.32	N V λ1242 z =2.804
7	5249.34	2.572 ± 0.149	Lyα z =3.32 N V λ1238 z =2.804	
8	5240.11	1.247 ± 0.175		
9	5230.51	0.832 ± 0.125		
10	5226.73	3.173 ± 0.159		
11	5220.36	0.996 ± 0.162		
12	5206.72	0.875 ± 0.124		
13	5203.27	2.867 ± 0.149		
14	5199.20	1.812 ± 0.144		
15	5190.33	1.550 ± 0.135		
16	5185.31	1.491 ± 0.181	N I λ1200 z =3.32	
17	5180.11	2.317 ± 0.129		
18	5174.64	1.983 ± 0.147		
19	5169.14	2.081 ± 0.183		
20	5158.54	1.041 ± 0.129		
21	5154.35	2.567 ± 0.146	Si II λ1193 z =3.32	
22	5146.74	1.586 ± 0.111		
23	5143.10	1.199 ± 0.104	Si II λ1190 z =3.32	
24	5139.32	3.833 ± 0.152	Lyα z =3.2266	
25	5117.30	1.391 ± 0.107		
26	5114.80	1.786 ± 0.100		
27	5107.93	3.703 ± 0.162		
28	5102.55	1.331 ± 0.127		
29	5097.35	2.182 ± 0.117	Si III λ1206 z =3.2266	
30	5093.67	2.954 ± 0.120		
31	5088.39	0.514 ± 0.096		
32	5084.24	0.664 ± 0.111		
33	5079.59	3.064 ± 0.139		
34	5074.30	2.152 ± 0.144		C II* λ1335 z =2.8004
35	5048.76	0.754 ± 0.109		
36	5041.28	1.203 ± 0.103	Si II λ1193 z =3.22	
37	5033.68	4.570 ± 0.150	Fe II λ2382 z =1.1127	
38	5029.32	1.101 ± 0.094	Si II λ1190 z =3.2266 Fe II λ2382 z =1.1109	
39	5026.96	0.836 ± 0.091		
40	5021.29	0.875 ± 0.100		
41	5017.16	1.002 ± 0.092		
42	5015.19	1.375 ± 0.095	Fe II λ2374 z =1.1127	Fe II λ2374 z =1.1109
43	5012.02	1.803 ± 0.109		
44	4995.71	2.100 ± 0.121		
45	4990.35	1.165 ± 0.107		
46	4986.26	0.686 ± 0.119		
47	4982.60	0.834 ± 0.119		
48	4968.77	1.200 ± 0.149		
49	4956.71	0.781 ± 0.096	Si II λ1302 z =2.8004	
50	4952.54	3.635 ± 0.106	Fe II λ2344 z =1.1127	

TABLE 2—*Continued*

No.	λ_{obs}	W_λ (Å)	Identification	Possible I.D.
51	4949.26	0.993 ± 0.087	Fe II λ2344 z =1.1109 O I λ1302 z =2.8004	
52	4938.15	2.935 ± 0.117		
53	4933.12	2.763 ± 0.126		
54	4922.78	1.042 ± 0.086		
55	4918.56	0.560 ± 0.090		
56	4899.49	1.102 ± 0.090		Si IV λ1402 z =2.49
57	4896.30	1.618 ± 0.084		
58	4881.59	2.033 ± 0.108		
59	4877.83	0.711 ± 0.081		
60	4875.46	1.781 ± 0.079		
61	4854.86	2.241 ± 0.092		
62	4852.62	1.750 ± 0.082		
63	4820.14	1.916 ± 0.099		
64	4817.59	0.406 ± 0.070		
65	4815.92	0.370 ± 0.064		
66	4813.18	1.680 ± 0.090		
67	4808.77	3.356 ± 0.100		
68	4800.54	3.192 ± 0.128		
69	4782.76	1.087 ± 0.070		
70	4780.73	0.430 ± 0.065		CII* λ1335 z =2.42
71	4776.21	1.318 ± 0.103	CII λ1334 z =2.42	
72	4769.96	2.494 ± 0.089		
73	4766.85	0.947 ± 0.084		
74	4762.08	0.760 ± 0.085		
75	4753.07	4.805 ± 0.106		
76	4748.75	0.419 ± 0.062		
77	4742.21	0.868 ± 0.103		
78	4738.27	0.522 ± 0.060		
79	4735.95	1.882 ± 0.076		
80	4733.10	1.257 ± 0.067		
81	4731.12	0.569 ± 0.069		
82	4724.95	0.872 ± 0.089	N V λ1242 z =2.8004	
83	4717.77	1.169 ± 0.082	Ly α z =2.879	
84	4708.42	0.691 ± 0.082	N V λ1238 z =2.8004	
85	4690.93	1.363 ± 0.066		
86	4689.34	0.994 ± 0.064		
87	4674.47	2.112 ± 0.093		
88	4666.65	3.012 ± 0.120		
89	4659.05	0.742 ± 0.086		
90	4651.35	1.715 ± 0.091		
91	4646.73	2.881 ± 0.093		
92	4642.42	0.502 ± 0.067		
93	4639.61	1.794 ± 0.091		
94	4627.93	1.314 ± 0.107		
95	4618.72	6.897 ± 0.129	Si II λ1190 z =2.87 Lyα z =2.8004	
96	4607.04	1.233 ± 0.078		
97	4602.53	1.463 ± 0.092		
98	4597.81	1.048 ± 0.103		
99	4585.45	3.827 ± 0.117	Si III λ1206 z =2.8004	
100	4581.55	0.409 ± 0.081	Si III λ1206 z =2.8004	N II λ1083 z =3.2266
101	4562.46	1.371 ± 0.077		
102	4558.92	1.441 ± 0.075		
103	4555.81	1.272 ± 0.081	Si II λ1304 z =2.49	
			Q 0029+073	
1	5321.67	1.260 ± 0.107	C IV λ1548 z =2.437	

TABLE 2—*Continued*

No.	λ_{obs}	W_λ (Å)	Identification	Possible I.D.
2	5281.61	0.699 ± 0.075	Si II λ1304 z =3.054	
3	5273.55	1.136 ± 0.063	O I λ1302 z =3.054	
4	5267.62	1.186 ± 0.064		
5	5260.04	0.350 ± 0.044		
6	5256.98	0.598 ± 0.047		
7	5251.74	2.696 ± 0.061		
8	5244.13	5.169 ± 0.059	Si II λ1526 z =2.437	
9	5236.56	3.236 ± 0.050		
10	5227.94	2.496 ± 0.080		
11	5216.26	5.836 ± 0.073	N V λ1242 z =3.198	C II* λ1334 z =2.904
12	5208.39	1.310 ± 0.052	C II λ1334 z =2.904	
13	5198.92	6.293 ± 0.089	N V λ1238 z =3.198	
14	5184.67	2.318 ± 0.091	Fe II λ2382 z =1.1759	
15	5167.12	1.585 ± 0.076	C II λ1334 z =2.8734 Fe II λ2374 z =1.1759	
16	5156.17	0.832 ± 0.086		
17	5142.65	3.395 ± 0.079		
18	5137.61	1.238 ± 0.061		
19	5133.25	0.826 ± 0.059		
20	5122.02	10.807 ± 0.110		Si IV λ1402 z =2.649
21	5112.57	4.081 ± 0.075		Si II λ1260 z =3.054
22	5103.26	8.120 ± 0.097	Lyα z =3.198 Fe II λ2344 z =1.1759 Si II λ1260 z =3.054	
23	5093.72	4.802 ± 0.081		Si II λ1304 z =2.904
24	5087.98	2.661 ± 0.068		
25	5083.76	2.268 ± 0.082	O I λ1302 z =2.904 Si IV λ1393 z =2.649	
26	5077.47	2.050 ± 0.084		
27	5069.80	5.225 ± 0.102	C II λ1334 z =2.798	C II* λ1335 z =2.798
28	5062.72	1.632 ± 0.099	Si III λ1206 z =3.198	
29	5051.02	3.717 ± 0.108	Si II λ1304 z =2.8734	
30	5041.83	5.734 ± 0.108	O I λ1302 z =2.8734	
31	5034.42	1.650 ± 0.087	N V λ1242 z =3.054	
32	5028.05	3.280 ± 0.106		
33	5021.79	1.820 ± 0.082		
34	5016.97	2.124 ± 0.099	N V λ1238 z =3.054	
35	5009.42	3.258 ± 0.106		Si II λ1193 z =3.198
36	5002.51	4.327 ± 0.135		Si II λ1190 z =3.198
37	4992.14	0.810 ± 0.105		
38	4987.27	0.542 ± 0.103		
39	4980.33	2.442 ± 0.125		
40	4967.34	1.520 ± 0.089		
41	4962.53	4.204 ± 0.107		
42	4957.34	1.382 ± 0.082		
43	4954.03	1.554 ± 0.099	Si II λ1304 z =2.798	
44	4947.44	0.789 ± 0.120	O I λ1302 z =2.798	
45	4940.02	1.370 ± 0.119		
46	4922.49	15.504 ± 0.244	Si II λ1260 z =2.904 Ly α z =3.054	
			Q 0114-089	
1	5118.03	0.352 ± 0.052	C IV λ1550 z =2.2995	
2	5116.53	0.401 ± 0.041	C IV λ1550 z =2.2995	
3	5109.48	0.571 ± 0.046	C IV λ1548 z =2.2995	
4	5107.96	0.445 ± 0.043	C IV λ1548 z =2.2995	
5	5087.59	1.270 ± 0.063		N V λ1238 z =3.1053
6	5077.08	0.682 ± 0.063		

TABLE 2—*Continued*

No.	λ_{obs}	W_λ (Å)	Identification	Possible I.D.
7	5072.11	1.321 ± 0.059		
8	5069.67	1.037 ± 0.055		
9	5066.57	0.512 ± 0.060		
10	5052.13	0.754 ± 0.076		
11	5049.14	0.775 ± 0.050		
12	5038.70	0.944 ± 0.084		Si II λ1526 z =2.2995
13	5033.66	0.620 ± 0.070		
14	5025.18	0.616 ± 0.059		
15	5022.64	0.395 ± 0.058		
16	5004.72	3.944 ± 0.094		
17	4992.02	7.351 ± 0.097	Lyα z =3.106	
18	4984.60	0.338 ± 0.054		
19	4981.72	0.508 ± 0.080		
20	4959.66	2.910 ± 0.071		
21	4954.48	1.237 ± 0.057	Si III λ1206 z =3.1053	
22	4952.04	1.532 ± 0.063		
23	4948.62	1.773 ± 0.080		
24	4944.17	1.569 ± 0.073		
25	4935.95	0.773 ± 0.062		
26	4933.41	0.827 ± 0.066		Si IV λ1393 z =2.539
27	4925.93	1.359 ± 0.056		
28	4924.20	1.298 ± 0.052		
29	4910.22	1.906 ± 0.076		
30	4902.65	0.813 ± 0.055		
31	4901.19	0.745 ± 0.046		
32	4898.78	0.423 ± 0.062		Si II λ1193 z =3.1053
33	4894.16	1.939 ± 0.082		
34	4886.98	2.031 ± 0.065		Si II λ1190 z =3.1053
35	4882.97	3.362 ± 0.064		
36	4879.92	1.017 ± 0.054		
37	4876.65	1.699 ± 0.063		
38	4873.10	1.724 ± 0.078		
39	4861.15	1.220 ± 0.070		
40	4854.80	0.343 ± 0.067		
41	4845.66	1.243 ± 0.068		
42	4842.76	0.552 ± 0.064		
43	4832.84	2.611 ± 0.077		
44	4828.78	0.320 ± 0.060		
45	4825.77	1.447 ± 0.065		
46	4823.29	0.851 ± 0.062		
47	4810.49	0.512 ± 0.065		
48	4806.47	0.416 ± 0.073		
49	4799.32	4.743 ± 0.085		
50	4791.57	3.982 ± 0.091		
51	4782.46	1.549 ± 0.070		
52	4779.18	1.610 ± 0.051		
53	4776.42	1.315 ± 0.062		
54	4771.27	0.360 ± 0.068		
55	4769.04	0.607 ± 0.059		
56	4753.66	4.578 ± 0.080		
57	4749.74	0.825 ± 0.061		
58	4745.01	0.409 ± 0.063		
59	4730.99	1.758 ± 0.086		
60	4709.50	1.221 ± 0.072		
61	4703.54	1.066 ± 0.062		
62	4695.83	4.490 ± 0.081		
63	4686.35	1.112 ± 0.073		
64	4680.34	0.417 ± 0.051		
65	4669.46	0.544 ± 0.064		
66	4666.10	2.373 ± 0.065		
67	4648.02	1.411 ± 0.075		

TABLE 2—*Continued*

No.	λ_{obs}	W_λ (Å)	Identification	Possible I.D.
68	4643.53	0.845 ± 0.062		
69	4639.30	0.576 ± 0.068		
70	4630.53	0.724 ± 0.070		
71	4623.48	0.359 ± 0.051		
72	4606.02	0.411 ± 0.056		
73	4601.64	0.276 ± 0.050		
74	4593.18	0.677 ± 0.057		
75	4589.98	0.523 ± 0.049		
76	4587.52	1.666 ± 0.068		
77	4580.17	0.623 ± 0.063		
78	4575.58	1.370 ± 0.065		
79	4571.04	1.847 ± 0.063		
80	4562.36	1.365 ± 0.074		
81	4537.35	3.363 ± 0.078		
82	4529.75	0.414 ± 0.064		
83	4522.89	2.305 ± 0.055		
84	4520.12	2.464 ± 0.062		
85	4506.28	0.437 ± 0.056		
86	4503.85	1.451 ± 0.063		
87	4488.92	1.600 ± 0.067		
88	4485.85	0.397 ± 0.049		
89	4482.58	0.933 ± 0.068		
			Q 0256-000	
1	5288.43	0.480 ± 0.050		
2	5286.56	1.104 ± 0.075		
3	5282.64	1.709 ± 0.079		
4	5268.96	0.654 ± 0.099		
5	5264.48	0.382 ± 0.077	Fe II λ2600 z =1.025	
6	5259.80	1.024 ± 0.092		
7	5256.42	2.478 ± 0.100		
8	5243.32	1.013 ± 0.094		
9	5239.53	0.558 ± 0.100		
10	5236.78	2.668 ± 0.117		Fe II λ2382 z =1.1983 Fe II λ2586 z =1.023
11	5228.07	1.475 ± 0.144		
12	5220.14	1.502 ± 0.141		
13	5218.13	1.287 ± 0.123		Fe II λ2374 z =1.1983
14	5212.07	1.489 ± 0.131		
15	5206.91	4.814 ± 0.181		
16	5202.12	3.624 ± 0.155		
17	5196.70	1.754 ± 0.167		
18	5192.61	0.849 ± 0.135		
19	5182.81	2.453 ± 0.245		
20	5177.39	1.262 ± 0.145		
21	5145.69	5.558 ± 0.193	Si II λ1260 z =3.082	
22	5140.44	1.327 ± 0.132		
23	5137.49	1.874 ± 0.121		
24	5134.45	2.877 ± 0.146		
25	5130.31	1.925 ± 0.160		
26	5104.71	2.661 ± 0.154		
27	5097.09	1.362 ± 0.128		
28	5081.68	2.180 ± 0.133		
29	5076.97	1.651 ± 0.154		
30	5066.28	0.856 ± 0.160		
31	5062.60	2.316 ± 0.139		
32	5044.59	1.394 ± 0.145		
33	5040.54	0.853 ± 0.121		

TABLE 2—*Continued*

No.	λ_{obs}	W_λ (Å)	Identification	Possible I.D.
34	5035.30	0.941 ± 0.099		
35	5033.63	1.051 ± 0.104		
36	5026.60	1.293 ± 0.131		
37	5023.76	1.142 ± 0.130		
38	5017.14	2.124 ± 0.143		
39	5012.63	2.207 ± 0.136		
40	5010.26	1.153 ± 0.131		
41	4985.38	2.297 ± 0.171		
42	4981.12	1.637 ± 0.130		
43	4971.92	4.570 ± 0.169	Lyα z =3.0916	
44	4963.31	9.689 ± 0.196	Lyα z =3.082	
45	4952.49	4.348 ± 0.176		
46	4938.80	0.659 ± 0.130	Si III λ1206 z =3.082	
47	4928.37	1.692 ± 0.146		
48	4907.18	1.482 ± 0.160		N I λ1200 z =3.0196
49	4899.68	1.425 ± 0.147	N I λ1200 z =3.082	
50	4885.15	3.762 ± 0.175		
51	4878.08	1.456 ± 0.153		
52	4872.57	1.664 ± 0.132	Si II λ1193 z =3.082	
53	4866.91	2.574 ± 0.147		
54	4863.98	0.693 ± 0.106		
55	4859.29	2.351 ± 0.147	Si II λ1190 z =3.082	
56	4854.56	1.327 ± 0.121		
57	4844.66	0.908 ± 0.123		
58	4841.79	1.170 ± 0.107		
59	4835.27	1.967 ± 0.137		
60	4832.46	1.018 ± 0.115		
61	4826.50	0.632 ± 0.122		
62	4817.97	0.773 ± 0.127		
63	4810.42	1.059 ± 0.133		
64	4807.30	1.306 ± 0.113		Fe II λ2374 z =1.025
65	4797.85	2.007 ± 0.114		
66	4795.66	0.627 ± 0.098		
67	4791.35	1.369 ± 0.118		
68	4787.82	1.049 ± 0.106		
69	4772.44	2.078 ± 0.122		
70	4766.64	0.854 ± 0.106		
71	4741.90	1.285 ± 0.104		
72	4737.58	1.369 ± 0.130		
73	4733.83	0.951 ± 0.108		
74	4724.13	2.946 ± 0.145		
75	4713.74	0.542 ± 0.098		
76	4709.31	1.792 ± 0.101		
77	4705.28	2.406 ± 0.137		
78	4698.25	0.617 ± 0.112		
79	4693.89	4.572 ± 0.122		
80	4687.53	0.527 ± 0.087		
81	4673.29	0.947 ± 0.096		
82	4666.23	0.718 ± 0.094		
83	4662.30	4.737 ± 0.131		
84	4651.92	1.766 ± 0.079		
85	4648.83	3.229 ± 0.094		
86	4642.89	0.633 ± 0.083		
87	4639.98	1.594 ± 0.096		
88	4632.70	0.989 ± 0.110		
89	4625.58	3.729 ± 0.121		
90	4620.72	2.522 ± 0.091		
91	4617.79	1.568 ± 0.067		
92	4616.02	0.814 ± 0.070		
93	4609.90	4.825 ± 0.116		
94	4605.21	1.371 ± 0.114		

TABLE 2—*Continued*

No.	λ_{obs}	W_λ (Å)	Identification	Possible I.D.
95	4601.73	1.019 ± 0.084		
96	4592.06	1.294 ± 0.099		
97	4589.16	1.010 ± 0.094		
98	4581.93	2.642 ± 0.100		
99	4578.84	0.856 ± 0.083		
100	4575.63	1.188 ± 0.107		
101	4563.37	1.281 ± 0.106		
102	4554.09	1.200 ± 0.102		
103	4546.44	0.940 ± 0.070		
104	4544.14	0.979 ± 0.079		
105	4540.55	0.902 ± 0.071		
106	4537.22	1.596 ± 0.068		
107	4534.83	2.055 ± 0.082		
108	4508.26	0.937 ± 0.078		
109	4502.54	1.314 ± 0.094		
110	4497.58	0.993 ± 0.086		
111	4492.22	0.863 ± 0.085		
112	4487.02	1.383 ± 0.100		
			Q 0301-005	
1	5107.96	0.253 ± 0.034		
2	5100.75	2.001 ± 0.046		
3	5098.26	1.236 ± 0.038		
4	5096.21	0.293 ± 0.040		
5	5090.91	1.166 ± 0.048		
6	5088.81	2.049 ± 0.053		
7	5086.03	0.391 ± 0.053		
8	5083.74	0.619 ± 0.055		
9	5080.84	1.401 ± 0.061		
10	5073.40	0.527 ± 0.061		
11	5064.67	0.546 ± 0.061		
12	5062.55	0.359 ± 0.056		
13	5058.49	0.885 ± 0.056		
14	5056.18	1.195 ± 0.071		
15	5053.01	0.500 ± 0.069		
16	5046.70	2.031 ± 0.072		
17	5044.30	0.950 ± 0.052		
18	5042.15	1.377 ± 0.078		
19	5036.00	1.421 ± 0.075		
20	5033.62	0.960 ± 0.075		
21	5024.64	0.850 ± 0.063		
22	5019.61	1.577 ± 0.093		
23	5017.42	0.952 ± 0.076		
24	5012.04	1.960 ± 0.095		
25	5002.75	2.315 ± 0.123		
26	4995.70	1.864 ± 0.107		
27	4990.23	4.574 ± 0.154		
28	4984.42	2.629 ± 0.153		
29	4969.62	5.793 ± 0.163	C II λ1334 z =2.7241 Si II λ1260 z =2.9406	C II* λ1335 z =2.7241
30	4955.92	1.903 ± 0.118		
31	4944.67	4.320 ± 0.154		
32	4934.96	2.808 ± 0.132		
33	4931.62	0.936 ± 0.098		

TABLE 2—*Continued*

No.	λ_{obs}	W_λ (Å)	Identification	Possible I.D.
			Q 0302-003	
1	5214.73	0.321 ± 0.050		
2	5201.18	0.232 ± 0.045		
3	5187.92	2.058 ± 0.070		
4	5184.95	0.701 ± 0.070		
5	5177.23	2.843 ± 0.094		
6	5172.07	0.417 ± 0.067		
7	5157.62	1.837 ± 0.178		
8	5146.86	2.706 ± 0.129		
9	5134.30	1.583 ± 0.111		
10	5130.88	2.673 ± 0.109	Lyα z =3.2195	
11	5127.81	1.460 ± 0.096		
12	5124.56	2.483 ± 0.119		
13	5115.02	0.650 ± 0.092		
14	5112.36	1.220 ± 0.127		
15	5063.47	0.720 ± 0.102		N I λ1200 z =3.2195
16	5044.12	1.217 ± 0.110		
17	5028.78	2.997 ± 0.140		
18	5023.99	1.646 ± 0.148		Si II λ1190 z =3.2195
19	5006.10	0.701 ± 0.124		
20	5001.18	0.872 ± 0.139		
21	4997.41	1.176 ± 0.124		
22	4994.50	1.160 ± 0.102		
23	4992.09	1.714 ± 0.122		
24	4979.73	1.508 ± 0.172		
25	4975.22	1.499 ± 0.123		
26	4963.47	0.872 ± 0.128		
27	4957.44	2.857 ± 0.130		Si IV λ1402 z =2.5359
28	4948.38	2.353 ± 0.172		
29	4938.78	4.165 ± 0.184		
30	4920.32	4.382 ± 0.166		
31	4914.23	0.813 ± 0.145		
32	4910.00	2.318 ± 0.167		
33	4902.88	3.420 ± 0.152		
34	4888.00	1.608 ± 0.124		
35	4881.37	1.603 ± 0.121		
36	4867.15	3.480 ± 0.134		
37	4858.41	1.885 ± 0.097		
38	4856.61	1.289 ± 0.085		
39	4854.66	1.220 ± 0.099		
40	4840.64	3.272 ± 0.120		
41	4836.91	2.629 ± 0.110		
42	4833.13	1.217 ± 0.131		
43	4829.87	0.964 ± 0.108		
44	4825.35	0.640 ± 0.100		
45	4816.92	0.652 ± 0.103		
46	4812.24	4.006 ± 0.156		
47	4803.25	1.184 ± 0.141		
48	4784.27	0.682 ± 0.106		
49	4778.45	1.438 ± 0.127		
50	4775.96	0.449 ± 0.086		
51	4773.89	0.476 ± 0.085		
52	4769.20	1.188 ± 0.165		
53	4762.06	2.213 ± 0.100		
54	4759.60	0.561 ± 0.084		
55	4747.72	1.283 ± 0.102		
56	4735.56	2.503 ± 0.137		
57	4716.91	2.767 ± 0.180	C II λ1334 z =2.5359	C II* λ1335 z =2.5359

TABLE 2—*Continued*

No.	λ_{obs}	W_λ (Å)	Identification	Possible I.D.
58	4708.49	1.954 ± 0.141		
59	4700.53	0.709 ± 0.104		
60	4696.81	1.887 ± 0.093		
61	4694.78	1.261 ± 0.072		
62	4692.11	1.334 ± 0.101		
63	4688.99	0.793 ± 0.099		
64	4683.80	1.395 ± 0.106		
65	4680.77	1.321 ± 0.094	Si II λ1304 z =2.5892	
66	4678.09	1.136 ± 0.069		
67	4675.77	2.520 ± 0.106		
68	4668.30	1.424 ± 0.145		
69	4651.05	2.734 ± 0.118		
70	4642.97	1.006 ± 0.094		
71	4638.81	2.671 ± 0.094		
72	4635.52	0.778 ± 0.072		
73	4633.31	1.714 ± 0.076		
74	4631.04	0.525 ± 0.064		
75	4628.15	2.163 ± 0.107		
76	4622.74	1.647 ± 0.101		
77	4613.98	1.219 ± 0.086		
78	4603.89	4.471 ± 0.114	O I λ1302 z =2.5359	
79	4582.27	0.470 ± 0.089		
80	4575.29	2.110 ± 0.130		N II λ1083 z =3.2195
81	4559.08	0.492 ± 0.098		
82	4555.89	1.319 ± 0.089		
83	4553.27	0.624 ± 0.083		
84	4545.05	1.576 ± 0.122		
85	4533.89	0.599 ± 0.100		
86	4530.21	1.951 ± 0.099		
87	4524.31	1.239 ± 0.123	Si II λ1260 z =2.5892	
88	4500.33	1.403 ± 0.115		
89	4496.67	2.112 ± 0.134		
			Q 0334-204	
1	5110.19	0.829 ± 0.056		Fe II λ1608 z =2.175
2	5094.98	0.377 ± 0.050	Si II λ1260 z =3.0432 Fe II λ1608 z =2.1671	
3	5047.01	0.541 ± 0.036		
4	5044.76	0.938 ± 0.032	Fe II λ2382 z =1.1174	
5	5042.76	0.190 ± 0.024		
6	5027.54	0.165 ± 0.017	Fe II λ2374 z =1.1174	C IV λ1550 z =2.2420
7	5021.58	0.207 ± 0.020		C IV λ1548 z =2.2420
8	5019.30	0.401 ± 0.021		C IV λ1548 z =2.2420
9	5011.69	1.179 ± 0.023		
10	5006.28	0.240 ± 0.024		Si II λ1526 z =2.2802
11	5003.98	0.302 ± 0.028		
12	5000.64	0.615 ± 0.036		
13	4996.86	0.370 ± 0.030		
14	4989.33	0.454 ± 0.046		
15	4985.97	0.308 ± 0.048		
16	4980.32	6.885 ± 0.097	Lyα z =3.0967	
17	4972.21	7.245 ± 0.086	Lyα z =3.0917	
18	4964.25	2.083 ± 0.063	Fe II λ2344 z =1.1174	
19	4957.06	1.171 ± 0.047		
20	4953.56	2.638 ± 0.061		
21	4948.84	0.643 ± 0.046		Si II λ1526 z =2.2420
22	4946.27	1.440 ± 0.037		
23	4942.85	3.747 ± 0.053	Si III λ1206 z =3.0967	

TABLE 2—*Continued*

No.	λ_{obs}	W_λ (Å)	Identification	Possible I.D.
24	4936.55	2.693 ± 0.072	Si III λ1206 z =3.0917	
25	4930.94	1.850 ± 0.056		
26	4924.33	5.243 ± 0.065		C IV λ1550 z =2.175
		Q 0636+681 (MMT)		
1	5034.05	1.883 ± 0.120		
2	5019.63	0.756 ± 0.082		
3	5015.83	0.460 ± 0.085		
4	5005.21	1.106 ± 0.093		
5	4997.55	1.884 ± 0.127		N V λ1242 z =3.0174
6	4991.27	1.877 ± 0.089		
7	4988.28	1.592 ± 0.092		
8	4983.54	2.542 ± 0.101		
9	4977.53	1.014 ± 0.085		N V λ1238 z =3.0174
10	4971.83	1.917 ± 0.092		
11	4968.13	0.836 ± 0.055		
12	4966.24	0.882 ± 0.071		
13	4962.45	0.827 ± 0.077		
14	4956.28	0.512 ± 0.080		
15	4948.99	0.689 ± 0.080		
16	4945.16	3.243 ± 0.095		
17	4942.32	0.901 ± 0.072		
18	4938.17	0.490 ± 0.087		
19	4921.46	1.110 ± 0.092	Si II λ1260 z =2.9054	
20	4914.99	2.120 ± 0.114		
21	4908.47	0.520 ± 0.090		
22	4901.78	0.415 ± 0.082		
23	4898.79	0.537 ± 0.066		
24	4894.23	0.540 ± 0.079		
25	4891.15	1.327 ± 0.083		
26	4888.32	1.388 ± 0.077		
27	4884.86	3.221 ± 0.101	Lyα z =3.0174	
28	4879.79	3.319 ± 0.101		
29	4875.83	2.321 ± 0.085	Si IV λ1402 z =2.4754	
30	4867.95	2.491 ± 0.080		
31	4864.09	1.493 ± 0.062		
32	4860.70	0.875 ± 0.062		
33	4857.92	1.042 ± 0.094		
34	4853.23	1.736 ± 0.069		
35	4849.88	0.922 ± 0.084		N V λ1242 z =2.9054 Si III λ1206 z =3.1074
36	4843.03	2.049 ± 0.084	Si IV λ1393 z =2.4754	
37	4840.57	1.262 ± 0.080		
38	4837.42	0.478 ± 0.074	N V λ1238 z =2.9054	
39	4831.75	1.166 ± 0.099		
40	4828.34	1.181 ± 0.074		
41	4810.42	0.597 ± 0.094		
42	4805.93	1.295 ± 0.096		
43	4802.72	1.381 ± 0.090		
44	4799.69	1.323 ± 0.101		
45	4790.07	1.675 ± 0.095		Si II λ1193 z =3.0174
46	4765.82	1.319 ± 0.103		
47	4759.00	2.327 ± 0.117		
48	4752.23	2.853 ± 0.119	Lyα z =2.9054	
49	4745.60	6.111 ± 0.136		
50	4738.31	0.561 ± 0.082		
51	4731.56	6.644 ± 0.140		
52	4711.03	3.071 ± 0.125	Si III λ1206 z =2.9054	

TABLE 2—*Continued*

No.	λ_{obs}	W_{λ} (Å)	Identification	Possible I.D.
53	4703.42	3.572 ± 0.119		
54	4698.90	1.565 ± 0.101		
55	4682.34	1.076 ± 0.097		
56	4678.23	0.707 ± 0.080		
57	4673.67	1.602 ± 0.100		
58	4668.84	1.512 ± 0.112		
59	4662.82	0.693 ± 0.084		
60	4659.31	1.948 ± 0.085	Si II λ1193 z =2.9054	
61	4655.27	0.919 ± 0.078		
62	4650.67	1.887 ± 0.100		
63	4647.62	0.901 ± 0.072	Si II λ1190 z =2.9054	
64	4645.00	0.473 ± 0.055		
65	4641.97	2.308 ± 0.093		C II* λ1335 z =2.4754
66	4638.82	0.384 ± 0.073		
67	4633.82	2.227 ± 0.117		
68	4620.70	0.477 ± 0.082		
69	4615.69	1.836 ± 0.093		
70	4612.55	1.289 ± 0.089		
71	4608.15	0.292 ± 0.056		
72	4596.64	1.165 ± 0.099		
73	4588.98	1.918 ± 0.114		
74	4577.11	0.691 ± 0.071		
75	4575.40	0.682 ± 0.057		
76	4565.94	1.622 ± 0.098		
77	4562.21	0.334 ± 0.063		
78	4559.01	0.597 ± 0.080		
79	4554.97	2.161 ± 0.106		
80	4549.53	0.695 ± 0.084		
81	4535.46	0.653 ± 0.079		
82	4527.06	0.420 ± 0.076		
83	4522.77	0.877 ± 0.076		
84	4519.19	0.612 ± 0.088		
85	4505.63	1.981 ± 0.092		
86	4493.03	0.805 ± 0.071		
87	4490.28	0.966 ± 0.050		
88	4487.98	1.142 ± 0.060		
89	4485.82	1.599 ± 0.071		
90	4482.16	1.810 ± 0.096		
91	4476.44	2.966 ± 0.074		
92	4473.46	1.583 ± 0.055		
93	4471.17	0.609 ± 0.038		
94	4468.72	1.702 ± 0.063		
95	4466.73	0.438 ± 0.051		
96	4463.31	0.369 ± 0.051		
97	4455.07	0.919 ± 0.073		
98	4449.43	1.100 ± 0.081		
99	4440.60	1.113 ± 0.088		
100	4436.67	0.683 ± 0.077		
101	4423.78	1.029 ± 0.075		
102	4420.84	0.927 ± 0.069		
103	4417.68	1.677 ± 0.072		
104	4414.85	2.247 ± 0.086		
105	4410.13	0.666 ± 0.071		
106	4405.94	0.842 ± 0.067		
107	4402.80	2.384 ± 0.067		
108	4394.32	0.451 ± 0.067		
109	4390.98	1.265 ± 0.080		
110	4385.78	1.120 ± 0.066		
111	4373.09	2.040 ± 0.090		
112	4368.40	2.163 ± 0.084		
113	4361.60	0.580 ± 0.069		

TABLE 2—*Continued*

No.	λ_{obs}	W_λ (Å)	Identification	Possible I.D.
114	4338.28	0.916 ± 0.079		
115	4332.65	1.844 ± 0.095		
116	4325.61	3.402 ± 0.097		
117	4320.20	0.980 ± 0.080		N V λ1242 z =2.4754
118	4316.88	2.354 ± 0.074		
119	4311.47	1.428 ± 0.064		
120	4308.38	0.688 ± 0.064		
121	4303.74	0.517 ± 0.069	N V λ1238 z =2.4754	
122	4295.40	0.531 ± 0.076		
123	4287.86	1.835 ± 0.093		
124	4282.58	1.139 ± 0.085		
125	4276.25	3.452 ± 0.113		Al III λ1862 z =1.2941
126	4267.50	0.871 ± 0.087		
127	4262.49	0.949 ± 0.074		
128	4258.65	0.752 ± 0.066		
129	4254.98	0.502 ± 0.076	Al III λ1854 z =1.2941	
130	4251.93	0.785 ± 0.063		
131	4249.36	1.011 ± 0.074		
132	4238.99	2.431 ± 0.115		
133	4231.91	1.348 ± 0.084		
134	4224.74	6.159 ± 0.122	Lyα z =2.4754	
135	4217.89	0.940 ± 0.086		
		Q 0636+681 (Palomar)		
1	5092.93	0.514 ± 0.017	Si II λ1304 z =2.9054	
2	5084.09	0.292 ± 0.020	O I λ1302 z =2.9054	
3	5075.33	2.241 ± 0.019		
4	5062.33	0.131 ± 0.016		
5	5058.94	0.323 ± 0.019		
6	5055.04	0.213 ± 0.021		
7	5051.33	0.597 ± 0.016		
8	5033.37	2.153 ± 0.027		
9	5025.17	0.423 ± 0.019		
10	5022.73	0.391 ± 0.015		
11	5019.05	0.962 ± 0.019		
12	5014.97	0.631 ± 0.022		
13	5009.72	0.376 ± 0.025		
14	5004.95	1.551 ± 0.026		
15	4997.47	2.396 ± 0.029		
16	4991.38	2.171 ± 0.020		
17	4988.00	1.614 ± 0.021		
18	4983.77	2.573 ± 0.024		
19	4977.71	1.232 ± 0.028		N V λ1238 z =2.9054
20	4971.65	2.173 ± 0.025		
21	4966.65	2.214 ± 0.025		
22	4962.30	1.121 ± 0.021		
23	4959.09	0.369 ± 0.022		
24	4955.44	0.639 ± 0.027		
25	4949.54	0.585 ± 0.022		
26	4944.75	4.259 ± 0.026		
27	4938.93	0.403 ± 0.022		
28	4936.13	0.245 ± 0.023		
29	4921.28	1.082 ± 0.021	Si II λ1260 z =2.9054	

TABLE 2—*Continued*

No.	λ_{obs}	W_λ (Å)	Identification	Possible I.D.
			Q 0731+653	
1	4962.67	0.914 ± 0.154	C IV λ1550 z =2.2001	
2	4954.48	1.218 ± 0.179	C IV λ1548 z =2.2001	Al III λ1854 z =1.6605
3	4933.53	0.742 ± 0.149	Al III λ1854 z =1.6605	
4	4929.42	1.220 ± 0.118	Si II λ1260 z =2.9099	
5	4926.92	1.349 ± 0.098	Si II λ1260 z =2.9099	
6	4896.61	0.782 ± 0.077	Si II λ1260 z =2.8861	
7	4881.95	1.499 ± 0.093		
8	4872.69	1.340 ± 0.150		
9	4852.91	1.631 ± 0.155		
10	4815.53	2.274 ± 0.254		N V λ1238 z =2.8861
11	4805.59	1.359 ± 0.216		
12	4787.17	1.766 ± 0.260		
13	4784.43	1.621 ± 0.227		
14	4780.84	1.300 ± 0.248		
15	4776.11	1.769 ± 0.265		
16	4753.50	11.053 ± 0.520	Lyα z =2.9099	
17	4718.75	9.752 ± 0.514	Lyα z =2.8861 Si III λ1206 z =2.9099	Si IV λ1402 z =2.362
18	4694.23	3.393 ± 0.376	Si III λ1206 z =2.8861 N I λ1200 z =2.9099	
19	4671.40	2.492 ± 0.301		
20	4666.63	1.294 ± 0.257		N I λ1200 z =2.8861
21	4663.01	1.865 ± 0.314	Si II λ1193 z =2.9099	
22	4654.08	3.819 ± 0.395	Si II λ1193 z =2.8861 Si II λ1190 z =2.9099	
23	4635.27	1.382 ± 0.255		
24	4614.10	1.552 ± 0.200		
25	4608.33	7.838 ± 0.379		Si IV λ1402 z =2.277
26	4599.87	5.906 ± 0.347	Fe II λ2382 z =2.9315	
27	4593.71	2.094 ± 0.273		
28	4589.87	1.419 ± 0.223		
29	4587.05	2.118 ± 0.272		Fe II λ2374 z =0.9315
30	4581.39	1.746 ± 0.321		
31	4575.29	1.678 ± 0.265		
32	4569.86	1.507 ± 0.222		
33	4566.68	2.238 ± 0.283		Si IV λ1393 z =2.277
34	4561.29	4.034 ± 0.289		
35	4556.11	4.771 ± 0.316		
36	4550.42	2.451 ± 0.294		
37	4534.47	1.326 ± 0.256		
38	4530.74	2.276 ± 0.240		
39	4522.83	2.780 ± 0.283		
40	4518.20	3.456 ± 0.302		
41	4503.97	1.620 ± 0.242		
42	4493.63	2.371 ± 0.315		
43	4487.89	3.217 ± 0.327	C II λ1334 z =2.362 C II* λ1335 z =2.362	
44	4479.82	3.397 ± 0.338		
			Q 0831+128	
1	4557.99	1.333 ± 0.099		
2	4534.28	2.930 ± 0.113		
3	4527.73	1.583 ± 0.109		
4	4509.93	1.128 ± 0.117		C II λ1334 z =2.3808

TABLE 2—*Continued*

No.	λ_{obs}	W_λ (Å)	Identification	Possible I.D.
5	4505.88	2.691 ± 0.126		
6	4500.55	1.857 ± 0.099		
7	4492.20	0.858 ± 0.105		
8	4487.96	2.237 ± 0.121		
9	4483.60	1.097 ± 0.132		
10	4476.52	1.511 ± 0.089		
11	4474.00	2.959 ± 0.113		
12	4468.97	1.026 ± 0.125		
13	4463.83	0.945 ± 0.119		
14	4452.17	3.158 ± 0.156		
15	4446.82	1.316 ± 0.155		
16	4439.29	0.594 ± 0.118		
17	4425.49	2.152 ± 0.163		
18	4413.71	2.948 ± 0.171		
19	4406.00	0.985 ± 0.141		Si II λ1304 z =2.3808
20	4397.45	0.735 ± 0.124		
21	4388.75	1.110 ± 0.190		
22	4380.48	2.479 ± 0.177		
23	4365.27	3.472 ± 0.242		
24	4325.94	3.070 ± 0.182	Si IV λ1402 z =2.0844	
25	4312.77	1.476 ± 0.177		
26	4310.07	1.120 ± 0.153		
27	4299.39	2.142 ± 0.214	Si IV λ1393 z =2.0844	
28	4289.72	1.405 ± 0.169		
29	4281.70	1.103 ± 0.144		
30	4272.88	1.344 ± 0.184		
31	4269.77	0.844 ± 0.152		
32	4261.30	2.119 ± 0.203		Si II λ1260 z =2.3808
33	4241.86	1.116 ± 0.159		
34	4231.34	2.021 ± 0.189		
35	4224.32	1.246 ± 0.171		
36	4220.42	1.396 ± 0.144		
37	4217.70	1.639 ± 0.143		
38	4200.59	1.675 ± 0.211		
39	4190.30	0.945 ± 0.180		
40	4185.66	3.390 ± 0.181		
41	4168.89	2.286 ± 0.191		
42	4165.21	2.168 ± 0.168		
43	4160.87	1.681 ± 0.212		
44	4146.49	2.513 ± 0.232		
45	4141.93	1.091 ± 0.193		
46	4132.69	0.779 ± 0.147		
47	4116.14	1.391 ± 0.189	C II λ1334 z =2.0844	
48	4110.01	8.411 ± 0.261		Lyα z =2.3808
49	4074.71	1.272 ± 0.167		
50	4055.14	1.442 ± 0.170		
51	4052.86	0.944 ± 0.182		
52	4039.26	1.728 ± 0.225		
53	3999.37	4.426 ± 0.268		
54	3956.74	1.316 ± 0.173		
55	3944.90	2.137 ± 0.180		
56	3941.39	2.031 ± 0.161		
57	3936.48	1.626 ± 0.196		
58	3912.34	2.085 ± 0.189		
59	3901.82	2.139 ± 0.186		
60	3894.56	1.376 ± 0.195		
61	3887.70	2.800 ± 0.220	Si II λ1260 z =2.0844	
62	3879.71	2.474 ± 0.235		
63	3868.58	0.950 ± 0.152		
64	3865.26	1.264 ± 0.142		
65	3852.81	3.815 ± 0.213		

TABLE 2—*Continued*

No.	λ_{obs}	W_λ (Å)	Identification	Possible I.D.
66	3825.66	1.340 ± 0.162		
67	3819.80	0.902 ± 0.178	N V λ1238 z =2.0844	
68	3801.42	1.837 ± 0.203		
69	3797.64	1.569 ± 0.169		
70	3783.78	2.518 ± 0.272		
71	3774.70	2.828 ± 0.343		
72	3751.46	9.834 ± 0.403	Lyα z =2.0844	
			Q 0905+151	
1	5093.52	0.179 ± 0.033		
2	5082.20	0.162 ± 0.022		
3	5058.39	0.734 ± 0.032		
4	5049.88	0.565 ± 0.030		
5	5047.33	0.126 ± 0.023		
6	5044.32	0.400 ± 0.023		
7	5039.13	0.529 ± 0.038		
8	5031.99	0.455 ± 0.035		
9	5029.19	0.461 ± 0.038		
10	5025.37	1.428 ± 0.035		
11	5021.17	2.787 ± 0.049		
12	5012.38	3.731 ± 0.059		
13	5002.85	4.610 ± 0.077		
14	4998.05	2.292 ± 0.059		
15	4992.71	2.829 ± 0.079		
16	4986.67	3.441 ± 0.089		
17	4982.30	0.812 ± 0.064		
18	4980.20	0.530 ± 0.061		
19	4974.63	1.635 ± 0.087		
20	4967.20	2.889 ± 0.085		
21	4961.10	0.731 ± 0.064		
22	4957.95	0.682 ± 0.079		
23	4949.44	1.331 ± 0.101		
24	4943.80	5.293 ± 0.090		
25	4939.93	1.449 ± 0.085		
26	4935.20	0.784 ± 0.099		
27	4928.31	1.529 ± 0.095		
			Q 0913+072	
1	4616.01	4.315 ± 0.035		
2	4582.09	0.654 ± 0.033		
3	4577.60	1.841 ± 0.034	Si II λ1260 z =1.9994	
4	4573.59	4.601 ± 0.033		
5	4568.13	1.365 ± 0.033		
6	4565.88	0.650 ± 0.030		
7	4561.80	1.081 ± 0.042	Si II λ1260 z =2.6193	
8	4558.06	0.262 ± 0.036		
9	4545.47	1.316 ± 0.045		
10	4541.53	0.233 ± 0.044		
11	4538.39	0.391 ± 0.035		
12	4536.36	0.382 ± 0.034		
13	4534.47	1.172 ± 0.035		
14	4529.58	0.807 ± 0.049		C II λ1334 z =2.3938
15	4520.30	0.229 ± 0.044		
16	4516.27	0.607 ± 0.050		
17	4512.24	2.683 ± 0.060		

TABLE 2—*Continued*

No.	λ_{obs}	W_λ (Å)	Identification	Possible I.D.
18	4506.24	0.640 ± 0.051		
19	4503.06	0.473 ± 0.053		
20	4500.37	0.529 ± 0.045		
21	4498.25	0.274 ± 0.040		N V λ1242 z =2.6193
22	4495.10	2.240 ± 0.058		Si II λ1260 z =2.5663
23	4486.04	0.820 ± 0.064		N V λ1238 z =2.6193
24	4479.87	1.003 ± 0.060		
25	4472.23	0.389 ± 0.058		
26	4466.46	0.265 ± 0.050		
27	4463.22	0.702 ± 0.069		
28	4459.29	0.463 ± 0.057		
29	4453.61	1.129 ± 0.086		
30	4443.10	1.195 ± 0.074		
31	4438.66	1.246 ± 0.086		
32	4432.43	0.947 ± 0.087		N V λ1242 z =2.5663
33	4427.15	1.500 ± 0.084		
34	4399.82	28.506 ± 0.245	Lyα z =2.6193 Si IV λλ1393,1402 z =2.1451	N V λ1238 z =2.5663
35	4375.30	1.664 ± 0.081		
36	4370.80	1.327 ± 0.066		
37	4369.40	0.498 ± 0.036		
38	4367.96	0.981 ± 0.046		
39	4366.34	1.302 ± 0.061	Si III λ1206 z =2.6193	
40	4363.41	0.599 ± 0.071		
41	4359.49	0.641 ± 0.117		
42	4349.57	0.767 ± 0.077		
43	4345.89	0.617 ± 0.086		
44	4342.76	0.526 ± 0.070	N I λ1200 z =2.6193	
45	4335.47	5.840 ± 0.128		Lyα z =2.5663
46	4320.52	1.329 ± 0.130	Si II λ1193 z =2.6193	
47	4313.22	1.211 ± 0.086		
48	4306.79	0.623 ± 0.093	Si II λ1190 z =2.6193	
49	4300.75	0.452 ± 0.073		Si III λ1206 z =2.5663
50	4296.30	4.648 ± 0.106	Si IV λ1402 z =2.0633	
51	4289.69	4.422 ± 0.112		
52	4283.24	0.669 ± 0.071		
53	4280.79	1.230 ± 0.081		
54	4269.13	1.412 ± 0.107	Si IV λ1402 z =2.0433 Si IV λ1393 z =2.063	
55	4265.44	0.599 ± 0.092		
56	4254.48	0.721 ± 0.101		Si II λ1193 z =2.5663
57	4250.16	0.591 ± 0.095		
58	4247.96	0.579 ± 0.086		
59	4245.83	0.808 ± 0.095		
60	4240.60	2.148 ± 0.106	Si IV λ1393 z =2.0433	
61	4237.54	1.474 ± 0.094		
62	4230.65	0.990 ± 0.104		
63	4203.49	0.660 ± 0.096		N V λ1238 z =2.3938
64	4200.75	1.907 ± 0.106		C II* λ1335 z =2.1451
65	4192.17	0.875 ± 0.097		
66	4186.92	0.909 ± 0.124		
67	4171.44	2.951 ± 0.148		
68	4164.31	1.469 ± 0.123		
69	4156.08	0.612 ± 0.112		
70	4137.76	1.044 ± 0.132		
71	4134.15	0.691 ± 0.097		
72	4131.27	0.961 ± 0.086		
73	4125.76	5.299 ± 0.126		Lyα z =2.3938
74	4120.69	1.588 ± 0.085		
75	4115.07	0.717 ± 0.070		
76	4108.51	1.961 ± 0.088		

TABLE 2—*Continued*

No.	λ_{obs}	W_λ (Å)	Identification	Possible I.D.
77	4102.94	0.939 ± 0.083		Si II λ1304 z =2.1451
78	4098.73	0.418 ± 0.074		
79	4095.13	0.472 ± 0.090	O I λ1302 z =2.145	Si III λ1206 z =2.3938
80	4080.56	2.220 ± 0.099		
81	4073.56	0.373 ± 0.065		
82	4071.05	1.394 ± 0.077		
83	4066.84	0.699 ± 0.072		
84	4061.22	0.979 ± 0.089	C II λ1334 z =2.0433	
85	4055.78	0.445 ± 0.068		
86	4052.79	0.535 ± 0.069		
87	4042.75	0.354 ± 0.063		
88	4040.16	0.420 ± 0.071		
89	4025.98	2.032 ± 0.076		
90	4022.13	0.578 ± 0.076		
91	4015.94	2.071 ± 0.098		
92	4003.27	1.104 ± 0.070		
93	4001.52	0.943 ± 0.068	C II λ1334 z =1.9994	
94	3997.32	2.670 ± 0.113		Si II λ1304 z =2.0633
95	3959.30	0.718 ± 0.094		
96	3908.12	0.399 ± 0.080	N V λ1242 z =2.1351	
97	3898.92	0.574 ± 0.050		
98	3895.29	3.189 ± 0.073		N V λ1238 z =2.1451
99	3887.36	0.571 ± 0.053		
100	3885.26	0.566 ± 0.059		
101	3877.90	0.978 ± 0.067		
102	3866.88	2.015 ± 0.082		
103	3862.68	1.713 ± 0.065		
104	3858.97	2.306 ± 0.078		
105	3842.76	0.557 ± 0.078		
106	3835.77	0.947 ± 0.087	Si II λ1260 z =2.0433	
107	3829.10	0.715 ± 0.082		
108	3823.26	3.515 ± 0.118	Lyα z =2.1451	
109	3815.99	0.886 ± 0.094		
110	3806.91	2.219 ± 0.125		N V λ1242 z =2.0633
111	3798.85	0.817 ± 0.134		
112	3792.84	1.265 ± 0.112	N V λ1238 z =2.0633 Si III λ1206 z =2.1451	
113	3780.11	0.591 ± 0.092	Si II λ1260 z =1.9994	N V λ1242 z =2.043
114	3773.39	1.058 ± 0.123		N V λ1238 z =2.043 N I λ1200 z =2.1451
115	3769.08	0.764 ± 0.095		
116	3755.62	1.253 ± 0.108	O VI λ1037 z =2.6193	
117	3750.47	0.565 ± 0.102	C II λ1036 z =2.6193	
118	3734.25	2.476 ± 0.116	O VI λ1031 z =2.6193	
119	3727.50	1.143 ± 0.104		N V λ1242 z =1.9994
			Q 0938+119	
1	5099.95	0.175 ± 0.019		
2	5094.48	0.138 ± 0.018		
3	5090.17	1.905 ± 0.026		C IV λ1548 z =2.879
4	5078.69	1.779 ± 0.030		
5	5075.62	0.722 ± 0.033		
6	5070.36	0.728 ± 0.043		
7	5067.10	0.617 ± 0.043		
8	5053.53	3.417 ± 0.067		
9	5046.23	3.183 ± 0.071		
10	5035.23	1.273 ± 0.064		
11	5019.31	1.618 ± 0.092		Si II λ1526 z =2.2879

TABLE 2—*Continued*

No.	λ_{obs}	W_λ (Å)	Identification	Possible I.D.
12	5015.76	0.633 ± 0.071		
13	5010.70	1.034 ± 0.059		
14	5009.17	0.335 ± 0.050		
15	5000.66	1.275 ± 0.091		
16	4996.99	1.486 ± 0.106		
17	4987.30	0.986 ± 0.118		Si II λ1808 z =1.75938
18	4977.26	2.076 ± 0.135		
19	4960.98	1.260 ± 0.118		
20	4956.64	2.433 ± 0.148		
21	4945.53	3.487 ± 0.148		
22	4940.59	1.762 ± 0.117		
23	4937.53	1.057 ± 0.143		
24	4932.66	2.317 ± 0.142		
			Q 1033+137	
1	5109.54	0.429 ± 0.053		
2	5006.46	0.318 ± 0.037		
3	4997.82	0.561 ± 0.035		
4	4995.15	0.330 ± 0.038		
5	4982.91	0.183 ± 0.029		
6	4978.45	1.062 ± 0.024		
7	4970.79	0.099 ± 0.020		
8	4966.50	0.142 ± 0.028		
9	4962.71	0.226 ± 0.025		
10	4960.11	0.381 ± 0.031		
11	4953.34	5.412 ± 0.045		
12	4947.71	1.203 ± 0.035		
13	4945.84	0.851 ± 0.031		
14	4937.46	1.565 ± 0.054		
15	4929.69	0.788 ± 0.046		
16	4922.75	2.579 ± 0.048		
17	4919.41	2.060 ± 0.050		
			Q 1206+115	
1	5183.96	0.356 ± 0.033		
2	5145.51	0.310 ± 0.035		Mg II λ2803 z =0.8355
3	5132.89	0.765 ± 0.036	Si II λ1526 z =2.3639	Mg II λ2796 z =0.8355
4	5069.43	3.399 ± 0.028	Si II λ1260 z =3.0222	
5	5054.54	0.225 ± 0.023		
6	5043.53	0.111 ± 0.017		
7	5012.01	2.762 ± 0.026	Si IV λ1402 z =2.5725	
8	5001.81	0.321 ± 0.022		
9	4997.65	0.395 ± 0.022	N V λ1242 z =3.0222	
10	4989.60	1.804 ± 0.022		
11	4983.99	0.704 ± 0.018	N V λ1238 z =3.0222	
12	4979.95	2.302 ± 0.022	Si IV λ1393 z =2.5725	
13	4964.49	0.571 ± 0.024		
14	4953.36	2.594 ± 0.032	N V λ1242 z =2.9871	
15	4946.14	2.617 ± 0.029		
16	4940.39	1.566 ± 0.028	N V λ1238 z =2.9871	
17	4912.63	0.555 ± 0.040		
18	4901.27	8.152 ± 0.044	Lyα z =3.0272	
19	4890.20	11.666 ± 0.059	Lyα z =3.0222	
20	4876.79	1.653 ± 0.049		
21	4860.36	4.757 ± 0.052		

TABLE 2—*Continued*

No.	λ_{obs}	W_λ (Å)	Identification	Possible I.D.
22	4852.94	3.374 ± 0.038	Si III λ1206 z =3.0222	
23	4846.72	5.831 ± 0.057	Lyα z =2.9871	
24	4833.05	1.677 ± 0.049		
25	4827.25	1.045 ± 0.057	N I λ1200 z =3.0222	
26	4822.25	0.905 ± 0.051		
27	4809.39	2.117 ± 0.056	Si II λ1193 z =3.0272	
			Si III λ1206 z =2.9871	
28	4804.70	2.144 ± 0.045		
29	4799.67	2.117 ± 0.041	Si II λ1193 z =3.0222	
			Si II λ1190 z =3.0272	
30	4795.72	0.967 ± 0.034		
31	4793.63	0.389 ± 0.043		
32	4788.12	1.869 ± 0.048	Si II λ1190 z =3.0222	N I λ1200 z =2.9871
33	4759.31	1.674 ± 0.070		Si II λ1193 z =2.9871
34	4747.79	1.668 ± 0.067		
35	4741.42	0.536 ± 0.054		
36	4732.41	1.475 ± 0.072		
37	4727.62	0.617 ± 0.045		
38	4722.09	3.471 ± 0.068		
39	4716.37	0.728 ± 0.053	Si IV λ1402 z =2.3639	
40	4709.95	0.928 ± 0.053		
41	4700.77	3.108 ± 0.068		
42	4687.15	2.248 ± 0.059	Si IV λ1393 z =2.3639	
43	4681.66	0.794 ± 0.054		
44	4669.25	3.801 ± 0.095		
45	4662.61	2.558 ± 0.064		
46	4654.56	0.920 ± 0.072		
47	4648.56	1.439 ± 0.083		
48	4633.93	5.286 ± 0.089		
49	4624.24	2.085 ± 0.071		
50	4614.41	1.558 ± 0.064		
51	4610.62	1.922 ± 0.059		
52	4606.44	2.217 ± 0.075		
		Q 1208+101		
1	6069.15	2.061 ± 0.088	C IV λ1550 z =2.9137	C II* λ1335 z =3.5440
2	6058.93	2.997 ± 0.092	C IV λ1548 z =2.9137	C II λ1334 z =3.5440
3	5989.83	1.585 ± 0.068	C IV λ1550 z =2.8606	
4	5984.98	0.894 ± 0.047	C IV λ1550 z =2.8593	
5	5980.17	1.677 ± 0.055	C IV λ1550 z =2.8573	
			C IV λ1548 z =2.8606	
6	5974.61	0.451 ± 0.047	Si II λ1526 z =2.9137	
			C IV λ1548 z =2.8593	
7	5969.81	1.441 ± 0.057	C IV λ1548 z =2.8573	
8	5858.57	1.341 ± 0.045		
9	5854.54	1.332 ± 0.043		
10	5840.73	4.380 ± 0.066		
11	5832.30	2.367 ± 0.045		
12	5826.94	1.673 ± 0.043		
13	5821.63	1.452 ± 0.052		
14	5815.02	0.986 ± 0.051		
15	5804.26	3.263 ± 0.077		
16	5785.63	5.380 ± 0.093		
17	5762.19	2.698 ± 0.090		
18	5753.85	1.422 ± 0.071		
19	5740.51	5.444 ± 0.104		
20	5725.17	1.850 ± 0.078		Si II λ1260 z =3.5440
21	5715.56	1.638 ± 0.093		Si II λ1260 z =3.5368

TABLE 2—*Continued*

No.	λ_{obs}	W_λ (Å)	Identification	Possible I.D.
22	5697.33	1.289 ± 0.112		
23	5688.23	3.763 ± 0.139		
24	5679.83	1.608 ± 0.084		
25	5670.44	4.126 ± 0.127		
26	5662.61	1.245 ± 0.073		
27	5655.42	4.761 ± 0.111		
28	5646.10	0.907 ± 0.078		N V λ1242 z =3.5440
29	5631.90	6.167 ± 0.117		
30	5625.13	5.398 ± 0.105		N V λ1238 z =3.5440
31	5606.72	4.554 ± 0.135	C II λ1334 z =3.1985	C II* λ1335 z =3.1985
32	5591.09	1.591 ± 0.101		
33	5586.46	1.524 ± 0.093		
34	5575.95	3.540 ± 0.256		
35	5570.71	3.785 ± 0.088		
36	5566.58	2.141 ± 0.099		
37	5559.18	0.792 ± 0.092		
38	5551.45	1.555 ± 0.093		
39	5545.37	6.704 ± 0.132		
40	5537.83	0.786 ± 0.100		
41	5531.50	2.406 ± 0.107		
42	5524.04	8.681 ± 0.144		Lyα z =3.5440
43	5515.26	7.223 ± 0.131		Lyα z =3.5368
44	5508.80	3.402 ± 0.118		
45	5503.02	1.693 ± 0.116		
46	5494.39	3.480 ± 0.111	Si IV λ1402 z =2.9137	
47	5490.31	2.311 ± 0.106	Si IV λ1402 z =2.9137	
48	5484.84	2.785 ± 0.122		
49	5480.01	2.440 ± 0.111		
			Q 1215+333	
1	4578.08	0.892 ± 0.081	Si II λ1526 z =1.9988	
2	4526.84	0.660 ± 0.063		
3	4413.66	0.567 ± 0.046		
4	4374.95	0.407 ± 0.032		
5	4368.92	0.770 ± 0.037		
6	4363.18	3.680 ± 0.053		
7	4358.46	0.525 ± 0.047		
8	4347.96	2.423 ± 0.060		
9	4329.17	0.837 ± 0.052		
10	4322.09	0.803 ± 0.060		
11	4310.84	0.350 ± 0.047		
12	4289.08	1.383 ± 0.068		
13	4284.03	2.771 ± 0.078		
14	4279.23	2.751 ± 0.099		
15	4267.61	1.559 ± 0.074		
16	4259.75	1.191 ± 0.093		
17	4237.21	0.326 ± 0.058		
18	4234.72	1.793 ± 0.054		
19	4231.86	3.096 ± 0.070		
20	4227.30	0.284 ± 0.045		
21	4224.93	1.414 ± 0.046		
22	4223.00	1.770 ± 0.055		
23	4220.22	0.637 ± 0.049		
24	4218.05	1.981 ± 0.057		
25	4212.83	4.581 ± 0.098		
26	4206.54	0.884 ± 0.073		Si IV λ1402 z =1.9988
27	4201.22	2.658 ± 0.089		
28	4195.69	3.008 ± 0.081		

TABLE 2—*Continued*

No.	λ_{obs}	W_λ (Å)	Identification	Possible I.D.
29	4189.63	0.612 ± 0.073		
30	4158.36	4.002 ± 0.092		
31	4154.59	0.637 ± 0.071		
32	4136.79	0.418 ± 0.082		
33	4124.77	2.686 ± 0.093		
34	4120.65	0.458 ± 0.085		
35	4109.18	0.661 ± 0.081		
36	4104.63	1.025 ± 0.070		
37	4102.66	0.612 ± 0.047		
38	4100.96	1.085 ± 0.069		
39	4096.17	2.275 ± 0.105		
40	4088.17	3.033 ± 0.120		
41	4060.92	1.243 ± 0.077		
42	4054.15	0.913 ± 0.068		
43	4052.21	0.519 ± 0.065		
44	4048.80	1.218 ± 0.079		
45	4046.36	0.732 ± 0.089		
46	4034.12	0.948 ± 0.091		
47	4023.19	2.106 ± 0.112		
48	4016.31	0.496 ± 0.078		
49	4012.76	0.581 ± 0.088		
50	4008.71	2.008 ± 0.105		
51	4001.96	1.424 ± 0.110	C II λ1334 z =1.9988	
52	3974.10	0.841 ± 0.071		
53	3967.56	0.757 ± 0.082		
54	3963.50	0.613 ± 0.068		
55	3959.63	2.241 ± 0.085		
56	3950.86	0.700 ± 0.089		
57	3941.35	1.518 ± 0.095		
58	3933.47	0.888 ± 0.073		
59	3930.70	0.339 ± 0.066		
60	3911.94	0.607 ± 0.076	Si II λ1304 z =1.9988	
61	3905.32	0.929 ± 0.083	O I λ1302 z =1.9988	
62	3894.65	1.026 ± 0.093		
63	3888.67	0.809 ± 0.087		
64	3880.02	0.464 ± 0.064		
65	3873.05	1.490 ± 0.079		
66	3867.39	0.695 ± 0.072		
67	3864.80	0.579 ± 0.071		
68	3849.53	0.414 ± 0.074		
69	3832.30	0.856 ± 0.080		
70	3808.60	0.480 ± 0.084		
71	3804.74	0.927 ± 0.091		
72	3800.57	0.713 ± 0.085		
73	3782.60	1.176 ± 0.104		
74	3779.49	1.399 ± 0.083	Si II λ1260 z =1.9988	
75	3776.35	1.708 ± 0.102		
76	3758.12	1.385 ± 0.108		
77	3732.45	0.679 ± 0.061		
78	3729.24	0.593 ± 0.086		
79	3719.35	1.601 ± 0.083		
80	3710.08	2.674 ± 0.108		
81	3705.51	1.817 ± 0.083		
82	3700.75	2.782 ± 0.108		
83	3683.56	2.262 ± 0.143		
84	3671.60	1.157 ± 0.229		

TABLE 2—*Continued*

No.	λ_{obs}	W_λ (Å)	Identification	Possible I.D.
		Q 1334-005		
1	4609.33	0.368 ± 0.031		
2	4605.46	0.505 ± 0.041		
3	4596.99	1.191 ± 0.038		
4	4594.80	0.420 ± 0.029		
5	4591.59	0.482 ± 0.036		
6	4584.75	1.560 ± 0.051		
7	4581.94	1.359 ± 0.027		
8	4579.41	1.411 ± 0.044		
9	4567.30	5.451 ± 0.067		
10	4557.77	0.867 ± 0.047		
11	4552.67	0.799 ± 0.040		
12	4549.86	0.231 ± 0.036		
13	4548.17	0.303 ± 0.036		
14	4540.95	0.687 ± 0.043		
15	4532.94	0.687 ± 0.044		
16	4519.57	0.380 ± 0.061		
17	4514.58	0.718 ± 0.057		
18	4510.42	0.436 ± 0.067		
19	4494.22	0.703 ± 0.053		
20	4490.13	0.600 ± 0.063		
21	4468.97	0.274 ± 0.049		
22	4465.03	3.683 ± 0.060		
23	4460.63	0.907 ± 0.044		
24	4458.95	1.307 ± 0.034		
25	4457.27	1.134 ± 0.037		
26	4454.14	0.617 ± 0.056		
27	4439.97	1.061 ± 0.052		
28	4437.33	0.793 ± 0.049		
29	4435.42	1.013 ± 0.046		
30	4429.11	0.417 ± 0.055		
31	4425.73	1.194 ± 0.058		
32	4423.29	0.756 ± 0.053		
33	4415.00	0.724 ± 0.062		
34	4407.43	1.518 ± 0.075		
35	4391.27	0.714 ± 0.065		
36	4386.59	0.560 ± 0.068		
37	4374.41	0.450 ± 0.052		
38	4369.57	1.150 ± 0.061		
39	4366.15	1.335 ± 0.058		
40	4359.38	1.883 ± 0.104		
41	4354.14	0.756 ± 0.059		
42	4351.57	1.538 ± 0.047		
43	4349.63	0.606 ± 0.042		
44	4346.74	1.064 ± 0.057		
45	4340.36	1.017 ± 0.058		
46	4324.67	1.108 ± 0.058		
47	4321.41	1.447 ± 0.055		
48	4318.42	0.398 ± 0.053		
49	4315.83	0.331 ± 0.062		
50	4305.68	0.348 ± 0.049		
51	4293.34	2.706 ± 0.067		
52	4289.65	1.066 ± 0.051		
53	4286.51	2.006 ± 0.047		
54	4283.45	0.291 ± 0.057		
55	4276.95	1.615 ± 0.056		
56	4274.26	0.326 ± 0.051		
57	4264.45	2.194 ± 0.067		
58	4243.39	0.371 ± 0.067		

TABLE 2—*Continued*

No.	λ_{obs}	W_λ (Å)	Identification	Possible I.D.
59	4234.26	0.985 ± 0.059		
60	4219.58	1.069 ± 0.055		
61	4217.17	0.921 ± 0.051		
62	4211.65	0.902 ± 0.056		
63	4203.45	0.807 ± 0.079		
64	4196.87	0.423 ± 0.060		
65	4183.03	0.627 ± 0.057		
66	4181.00	1.525 ± 0.054		
67	4176.05	1.455 ± 0.071		
68	4172.93	1.008 ± 0.058		
69	4165.38	0.610 ± 0.063		
70	4162.29	0.908 ± 0.063		
71	4160.29	0.746 ± 0.046		
72	4140.61	0.274 ± 0.048		
73	4131.43	1.373 ± 0.068		
74	4126.60	2.330 ± 0.070		
75	4121.91	0.990 ± 0.069		
76	4116.73	1.004 ± 0.071		
77	4111.74	0.440 ± 0.055		
78	4107.85	3.077 ± 0.072		
79	4102.39	0.765 ± 0.059		
80	4087.91	1.893 ± 0.074		
81	4077.34	0.491 ± 0.068		
82	4073.73	1.326 ± 0.060		
83	4071.60	1.047 ± 0.049		
84	4058.38	0.841 ± 0.066		
85	4052.14	1.053 ± 0.065		
86	4046.99	0.554 ± 0.079		
87	4018.63	0.443 ± 0.071		
88	4007.79	0.737 ± 0.075		
89	4000.71	0.765 ± 0.070		
90	3988.83	0.707 ± 0.062		
91	3971.73	0.975 ± 0.101		
92	3963.76	0.925 ± 0.059		
93	3928.99	1.212 ± 0.061		
94	3920.09	0.676 ± 0.058		
95	3900.08	1.452 ± 0.070		
96	3891.98	3.737 ± 0.082		
97	3876.98	1.347 ± 0.058		
98	3875.25	0.640 ± 0.050		
99	3866.90	0.412 ± 0.069		
100	3861.85	2.190 ± 0.096		
101	3853.62	2.792 ± 0.105		
102	3836.37	0.536 ± 0.087		
103	3809.81	0.440 ± 0.075		
104	3801.04	0.408 ± 0.064		
105	3798.53	1.162 ± 0.083		
106	3771.24	1.685 ± 0.091		
107	3767.30	1.895 ± 0.080		
108	3764.53	1.082 ± 0.060		
109	3761.92	1.149 ± 0.072		
110	3755.52	1.882 ± 0.091		
111	3751.98	0.882 ± 0.083		
112	3745.81	0.970 ± 0.077		
113	3743.04	1.732 ± 0.087		
114	3734.67	0.754 ± 0.091		
115	3719.92	0.760 ± 0.103		
116	3706.20	0.689 ± 0.094		
117	3701.85	0.467 ± 0.083		

TABLE 2—*Continued*

No.	λ_{obs}	W_λ (Å)	Identification	Possible I.D.
		Q 1400+114		
1	5102.82	0.776 ± 0.087		
2	5095.42	0.365 ± 0.060		
3	5092.13	0.358 ± 0.060		
4	5071.96	0.867 ± 0.051		
5	5069.79	1.267 ± 0.046		
6	5067.41	1.838 ± 0.060		
7	5059.62	1.731 ± 0.065		
8	5045.30	0.392 ± 0.070		
9	5036.00	1.335 ± 0.070		
10	5033.57	0.464 ± 0.053		
11	5029.28	4.124 ± 0.110		
12	5021.78	0.784 ± 0.071		
13	5018.27	2.641 ± 0.082		
14	5010.89	0.995 ± 0.086		
15	5006.75	1.076 ± 0.054		
16	5004.96	1.396 ± 0.050		
17	5002.84	1.219 ± 0.080		
18	4995.82	1.492 ± 0.076		
19	4993.44	1.378 ± 0.061		
20	4990.93	2.551 ± 0.072		
21	4988.62	1.043 ± 0.073		
22	4981.06	0.638 ± 0.079		
23	4979.20	1.213 ± 0.082		
24	4977.09	0.811 ± 0.094		
25	4974.43	0.752 ± 0.089		
26	4968.03	0.450 ± 0.083		
27	4965.88	0.631 ± 0.099		
28	4960.96	0.544 ± 0.092		
29	4956.74	2.072 ± 0.103		
30	4953.67	3.096 ± 0.094		
31	4950.90	2.084 ± 0.100		
32	4947.58	1.608 ± 0.094		
33	4945.08	1.547 ± 0.106		
34	4942.17	0.588 ± 0.106		
35	4932.50	0.966 ± 0.105		
36	4930.71	0.741 ± 0.085		
37	4928.90	1.541 ± 0.116		
38	4925.76	1.134 ± 0.133		
39	4922.65	0.604 ± 0.098		
40	4920.35	0.582 ± 0.082		
		Q 1402+044		
1	5109.38	0.953 ± 0.026		
2	5106.26	0.371 ± 0.030		
3	5090.42	0.452 ± 0.034		
4	5086.01	1.632 ± 0.065		
5	5065.71	1.541 ± 0.076		
6	5060.43	0.475 ± 0.062		
7	5048.64	0.695 ± 0.085		
8	5031.26	0.479 ± 0.073		
9	5028.09	0.675 ± 0.071		
10	5024.44	0.913 ± 0.103		
11	5017.94	1.100 ± 0.087		
12	5011.80	2.029 ± 0.118		
13	5001.20	1.140 ± 0.113		

TABLE 2—*Continued*

No.	λ_{obs}	W_λ (Å)	Identification	Possible I.D.
14	4986.14	1.521 ± 0.166		
15	4980.49	1.765 ± 0.141		
16	4976.82	0.600 ± 0.091		
17	4973.52	1.318 ± 0.124		
18	4968.98	2.099 ± 0.135		
19	4947.01	0.980 ± 0.123		
20	4936.90	0.697 ± 0.123		
		Q 1410+096		
1	5315.16	0.950 ± 0.023		
2	5300.23	1.300 ± 0.032		
3	5285.23	0.809 ± 0.022		
4	5279.48	0.635 ± 0.024		
5	5270.61	0.183 ± 0.017		
6	5259.65	0.925 ± 0.022		
7	5250.11	1.129 ± 0.016		
8	5244.97	0.973 ± 0.018		
9	5238.75	0.188 ± 0.016		
10	5233.11	0.803 ± 0.020		
11	5224.52	0.221 ± 0.019		
12	5219.33	1.481 ± 0.014		
13	5215.19	0.573 ± 0.018		
14	5208.82	1.184 ± 0.022		
15	5203.31	0.706 ± 0.015		
16	5200.37	0.789 ± 0.014		
17	5196.85	0.974 ± 0.019		
18	5181.05	4.081 ± 0.024		
19	5171.16	2.307 ± 0.023		
20	5162.99	1.511 ± 0.028		
21	5153.11	1.686 ± 0.022		
22	5147.35	2.039 ± 0.027		
23	5131.27	4.257 ± 0.035		
24	5097.38	0.495 ± 0.028		
25	5087.53	1.521 ± 0.032		
26	5080.45	1.498 ± 0.026		
27	5074.28	3.309 ± 0.028		
28	5067.92	0.376 ± 0.028		
29	5059.13	0.353 ± 0.029		
30	5048.08	0.848 ± 0.033		
31	5037.00	4.150 ± 0.031		
32	5029.54	2.214 ± 0.036		
33	5017.03	0.868 ± 0.037		
34	5011.69	0.423 ± 0.035		
35	4987.78	1.651 ± 0.037		
36	4973.36	0.406 ± 0.028		
37	4957.31	1.201 ± 0.034		
38	4952.42	0.766 ± 0.030		
39	4948.22	0.626 ± 0.031		
40	4941.40	0.190 ± 0.023		
41	4933.02	0.453 ± 0.027		
42	4919.71	0.992 ± 0.042		
43	4914.18	0.320 ± 0.025		
		Q 1442+101 (1)		
1	5526.24	2.676 ± 0.046	C IV λ1550 z =2.565	

TABLE 2—*Continued*

No.	λ_{obs}	W_λ (Å)	Identification	Possible I.D.
2	5516.95	3.151 ± 0.045	C IV λ1548 z =2.565	
3	5501.29	1.735 ± 0.041		
4	5486.31	0.954 ± 0.040	C II λ1334 z =3.1102	Si II λ1260 z =3.3534
5	5482.00	0.563 ± 0.043		
6	5477.78	0.320 ± 0.047		
7	5471.86	1.731 ± 0.048		
8	5467.64	0.279 ± 0.042		
9	5460.71	1.042 ± 0.066		
10	5453.01	2.855 ± 0.059		
11	5448.38	0.204 ± 0.040		
12	5440.32	1.055 ± 0.058	Si II λ1526 z =2.565	
13	5433.95	0.917 ± 0.049		
14	5430.31	0.958 ± 0.049		
15	5423.63	0.785 ± 0.047		
16	5419.95	1.469 ± 0.038		
17	5415.41	0.432 ± 0.046		
18	5407.97	2.006 ± 0.035		
19	5404.69	1.402 ± 0.040		C II* λ1335 z =3.0474
20	5399.10	2.857 ± 0.064	C II λ1334 z =3.0474	
21	5387.57	1.703 ± 0.058		
22	5372.67	3.705 ± 0.091		
23	5363.73	0.589 ± 0.054		
24	5360.85	0.430 ± 0.041	Si II λ1304 z =3.1102	
25	5358.28	1.191 ± 0.051		
26	5353.90	1.749 ± 0.052	O I λ1302 z =3.1102	
27	5349.86	0.554 ± 0.046		
28	5344.25	1.411 ± 0.055		
29	5339.16	3.364 ± 0.061		
30	5332.24	0.537 ± 0.066		
31	5323.06	0.515 ± 0.058		
32	5315.81	1.280 ± 0.058		
33	5311.58	3.508 ± 0.063		
34	5302.70	4.022 ± 0.076		
35	5292.38	6.580 ± 0.067		Al II λ1670 z =2.1712 Lyα z =3.35346
36	5286.90	1.408 ± 0.042		
37	5284.28	1.560 ± 0.040		
38	5279.46	3.895 ± 0.067		Si II λ1304 z =3.0474
39	5269.30	4.825 ± 0.077	O I λ1302 z =3.0474	
40	5263.07	0.318 ± 0.052		
41	5256.51	1.712 ± 0.082		
42	5250.29	2.287 ± 0.070		Si III λ1206 z =3.3534
43	5242.18	2.355 ± 0.066		
44	5236.81	1.592 ± 0.050		
45	5234.04	1.242 ± 0.058		
46	5223.45	2.523 ± 0.075		N I λ1200 z =3.3534
47	5217.19	0.457 ± 0.059		
48	5213.60	0.617 ± 0.064		
49	5202.05	0.070 ± 0.064		
50	5196.23	1.242 ± 0.070		
51	5189.40	4.561 ± 0.067		
52	5183.87	1.388 ± 0.062	Si II λ1206 z =3.1102	
53	5176.44	0.924 ± 0.050		
54	5172.05	1.298 ± 0.058		Fe II λ2600 z =0.9893 Si II λ1193 z =3.35346
55	5167.98	3.762 ± 0.062		
56	5158.56	0.462 ± 0.055		
57	5155.78	1.521 ± 0.065		
58	5150.92	0.824 ± 0.059		
59	5146.45	0.765 ± 0.052		Fe II λ2586 z =0.9893 Si II λ1190 z =3.3534

TABLE 2—*Continued*

No.	λ_{obs}	W_λ (Å)	Identification	Possible I.D.
60	5143.23	1.868 ± 0.049		
61	5140.57	2.329 ± 0.044		
62	5137.09	1.181 ± 0.049		
63	5134.59	0.242 ± 0.043		
			Q 1442+101 (2)	
1	5143.44	1.577 ± 0.037		
2	5140.74	2.700 ± 0.038		
3	5137.14	1.398 ± 0.039		
4	5134.25	0.499 ± 0.048		
5	5130.69	0.953 ± 0.049		
6	5126.52	3.316 ± 0.068		
7	5119.14	0.911 ± 0.063		
8	5112.02	1.253 ± 0.056		
9	5108.78	0.319 ± 0.054		N V λ1242 z =3.1102
10	5102.81	1.667 ± 0.067		Si II λ1206 z =3.0474
11	5094.89	2.176 ± 0.075		N V λ1238 z =3.1102
12	5079.91	1.420 ± 0.089		
13	5074.21	0.277 ± 0.049		
14	5066.64	3.474 ± 0.059	Si IV λ1393 z =2.6336	
15	5062.08	0.613 ± 0.046		
16	5055.79	2.708 ± 0.079		
17	5047.60	2.791 ± 0.049		
18	5042.58	2.776 ± 0.071		
19	5033.35	3.707 ± 0.062		
20	5027.85	1.335 ± 0.045		N V λ1242 z =3.0474
21	5023.75	1.290 ± 0.056		
22	5018.70	1.565 ± 0.071		
23	5008.70	0.655 ± 0.069		
24	5003.76	0.966 ± 0.054		
25	4998.02	3.901 ± 0.061	Lyα z =3.1102	Si IV λ1402 z =2.565
26	4989.68	4.129 ± 0.061		
27	4984.08	1.755 ± 0.044		
28	4978.99	5.888 ± 0.054		
29	4972.62	3.111 ± 0.035		
30	4967.19	3.068 ± 0.078		Si IV λ1393 z =2.565
31	4957.72	0.971 ± 0.075	Si III λ1206 z =3.1102	
32	4947.31	2.392 ± 0.053		
33	4943.53	1.184 ± 0.034		
34	4940.28	2.573 ± 0.056		
35	4925.65	1.620 ± 0.067		
36	4918.89	6.296 ± 0.070	Lyα z =3.0474	
37	4910.87	0.392 ± 0.058		
38	4906.02	1.604 ± 0.059	Si II λ1193 z =3.1102	
39	4901.22	1.124 ± 0.053		
40	4896.73	2.772 ± 0.060	Si II λ1190 z =3.1102	
41	4873.87	0.352 ± 0.054		
42	4868.99	1.554 ± 0.075		
43	4860.69	2.225 ± 0.059		
44	4852.93	3.905 ± 0.069		C II λ1334 z =2.6336
45	4846.33	2.282 ± 0.071		
46	4839.90	1.701 ± 0.059		Fe II λ1608 z =2.1712
47	4835.92	0.544 ± 0.053		
48	4832.51	0.329 ± 0.060		
49	4825.67	1.104 ± 0.058		
50	4814.38	0.744 ± 0.065		
51	4809.70	1.047 ± 0.062		
52	4805.34	0.573 ± 0.057		

TABLE 2—*Continued*

No.	λ_{obs}	W_λ (Å)	Identification	Possible I.D.
53	4795.70	0.309 ± 0.054		
54	4791.06	2.941 ± 0.048		
55	4787.70	1.223 ± 0.046		
56	4783.74	2.337 ± 0.047		
57	4779.00	3.314 ± 0.055		
58	4773.21	1.220 ± 0.046		
59	4769.61	1.813 ± 0.052		
60	4765.96	0.942 ± 0.049		
61	4761.65	2.574 ± 0.051		C II* λ1335 z =2.565
62	4757.74	0.455 ± 0.047	C II λ1334 z =2.565	
63	4753.56	3.278 ± 0.064		
64	4743.44	1.613 ± 0.071		Si II λ1304 z =2.6336 Fe II λ2382 z =0.9893
65	4736.95	0.487 ± 0.053		
66	4730.24	1.227 ± 0.086		O I λ1302 z =2.6336
67	4722.20	0.696 ± 0.064		Fe II λ2374 z =0.9893
68	4717.26	0.903 ± 0.054		N II λ1083 z =3.3534
69	4713.80	1.998 ± 0.060		
			Q 1451+123	
1	5301.23	0.637 ± 0.088		
2	5297.43	0.678 ± 0.109		Si II λ1526 z =2.4698
3	5261.68	0.602 ± 0.073		
4	5257.40	1.140 ± 0.093	Si II λ1260 z =3.1714	
5	5235.38	0.692 ± 0.084		Fe II λ1608 z =2.2538
6	5164.70	1.081 ± 0.039		N V λ1238 z =3.1714
7	5144.14	0.830 ± 0.046		
8	5138.52	0.473 ± 0.039		
9	5134.96	1.092 ± 0.046		
10	5130.42	0.397 ± 0.048		
11	5119.58	6.392 ± 0.095		
12	5109.85	2.008 ± 0.100		
13	5105.14	0.907 ± 0.103		
14	5098.42	0.966 ± 0.113		
15	5087.48	2.995 ± 0.164		
16	5071.10	19.729 ± 0.301	Lyα z =3.1714	
17	5052.64	1.348 ± 0.143		
18	5046.10	1.381 ± 0.143		C IV λ1550 z =2.2538
19	5042.40	0.968 ± 0.122		
20	5038.62	1.871 ± 0.128		C IV λ1548 z =2.2538
21	5033.37	3.579 ± 0.181	Si III λ1206 z =3.1714	
22	5017.27	6.030 ± 0.217		
23	5007.95	1.631 ± 0.171	N I λ1200 z =3.1714	
24	4987.72	2.539 ± 0.205		
25	4977.61	1.515 ± 0.144	Si II λ1193 z =3.1714	
26	4971.47	6.435 ± 0.217		Si II λ1190 z =3.1714 Si II λ1526 z =2.2538
27	4960.66	1.776 ± 0.161		
28	4951.95	1.881 ± 0.155		
29	4942.08	1.980 ± 0.134		
30	4938.71	2.720 ± 0.167		
31	4925.29	4.385 ± 0.211		
32	4908.34	4.159 ± 0.264		

TABLE 2—*Continued*

No.	λ_{obs}	W_λ (Å)	Identification	Possible I.D.
			Q 1512+132	
1	5030.33	0.319 ± 0.046		
2	5024.90	0.310 ± 0.047	Si II λ1260 z =2.9859	
3	5000.88	0.731 ± 0.059		
4	4991.99	0.795 ± 0.040		
5	4975.17	0.553 ± 0.040		
6	4965.61	0.212 ± 0.036		
7	4961.22	0.261 ± 0.047		
8	4947.09	2.012 ± 0.059		
9	4940.82	0.371 ± 0.057		
10	4929.71	0.914 ± 0.055		
11	4923.90	1.178 ± 0.062		
12	4918.13	0.477 ± 0.060		
13	4901.93	1.773 ± 0.086		
14	4885.34	0.336 ± 0.067		
15	4881.69	0.413 ± 0.078		
16	4864.86	0.648 ± 0.105		
17	4857.50	2.310 ± 0.092		
18	4845.62	8.155 ± 0.159	Lyα z =2.9859	
19	4827.52	3.913 ± 0.131		
20	4807.00	2.944 ± 0.124	Si III λ1206 z =2.9859	
21	4795.37	2.609 ± 0.109		
22	4790.23	1.038 ± 0.059		
23	4785.78	2.533 ± 0.115		
24	4763.83	0.497 ± 0.068		
25	4760.95	0.562 ± 0.089		
26	4755.12	1.102 ± 0.101	Si II λ1193 z =2.9859	
27	4750.49	0.889 ± 0.091		
28	4742.21	1.825 ± 0.135		Si II λ1190 z =2.9859
29	4736.44	0.645 ± 0.093		
30	4724.08	0.771 ± 0.077		
31	4718.88	1.058 ± 0.086		
32	4713.31	0.855 ± 0.095		
			Q 1548+092	
1	4627.10	0.379 ± 0.076	Si IV λ1393 z =2.3187	
2	4559.02	0.295 ± 0.035		
3	4557.54	0.304 ± 0.035		
4	4554.46	0.292 ± 0.047	Si IV λ1402 z =2.2475	Si II λ1304 z =2.4906
5	4547.07	0.462 ± 0.055	O I λ1302 z =2.4906	Si II λ1260 z =2.6092
6	4537.15	0.466 ± 0.054		
7	4534.36	0.301 ± 0.049		
8	4528.32	2.396 ± 0.052		
9	4525.60	1.768 ± 0.029		
10	4523.42	1.698 ± 0.047	Si IV λ1393 z =2.2475	
11	4518.41	1.718 ± 0.067		
12	4514.41	1.214 ± 0.059		
13	4507.14	0.888 ± 0.088		
14	4501.51	1.697 ± 0.063		
15	4497.82	3.078 ± 0.062		
16	4493.99	0.532 ± 0.058		
17	4489.30	4.924 ± 0.110		
18	4477.44	1.866 ± 0.107		
19	4466.61	0.915 ± 0.084		
20	4462.96	2.198 ± 0.085		
21	4459.36	0.566 ± 0.064		

TABLE 2—*Continued*

No.	λ_{obs}	W_λ (Å)	Identification	Possible I.D.
22	4456.12	3.233 ± 0.092		
23	4446.13	0.604 ± 0.097		
24	4424.67	1.031 ± 0.115		
25	4411.14	0.888 ± 0.131		
26	4394.54	1.128 ± 0.099		
27	4387.60	6.271 ± 0.136		Lyα z =2.6092
28	4382.78	1.723 ± 0.097		
29	4379.54	0.780 ± 0.131		
30	4372.58	0.954 ± 0.100		
31	4370.30	1.151 ± 0.113		
32	4361.00	1.486 ± 0.242		
33	4353.64	1.344 ± 0.164		Si III λ1206 z =2.6092
34	4341.66	1.010 ± 0.141		
35	4337.01	2.680 ± 0.159		C II* λ1335 z =2.2475
36	4324.70	3.272 ± 0.176		N V λ1238 z =2.4906
37	4314.27	1.627 ± 0.179		
38	4304.42	1.005 ± 0.157		Si II λ1193 z =2.6092
39	4292.04	1.526 ± 0.175		
40	4287.37	1.232 ± 0.185		
41	4268.51	1.114 ± 0.143		
42	4266.16	1.475 ± 0.143		
43	4261.91	1.131 ± 0.202		
44	4244.81	2.182 ± 0.171	Lyα z =2.4906	
45	4228.45	2.399 ± 0.183	O I λ1302 z =2.2475	
46	4220.83	1.299 ± 0.158		
47	4215.69	3.589 ± 0.238		Fe II λ2382 z =0.7703
48	4210.05	2.808 ± 0.214		
49	4155.00	1.375 ± 0.265		
50	4084.04	4.290 ± 0.824		
			Q 1601+182	
1	5317.03	3.767 ± 0.238	Si II λ1526 z =3.218	
2	5282.07	0.818 ± 0.145		
3	5239.94	2.905 ± 0.118	N V λ1242 z =3.218	
4	5236.03	1.309 ± 0.071	N V λ1242 z =3.218	
5	5232.01	2.612 ± 0.113	N V λ1242 z =3.218	
6	5222.73	3.847 ± 0.121	N V λ1238 z =3.218	
7	5218.71	1.767 ± 0.070	N V λ1238 z =3.218	
8	5214.98	2.622 ± 0.080	N V λ1238 z =3.218	
9	5180.05	0.406 ± 0.070		
10	5128.41	12.773 ± 0.057	Lyα z =3.218	
11	5118.40	4.099 ± 0.040	Lyα z =3.218	
12	5113.64	4.021 ± 0.079		
13	5100.71	1.579 ± 0.088		
14	5090.80	8.117 ± 0.121	Si III λ1206 z =3.218	
15	5081.06	2.549 ± 0.145	Si III λ1206 z =3.218	
16	5061.63	0.776 ± 0.140	N I λ1200 z =3.218	
17	5051.41	1.781 ± 0.127		
18	5046.15	1.154 ± 0.119		
19	5042.35	0.920 ± 0.113		
20	5035.16	2.009 ± 0.147	Si II λ1193 z =3.218	
21	5030.33	3.433 ± 0.143		
22	5022.02	5.766 ± 0.168	Si II λ1190 z =3.218	
23	5014.90	4.464 ± 0.148		
24	5009.24	2.471 ± 0.166		
25	4984.30	1.020 ± 0.164		
26	4981.27	1.703 ± 0.168		
27	4957.69	1.665 ± 0.152		

TABLE 2—*Continued*

No.	λ_{obs}	W_λ (Å)	Identification	Possible I.D.
28	4952.76	1.105 ± 0.165		
29	4938.52	1.993 ± 0.144		
30	4935.73	1.459 ± 0.122		
31	4933.09	1.145 ± 0.144		
32	4926.24	1.985 ± 0.176		
33	4907.41	1.878 ± 0.171		
			Q 1602+178	
1	4987.09	0.903 ± 0.144		N V λ1242 z =3.01274 Si II λ1304 z =2.8231
2	4971.02	1.736 ± 0.140		N V λ1238 z =3.01274
3	4967.60	1.439 ± 0.127	C IV λ1550 z =2.2033	
4	4959.41	1.883 ± 0.124	C IV λ1548 z =2.2033	
5	4920.53	0.593 ± 0.086		
6	4917.45	2.309 ± 0.111		
7	4900.62	0.781 ± 0.117		
8	4875.66	7.049 ± 0.092	Mg II λ2803 z =0.73925	
9	4870.97	0.708 ± 0.045	Mg II λ2803 z =0.73738	
10	4863.96	6.174 ± 0.072	Mg II λ2796 z =0.73925	
11	4858.15	1.218 ± 0.070	Mg II λ2796 z =0.73738	
12	4845.87	0.500 ± 0.086		
13	4840.46	1.783 ± 0.065		
14	4835.46	6.662 ± 0.077	Lyα z =2.98	
15	4829.24	3.495 ± 0.113		
16	4821.41	1.835 ± 0.087		
17	4818.76	1.104 ± 0.075		Si II λ1260 z =2.8231
18	4814.33	2.030 ± 0.119		
19	4810.63	0.658 ± 0.097		
20	4805.38	0.723 ± 0.131		
21	4799.10	4.645 ± 0.171	Si III λ1206 z =2.98	
22	4780.98	2.592 ± 0.197		
23	4761.16	0.920 ± 0.176		
24	4757.06	2.032 ± 0.178		
25	4747.38	4.969 ± 0.256	Si II λ1193 z =2.98	
26	4736.10	2.401 ± 0.177	Si II λ1190 z =2.98	
27	4732.41	2.081 ± 0.185		
28	4708.39	4.290 ± 0.295		
29	4699.03	3.328 ± 0.247		
30	4693.90	2.408 ± 0.231		
31	4689.23	1.421 ± 0.249		
32	4684.86	1.989 ± 0.280		
33	4678.94	2.073 ± 0.263		
34	4669.44	2.103 ± 0.270		
35	4655.19	1.569 ± 0.273		
36	4647.65	5.932 ± 0.374		Lyα z =2.8231
37	4636.68	1.938 ± 0.299		
38	4630.11	1.510 ± 0.273		
39	4620.80	2.439 ± 0.241		
40	4615.52	1.657 ± 0.320		
41	4602.11	1.667 ± 0.315		
42	4595.65	1.444 ± 0.271		
43	4577.70	5.223 ± 0.427		
			Q 1614+051	
1	5134.63	0.792 ± 0.074		

TABLE 2—*Continued*

No.	λ_{obs}	W_λ (Å)	Identification	Possible I.D.
2	5121.27	1.013 ± 0.042		
3	5118.24	3.293 ± 0.041		
4	5100.93	1.719 ± 0.108		
5	5092.36	3.625 ± 0.125		
6	5082.09	4.229 ± 0.176		
7	5070.49	4.299 ± 0.169		
8	5064.57	3.276 ± 0.120		
9	5060.29	2.855 ± 0.170		
10	5052.60	1.298 ± 0.164		
11	5043.75	2.152 ± 0.180		
12	5026.48	1.610 ± 0.195		
13	5008.63	1.116 ± 0.166		
14	4996.07	0.962 ± 0.176		
15	4980.53	9.051 ± 0.341		Lyα z =3.0969
16	4970.11	0.907 ± 0.164		
17	4960.11	1.051 ± 0.159		
18	4953.08	4.954 ± 0.230		
19	4948.20	1.702 ± 0.166		
20	4943.09	2.470 ± 0.222		Si III λ1206 z =3.0969
21	4930.34	6.650 ± 0.275		
22	4909.61	4.500 ± 0.276		
			Q 1738+350	
1	5142.91	2.163 ± 0.055		
2	5139.20	2.584 ± 0.038		
3	5135.79	2.897 ± 0.047		
4	5131.78	2.279 ± 0.068		
5	5127.12	1.857 ± 0.098		
6	5117.54	5.025 ± 0.154		
7	5099.63	0.833 ± 0.106		
8	5094.69	2.219 ± 0.190		
9	5075.64	2.435 ± 0.217		
10	5068.45	2.499 ± 0.225		
11	5054.86	2.131 ± 0.202		
12	5048.39	1.829 ± 0.292		
13	5037.50	1.846 ± 0.257		
14	5030.56	4.584 ± 0.257		
15	5024.07	5.208 ± 0.265		
16	5017.38	1.156 ± 0.228		
17	5008.92	1.027 ± 0.204		
18	4998.95	2.258 ± 0.279		
19	4970.49	2.661 ± 0.277		
20	4965.26	3.434 ± 0.334		
21	4959.45	1.337 ± 0.237		
22	4949.13	3.394 ± 0.328		
23	4930.83	1.950 ± 0.289		
24	4907.04	4.528 ± 0.372		
			Q 2233+131	
1	5231.95	2.378 ± 0.039	Si II λ1260 z =3.1519	
2	5229.39	1.857 ± 0.051	Si II λ1260 z =3.1519	
3	5222.02	0.253 ± 0.047		
4	5217.79	0.439 ± 0.050		
5	5199.56	0.521 ± 0.056		
6	5196.61	1.227 ± 0.061		

TABLE 2—*Continued*

No.	λ_{obs}	W_λ (Å)	Identification	Possible I.D.
7	5188.64	1.000 ± 0.066		
8	5181.70	0.933 ± 0.052		
9	5178.59	1.226 ± 0.072		
10	5171.82	1.441 ± 0.066		
11	5167.45	2.954 ± 0.071		
12	5160.52	1.182 ± 0.063	N V λ1242 z =3.1519	
13	5156.97	3.302 ± 0.079		
14	5151.19	0.493 ± 0.081		
15	5144.19	1.296 ± 0.093	N V λ1238 z =3.1519	
16	5135.76	2.521 ± 0.069		
17	5132.62	1.249 ± 0.059		
18	5125.16	2.552 ± 0.082		
19	5121.67	1.450 ± 0.073		
20	5113.07	1.993 ± 0.090		C II* λ1335 z =2.8284
21	5108.47	1.747 ± 0.081	C II λ1334 z =2.8284	
22	5103.77	2.327 ± 0.091		
23	5096.24	2.664 ± 0.105		
24	5090.29	1.706 ± 0.123		
25	5084.51	1.174 ± 0.090		
26	5077.86	4.166 ± 0.128		
27	5069.01	1.358 ± 0.113		
28	5062.12	1.295 ± 0.100		
29	5045.76	20.830 ± 0.248	Lyα z =3.1519	
30	5017.05	4.971 ± 0.132	Si III λ1206 z =3.1519	
31	5010.32	6.855 ± 0.119	Si III λ1206 z =3.1519	
32	5002.04	7.632 ± 0.118	Si III λ1206 z =3.1519	
33	4995.44	3.029 ± 0.106		
34	4990.34	2.043 ± 0.097		
35	4986.89	2.411 ± 0.121		
36	4980.39	1.750 ± 0.126		Si IV λ1402 z =2.5510
37	4957.58	1.294 ± 0.115		
38	4951.55	5.299 ± 0.162	Si II λ1193 z =3.1519	Si IV λ1393 z =2.5510
39	4939.97	2.947 ± 0.123	Si II λ1190 z =3.1519	
40	4930.87	0.971 ± 0.140		
41	4920.04	1.510 ± 0.135		
42	4912.08	2.830 ± 0.124		
43	4904.64	0.828 ± 0.104		
			Q 2233+136	
1	5290.82	1.914 ± 0.076	Al II λ1670 z =2.1690	O I λ1302 z =3.0625
2	5138.87	0.249 ± 0.043		
3	5127.46	0.249 ± 0.032		
4	5118.01	2.887 ± 0.039		
5	5114.10	0.770 ± 0.030		
6	5101.30	0.981 ± 0.041		
7	5097.13	1.328 ± 0.035		
8	5093.09	1.313 ± 0.051	Fe II λ1608 z =2.1690	
9	5077.03	0.729 ± 0.062		
10	5071.53	2.530 ± 0.048		Si II λ1304 z =2.8894
11	5067.37	2.439 ± 0.059		
12	5056.90	3.711 ± 0.074		
13	5050.43	1.222 ± 0.057		
14	5044.99	0.450 ± 0.070		
15	5038.05	2.398 ± 0.072		
16	5020.94	2.523 ± 0.070		
17	5012.90	6.893 ± 0.082		
18	5003.91	2.385 ± 0.087		
19	4998.11	0.435 ± 0.064		

TABLE 2—*Continued*

No.	λ_{obs}	W_λ (Å)	Identification	Possible I.D.
20	4992.53	0.979 ± 0.073	Fe II λ2382 z =1.0957	
21	4989.16	1.051 ± 0.062		
22	4983.65	2.132 ± 0.079		
23	4977.43	1.822 ± 0.079		Fe II λ2374 z =1.0957
24	4971.62	0.418 ± 0.076		
25	4963.64	0.620 ± 0.079		
26	4946.46	5.172 ± 0.075		
27	4938.68	6.856 ± 0.076		Lyα z =3.0625
28	4931.78	0.898 ± 0.079		
29	4921.22	0.542 ± 0.071		
30	4917.96	0.399 ± 0.067		
31	4911.37	4.845 ± 0.080	C IV λ1550 z =2.1690	Fe II λ2344 z =1.0957
		Q 2311-036		
1	4995.48	0.736 ± 0.071	Mg II λ2803 z =0.7819	
2	4982.98	1.205 ± 0.084	Mg II λ2793 z =0.7819	
3	4916.41	3.034 ± 0.034		
4	4905.09	1.320 ± 0.026		O I λ1302 z =2.7685
5	4901.41	1.710 ± 0.044		
6	4882.71	1.955 ± 0.064		
7	4872.96	2.536 ± 0.095		
8	4860.91	2.224 ± 0.087		
9	4853.24	0.804 ± 0.072		
10	4847.33	0.849 ± 0.066		
11	4843.15	0.371 ± 0.073		
12	4819.32	2.435 ± 0.114		
13	4803.18	3.082 ± 0.128		
14	4797.59	3.093 ± 0.170		
15	4786.13	0.747 ± 0.113		
16	4773.20	1.413 ± 0.157		
17	4766.06	2.451 ± 0.168		
18	4760.56	2.273 ± 0.201		
19	4747.42	1.695 ± 0.183		Si II λ1260 z =2.7685
20	4742.90	1.007 ± 0.148		
21	4737.93	1.724 ± 0.195		
22	4716.61	4.332 ± 0.222		
23	4706.87	1.205 ± 0.197		
24	4680.84	2.108 ± 0.268		N V λ1242 z =2.7685
25	4666.74	2.730 ± 0.299		N V λ1238 z =2.7685
26	4648.72	3.854 ± 0.241		
27	4635.41	1.187 ± 0.232		Fe II λ2600 z =0.7819
28	4629.47	0.920 ± 0.163		
29	4607.42	4.252 ± 0.286		Fe II λ2600 z =0.7819
30	4597.42	2.504 ± 0.192		
31	4581.29	5.975 ± 0.303		Lyα z =2.7685

by York et al. (1991). Otherwise, any ratio of ionization species or metallicity was considered acceptable.

2.2. *Spectrophotometry*

Spectrophotometry for five of the QSOs were obtained for this work at the Steward Observatory 2.3 m Telescope with the Boller and Chivens spectrograph and TI-CCD. A 300 line mm^{-1} grating blazed at 6900 Å was used in first order with a 4″5 slit to obtain spectral coverage from 3500–6900 Å at a resolution of 15 Å (FWHM). Second-order light was eliminated by an order-blocking filter. QSOs were observed for a maximum exposure of 3000 s, with the slit oriented at the average parallactic angle for each exposure. For the flux calibration, an IIDS standard star nearby in the sky was observed immediately before and after each QSO observation. Bias frames, quartz-lamp flats, and helium-neon-argon lamp exposures were used as described above. The data were reduced in IRAF, and the default standard star flux values and extinction curves for Kitt Peak, as supplied by IRAF, were used. The analysis followed that described by Pei, Fall, & Bechtold (1991); further details may be found there.

Observations of 1159+124, 1208+101, 1442+101, and 1548+092 were obtained on the night of 1990 May 21. Thin cirrus was present all night, and the seeing was 1″ or better. Observations of 1602+178 were obtained on 1991 May 18. Conditions were photometric, with subarcsecond seeing. Results are described below in § 4.1.

3. Lyα FOREST STATISTICS FOR $z_{abs} \ll z_{em}$

3.1. *Absorption-Line Sample*

In order to study the statistics of the Lyα forest at $z_{abs} \ll z_{em}$, a sample was compiled from the data described in the previous section, and the literature. For data from the literature, the criteria for inclusion in the sample were (1) the QSO was not a broad absorption line QSO; (2) the spectral resolution of the data was better than 200 km s^{-1} FWHM; and (3) errors in the absorption line equivalent widths were published. The third criterion excluded 0805+046 which was included in the previous compilations of BDO and LWT. Objects with associated C IV complexes or other metal-line system near z_{em} were included in this part of the analysis, provided the complexes did not extend bluer than $\Delta z = 0.15$ from the emission line redshift. Finally, echelle data for 0014+813 (Rauch et al. 1992), 0420−388 (Atwood, Baldwin, & Carswell 1985), 1101−264 (Carswell et al. 1991a), 2000−330 (Carswell et al. 1987), and 2206−199 (Pettini et al. 1990) were excluded, since these spectra have much higher resolution, were analyzed differently, and in any case do not contribute substantially to the line sample. As it turns out, the results for the moderate-resolution sample compiled here are in excellent agreement with the results derived from the echelle data (see § 3.3 below).

The entire absorption line sample, including the QSOs presented in this paper, is described in Table 3. It includes 2792 lines in the spectra of 78 QSOs and differs significantly from both the BDO and LWT samples. Table 3 lists the minimum and maximum redshifts covered by the spectra, z_{min} and z_{max}. In most cases z_{min} was determined by either the end of the spectral coverage, or the Lyβ emission wavelength, whichever was redder. In a few cases, I increased z_{min} compared to BDO or LWT in order to eliminate a noisy part of the spectrum. The value for z_{max} is determined either by the wavelength of the peak of Lyα emission or the end of the spectral coverage, whichever is bluer. The spectral resolution of the data, R, is listed as either M for moderate, which is taken to be between 50 and 100 km s^{-1} FWHM; or L for low, which signifies greater than 100 km s^{-1} FWHM, but less than 200 km s^{-1}.

The rest equivalent width limit for Lyα for the two ranges (z_{min}, z_{em}–0.15) and (z_{em}–0.15, z_{max}) are given in Table 3, as E_2 and E_1 respectively. For the data presented here, and in Dobrzycki & Bechtold (1994), the equivalent width limit was computed directly as a function of wavelength from the continuum fit, and the signal-to-noise in each pixel. The upper limit to the 5 σ rest equivalent width limit for an unresolved line in each of the two redshift ranges is listed; E_2 is generally larger than E_1 since the signal-to-noise is substantially better in the wings of the Lyα emission line than in the continuum. For the data from the literature, the rest equivalent width limit listed is either what was quoted by the authors, or, if not discussed, was estimated by taking 5 times the largest observed error in equivalent width of any absorption line in the relevant redshift region and dividing it by $(1 + z_{min})$. In a few cases, the result estimated this way was worse than 0.36 Å, the limit assumed in the previous compilation of LWT. N_1 is the number of lines stronger than E_1 in the interval (z_{em}–0.15, z_{max}), and N_2 is the number of lines stronger than E_2 in the interval (z_{min}, z_{em}–0.15). Note that in some cases the spectra covered the region containing the Lyα emission line, but not much else, in which case $N_1 > N_2$.

Absorption lines for the spectra presented here were excluded if they have an entry in Table 2, column (4) indicating that they are "sure" to be associated with a metal-line system. For the QSO spectra from the literature, the identification of metal lines was reexamined by Ms. B. Frye. All redshift systems listed by York et al. (1991) as class A or B were considered and the corresponding transitions in the line list of Morton, York, & Jenkins 1988 (their Table 4) were examined. Since in a few cases new metal-line systems had been discovered since the publication of the Lyα forest spectrum, the result was that a small number of additional lines were disgarded. Details, including the list of disgarded lines, can be found in Frye et al. (1993). The effect of removing these lines turned out to be negligible.

3.2. *Best Estimates of γ, W^*, and A_0*

Following previous work, the number of absorption lines per unit redshift per unit equivalent width can be expressed as

$$\frac{\delta^2 N}{\delta z \delta W} = \frac{A_0}{W^*}(1+z)^\gamma \exp\left(-\frac{W}{W^*}\right). \quad (1)$$

The maximum-likelihood method of Murdoch et al. (1986) (with their eqs. [A8] and [A2a] corrected) was used to estimate the Lyα forest parameters γ and W^* with a code kindly provided by A. Dobrzycki. In addition, the number of lines per unit redshift stronger than a *fixed* rest equivalent width limit is often written as

$$\frac{dN}{dz} = A_0(1+z)^\gamma . \quad (2)$$

For $0 \le q_0 \le 0.5$, if $\gamma > 1$, then there is intrinsic evolution in the observed number density of absorbers (i.e., in their space density, cross section for absorption, or both) in the sense that the mean-free-path for absorption was smaller in the past. A_0 was computed by integrating equation (2) over the redshift ranges of the sample used and comparing the expected total number of lines to the observed total, after γ had been determined by the maximum-likelihood technique.

Results for γ, W^*, and A_0 are listed in Table 4. Several subsamples of the total sample listed in Table 3 were formed, in order to get some idea of the effect of the inclusion or exclusion of different types of data, the dependence of parameters on the equivalent width threshold, and to facilitate comparisons with previously reported results. Column (1) lists a number designating each subsample (used in the discussion below), column (2) lists the number of lines used in the fit, column (3) lists the number of QSOs in the subsample, column (4) lists the rest equivalent width limit in angstroms, column (5) lists the redshift interval excluded to avoid the proximity effect, and column (6) lists the resolution of the data included. Columns (7), (8), and (9) list the results of the fits,

TABLE 3

TOTAL SAMPLE: ABSORPTION-LINE PROPERTIES

QSO	z_{em}	z_{min}	z_{max}	R	E_1	E_2	N_1	N_2	Refn.
0000-263*	4.111	3.796	4.111	M	0.044	0.060	-	33	1
0001+087	3.243	3.035	3.243	M	0.13	0.14	15	9	1
0002+051	1.899	1.764	1.899	M	0.16	0.16	10	-	2
0002-422	2.763	2.175	2.763	M	0.32	0.32	8	26	3,4
0014+813*	3.384	2.743	3.384	M	0.15	0.15	-	53	1
0029+073*	3.294	3.033	3.294	M	0.090	0.14	-	8	1
0058+019	1.959	1.756	1.959	M	0.13	0.13	18	2	5
0100+130	2.690	2.359	2.690	M	0.16	0.16	9	16	4
0114-089	3.205	2.685	3.205	M	0.080	0.080	17	61	1
0119-046*	1.937	1.682	1.937	M	0.16	0.16	-	7	6
0122-380	2.181	1.797	2.181	L	0.36	0.36	10	8	7
0142-100	2.727	2.145	2.727	M	0.13	0.13	22	41	5
0207-003*	2.855	2.253	2.855	L	0.30	0.30	-	30	8
0216+080	2.990	2.916	2.990	L	0.064	0.064	7	-	5
0237-233	2.222	1.719	2.222	M	0.13	0.13	13	33	5
0256-000	3.374	2.685	3.374	M	0.18	0.18	16	74	1
0301-005	3.223	3.043	3.212	M	0.10	0.12	25	3	1
0302-003*	3.286	2.685	3.286	M	0.15	0.17	-	54	1
0334-204	3.126	3.043	3.126	M	0.060	0.060	10	-	1
0347-383	3.230	2.569	3.230	L	0.46	0.81	4	11	8
0421+019	2.051	1.772	2.051	M	0.16	0.16	8	11	2
0424-131*	2.166	1.879	2.166	M	0.12	0.12	-	7	5
0449-135*	3.097	2.916	3.097	L	0.18	0.18	-	1	5
0453-423	2.656	2.209	2.656	M	0.32	0.32	12	25	3,4
0636+680m	3.174	2.522	3.174	M	0.099	0.13	21	79	1
0636+680p	3.174	3.043	3.174	M	0.023	0.023	24	-	1
0731+653*	3.033	2.677	3.033	M	0.30	0.31	-	18	1
0831+128	2.739	2.155	2.739	M	0.22	0.29	18	32	1
0836+113	2.669	2.096	2.669	L	0.45	0.45	3	12	9
0837+109	3.326	2.989	3.326	M	0.10	0.10	34	44	5
0848+163*	1.925	1.747	1.925	M	0.073	0.073	-	2	5
0854+191*	1.896	1.838	1.896	L	0.14	0.14	-	-	5
0905+151	3.173	3.043	3.173	M	0.074	0.074	24	-	1
0913+072	2.784	2.193	2.784	M	0.094	0.19	21	26	1
0938+119	3.192	3.043	3.192	M	0.12	0.12	18	-	1
1017+280	1.928	1.632	1.928	M	0.095	0.095	8	11	5
1033+137	3.092	3.043	3.092	M	0.045	0.045	9	-	1
1054-034	2.114	2.085	2.114	L	0.15	0.15	3	-	5
1101-264	2.143	1.784	2.143	L	0.27	0.27	8	10	7
1115+080*	1.725	1.682	1.725	M	0.16	0.16	-	0	2
1151+068	2.760	2.173	2.760	M	0.32	0.32	9	33	9
1159+124*	3.502	2.799	3.502	M	0.20	0.20	-	56	5
1206+119*	3.108	2.784	3.108	M	0.063	0.087	-	20	1
1206+119*	3.108	2.466	3.108	M	0.088	0.11	-	77	10
1208+101	3.822	3.500	3.822	M	0.16	0.11	15	18	1
1213+093	2.719	2.537	2.719	L	0.17	0.17	16	1	5
1215+33	2.606	2.043	2.606	M	0.10	0.15	19	47	1
1225-017	2.831	2.317	2.831	M	0.11	0.13	21	62	10
1225+317	2.200	1.800	2.200	M	0.16	0.16	11	23	4
1228+076	2.391	2.208	2.391	L	0.47	0.15	7	2	11
1247+267	2.039	1.632	2.039	M	0.076	0.076	18	25	5
1315+472	2.590	2.029	2.590	M	0.079	0.14	16	48	1
1334-005	2.842	2.242	2.833	M	0.096	0.070	18	72	1
1337+113	2.919	2.661	2.919	L	0.25	0.25	3	4	9
1347+112*	2.697	2.488	2.697	L	0.49	0.49	-	1	9
1400+114	3.177	3.043	3.177	M	0.13	0.13	34	-	1
1402+044	3.206	3.032	3.206	M	0.33	0.33	6	0	1
1410+096	3.313	3.032	3.313	M	0.067	0.087	18	12	1
1442+101	3.554	2.872	3.554	M	0.064	0.085	16	70	1
1451+123*	3.251	3.032	3.251	M	0.18	0.20	-	6	1
1510+115*	2.106	1.879	2.106	L	0.24	0.24	-	6	5
1511+091*	2.878	2.455	2.878	L	0.17	0.17	-	29	5
1512+132*	3.120	2.872	3.120	M	0.20	0.25	-	4	1
1548+092	2.748	2.455	2.748	M	0.16	0.29	18	10	1
1601+182*	3.227	3.032	3.227	M	0.19	0.22	-	6	1
1602+178*	2.989	2.749	2.989	M	0.33	0.40	-	6	1
1607+183	3.134	2.488	3.113	M	0.11	0.13	17	72	10
1614+051	3.216	3.032	3.216	M	0.23	0.25	16	2	1
1623+268	2.605	2.249	2.605	M	0.32	0.32	19	43	12
1623+269*	2.526	1.975	2.526	M	0.089	0.12	-	12	10
1700+642	2.744	2.159	2.744	M	0.058	0.076	29	57	10
1738+350	3.239	3.032	3.239	M	0.33	0.32	15	6	1
2126-158	3.280	2.500	3.280	M	0.32	0.32	9	39	4
2204-408	3.220	2.561	3.220	L	0.27	0.27	9	59	8
2206-199	2.559	2.126	2.559	L	0.22	0.22	7	24	5
2233+131*	3.295	3.032	3.295	M	0.13	0.14	-	8	1
2233+136	3.209	3.032	3.209	M	0.091	0.092	18	3	1
2311-036	3.041	2.750	3.041	M	0.22	0.37	12	3	1
2348-011	3.030	2.718	3.030	L	0.63	0.63	2	8	9

NOTES.—z_{min}: lowest redshift considered. z_{max}: highest redshift considered. R: Resolution class; M: better than 100 km s^{-1}; L: worse than 100 km s^{-1}. E1: rest equivalent width limit for $z_{em} - 0.15 < z_{abs} < z_{max}$, that is, near Ly$\alpha$ emission. E: rest equivalent width limit for $z_{min} < z_{abs} < z_{em} - 0.15$, that is, far from Ly$\alpha$ emission. N1: number of lines stronger than E1 in redshift interval $z_{em} - 0.15 < z_{abs} < z_{max}$. N2: number of lines stronger than E2 in redshift interval $z_{min} < z_{abs} < z_{em} - 0.15$. For 0636+680, m: MMT, p: Palomar.

REFERENCES.—(1) This paper. (2) Young, Sargent, & Boksenberg 1982a. (3) Sargent et al. 1979. (4) Sargent et al. 1980. (5) Sargent, Boksenberg, & Steidel 1988. (6) Sargent, Young, & Boksenberg 1982. (7) Carswell et al. 1982. (8) Williger et al. 1989. (9) Turnshek et al. 1989. (10) Dobrzycki & Bechtold 1994. (11) Robertson & Shaver 1983. (12) Sargent, Young, & Schneider 1982.

TABLE 4

MAXIMUM LIKELIHOOD ESTIMATIONS OF γ, W^*, AND A_0

No. (a)	N_{lines} (b)	N_{QSOs} (c)	W_{λ_0}(Å) (d)	ΔZ (e)	R (f)	γ	W*	A_0	P_{KS} (g)
1	984	59	> 0.32	1	M, L	1.85 ± 0.27	0.285 ± 0.009	5.97	0.10
2	955	46	> 0.24	1	M, L	1.72 ± 0.25	0.268 ± 0.009	9.26	0.096
3	924	33	> 0.16	1	M, L	1.34 ± 0.24	0.271 ± 0.009	19.8	0.060
4	1701	67	> E_2	1	M, L	1.09 ± 0.19	0.296 ± 0.007		0.39
5	2149	73	> E_2	2	M, L	1.05 ± 0.17	0.299 ± 0.006		0.98
6	376	52	> 0.56	1	M	2.12 ± 0.43	0.268 ± 0.014	1.78	0.50
7	498	52	> 0.48	1	M	2.40 ± 0.38	0.271 ± 0.012	1.64	0.43
8	661	52	> 0.40	1	M	2.01 ± 0.33	0.274 ± 0.011	3.60	0.32
9	859	49	> 0.32	1	M	1.89 ± 0.28	0.276 ± 0.009	5.62	0.17
10	898	39	> 0.24	1	M	1.81 ± 0.26	0.264 ± 0.009	8.22	0.064
11	922	33	> 0.16	1	M	1.32 ± 0.24	0.272 ± 0.009	20.2	0.063
12	1495	52	> E_2	1	M	1.01 ± 0.20	0.287 ± 0.007		0.73
13	929	52	> 0.36	2	M	1.85 ± 0.27	0.276 ± 0.009	5.04	0.29
14	1060	51	> 0.32	2	M	1.80 ± 0.25	0.278 ± 0.009	6.12	0.26
15	1079	40	> 0.24	2	M	1.76 ± 0.22	0.266 ± 0.008	8.49	0.05
16	1140	34	> 0.16	2	M	1.27 ± 0.21	0.270 ± 0.008	21.2	0.06
17	1854	54	> E_2	2	M	0.99 ± 0.18	0.287 ± 0.007		0.68
18	417	33	0.16 < W < 0.32	1	M	0.47 ± 0.35		26.9	0.34
19	508	34	0.16 < W < 0.32	2	M	0.46 ± 0.31		26.6	0.10
20	627	67	E_2 < W < 0.32	1	M	0.048 ± 0.29			0.20
21a	552	35	> 0.32	1	M	1.46 ± 0.58	0.277 ± 0.012	9.93	0.35
21b	306	26	> 0.32	1	M	3.76 ± 0.81	0.274 ± 0.016	0.64	0.82
22a	530	18	> 0.16	1	M	-0.21 ± 0.56	0.287 ± 0.012	169.3	0.23
22b	373	19	> 0.16	1	M	2.63 ± 0.67	0.254 ± 0.013	4.41	0.70
23a	223	18	0.16 < W < 0.32	1	M	-2.05 ± 0.90		884.	0.56
23b	181	19	0.16 < W < 0.32	1	M	1.60 ± 0.93		6.94	0.97

[a] Sample number (see text). Samples 21a, 22a, and 23a include lines with $z_{abs} > 2.5$ only; samples 21b, 22b, and 23b include lines with $z_{abs} < 2.5$ only.
[b] Number of lines included in estimation of γ, W^*, and A_0.
[c] Number of QSOs included in sample.
[d] Rest equivalent width of Lyα used, in Å.
[e] Redshift interval used; 1 = z_{min} to $z_{em} - 0.15$, or z_{max}; 2 = z_{min} to $z_{em} - z(8\ Mpc)$ or z_{max}. See text.
[f] Resolution of spectra included (see Table 3).
[g] P_{KS} is the K-S probability that $(1 + z)^\gamma$ is a good fit to the distribution of line redshifts, for γ listed in col. (7). Large numbers indicate good fits.

γ, W^*, and A_0, respectively. (Objects where the equivalent width threshold listed in Table 3 is greater than the minimum value listed in col. [4] of Table 4 were of course completely excluded from each fit.) Errors in A_0 are not tabulated, because they are highly correlated with errors in γ. The results for samples 4, 5, 12, 17, and 20 were derived using the individual equivalent width threshold, E_2, appropriate to each QSO. This formally gives the best determination of γ since the largest number of lines is included, but since E_2 varied widely from QSO to QSO, these results are mostly of academic interest. In particular, A_0 was not calculated for these samples.

In order to test how well equation (1) describes the data, the Kolmogorov test was performed for each subsample, as described by Murdoch et al. (1986, their eqs. [A14]–[A16]). In column (10) of Table 4, I list P_{KS}, the Kolmogorov-Smirnov probability that $(1 + z)^\gamma$ is a good fit to the distribution of line redshifts. In all cases, the fit is acceptable, that is, $P_{KS} > 0.01$.

In addition, for each subsample, the Q-test described by Murdoch et al. (1986) was used to test whether the form of the redshift evolution of equations (1) and (2) is a good description to the data. For each line in each spectrum, I calculated the ratio, Q_i, of the number of lines expected between z_{min} and the redshift of the line to the total number of lines expected. Then the average of the Q_i's for each QSO, Q_{qso}, was computed. For a good fit, the Q_{qso}'s for the objects in the sample should be drawn from a distribution with mean 0.5. The one-sample Wilcoxon test (LWT, Appendix A) was used to test this. In all cases the the functional form of equations (1) or (2) is acceptable: in the worst case, the data is inconsistent with the functional form of equations (1) or (2) at the 2 σ level.

I now discuss the results from the comparison of various subsamples of the total sample. First, samples were constructed to examine the effect of the spectral resolution on γ. Table 4 shows that there is little effect on γ, W^*, or A_0 when lines of "L" resolution are excluded. This supports the conclusions of Parnell & Carswell (1988), who argued from simulations that the value of γ is almost independent of spectral resolution. On the other hand, it may result from the fact that the "L" spectra contribute relatively few of the lines in the sample (see Table 3).

In order to avoid the proximity effect, BDO excluded lines within $\Delta z = 0.15$ of the emission-line redshift, whereas LWT excluded lines within 8 Mpc from z_{em}. The effective difference between these two assumptions is that for the lowest redshift

QSOs, the entire observed spectrum above the atmospheric cutoff is excluded in the first case, whereas in the second case, some portion is used in the fit. Table 4 shows that even though one might think that the lowest redshift objects have a lot of leverage in the determination of γ, the results for γ under the two assumptions were virtually the same.

In addition, several other subsamples were tried, with the results so similar to those given in Table 4, that they are not shown. In one case, the lines listed in Table 2 as "Possible" metal lines were excluded as well as those listed as sure "Identifications." In the second subsample, the highest and lowest redshift QSOs (1115+080 and 0000−263) were excluded from the fits. Finally, the echelle data of the five QSOs discussed above were included. In every case, the change in γ was less than 0.5 σ from the results listed in Table 4, compared to subsamples with otherwise the same criteria.

The only possible effect is a dependence of γ on the equivalent width threshold. For example, for the "M" resolution data only, the lines stronger than 0.32 Å have a best-fit $\gamma = 1.89 \pm 0.28$. By contrast, the lines with 0.16 Å $< W_\lambda <$ 0.32 Å have $\gamma = 0.47 \pm 0.35$. The probability that γ is the same for the two samples can be estimated with the K-S test. The P_{KS} that γ = 1.89 for the weak line sample is 1.5×10^{-5} and the P_{KS} that γ = 0.47 for the strong line sample is 4.2×10^{-4}. Thus this difference in γ is very significant. However, it is possible that this trend is *not* evidence for a physical effect, but rather results from some subtle line blending or variable signal-to-noise problem. Note, that this trend of decreasing γ with decreasing W_λ is in the *opposite* sense of the trend found by Giallongo (1991) in the higher resolution echelle data (none of which is included here). However, Trevese, Giallongo, & Camurani 1992 have argued that this trend is expected if line blending is significant. Clearly a very large, high-resolution sample would be ideal to verify any trend.

The value of W^* is virtually independent of sample with a best-fit value of ∼0.27 Å. This is consistent with previous work (e.g., Murdoch et al. 1986; Rauch et al. 1992). A representative plot of the equivalent width distribution, shown in Figure 2, was derived from sample 11, and includes "M" resolution lines with equivalent widths greater than 0.16 Å. The data has been binned for presentation and is normalized to the total number of lines at z = 2.44 (see Murdoch et al. 1986, their eq. [6]). The best fit is shown by the solid line, and is a very good description of all of the data. In particular, there is no obvious break or other feature in the distribution, which might suggest a characteristic equivalent width at which the evolutionary parameter γ might change on purely empirical grounds.

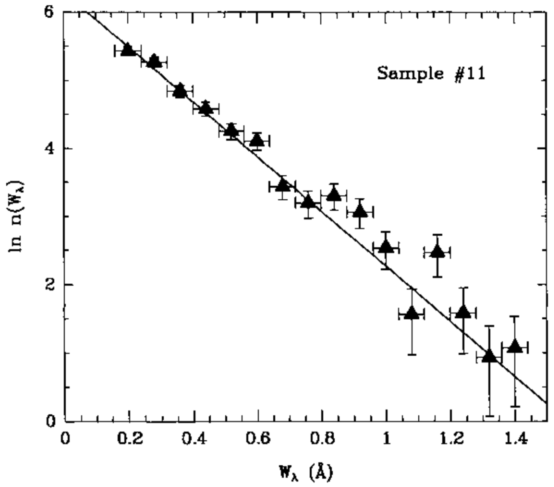

FIG. 2.—Distribution of rest equivalent widths for sample 11, normalized to the number density of absorbers at z = 2.44. Data have been binned for presentation only. *Solid line* shows fit of eq. (1) with W^* = 0.27 Å.

Figure 3 shows plots of the logarithm of the number of lines per unit redshift, log (dN/dz), versus log $(1 + z)$, where the data have been binned for presentation. The maximum likelihood fit of equation (2) is shown as a dotted line. Figures 3*a*, 3*b*, and 3*c* show the results for W_{thr} = 0.32 Å (sample 9), W_{thr} = 0.16 Å (sample 11) and 0.32 Å $> W_\lambda >$ 0.16 Å (sample 18), respectively. Figure 4*a* shows a histogram of the number of QSOs as a function of redshift included in sample 9. Figure 4*b* shows the number of lines as a function of redshift included in sample 9. The statistics are well determined for $2.2 < z < 3.2$, with some information over a more extended range, $1.6 < z < 4.0$.

LWT suggested that a "broken" power law fitted the data better than the single power law of equation (2). Although the results of the Kolmogorov-Smirnov test show that a single power law is an acceptable to the data for all subsamples, the points in Figure 3*a*, for example, are suggestively curved. To investigate any significant curvature, I have considered subsamples at high and low redshift separately. The simplest question to then ask is, does the best fit to the lines at high redshift predict the number of lines seen at low redshift? For the strong lines, the answer is yes. If I fit the lines with $z_{abs} > 2.5$ and $W_\lambda >$ 0.32 Å then $\gamma = 1.46 \pm 0.58$ and A_0 = 9.93 (sample 21.a in Table 4). For $z < 2.5$, these parameters predict 322 lines and 306 are seen. For the weak lines, however, if one fits the $z > 2.5$ data, then $\gamma = -0.205 \pm 0.560$ and A_0 = 169.3 (sample 22a in Table 4). Then one predicts that 556 lines should have been seen in the $z < 2.5$ sample, but 373 were seen, a 9.5 σ difference. The weak lines alone (0.16 Å $< W_\lambda <$ 0.32 Å, samples 23a and 23b in Table 4), show a similar discrepency. The lines with $z > 2.5$ have $\gamma = -2.05 \pm 0.93$ (sample 23a); a simple extrapolation predicts that 360 lines should have been seen with $z < 2.5$, but 181 were actually observed. Similar results occur if one considers other redshift divisions suggested by Figure 3, e.g., z = 2.16 [which corresponds to log $(1 + z) = 0.5$].

One can also ask if the best-fit γ for the high-redshift sample describes the redshift distribution of the lines in the low-redshift sample. Results are given in Table 4. For lines with $W_\lambda >$ 0.32 Å, the data for $z > 2.5$ has $\gamma = 1.46 \pm 0.58$ (sample 21a), whereas for $z < 2.5$, $\gamma = 3.76 \pm 0.81$ (sample 21b). The K-S probability that γ = 1.46 describes the low-redshift data is P_{KS} = 0.073, an acceptable fit. Thus, for the W_{thr} = 0.32 Å, there is no evidence for a change in slope in the log dN/dz versus log $(1 + z)$ relation. However, for the W_{thr} = 0.16 Å sample, the best fit γ's are significantly different. For the high-redshift lines, $\gamma = -.205 \pm 0.56$ (sample 22a), whereas the low-redshift lines give $\gamma = 2.63 \pm 0.67$ (sample 22b). The P_{KS} that $\gamma = -0.205$ for the low-redshift sample is 0.0018. That is, the best-fit γ for the $z > 2.5$ lines does not describe the redshift

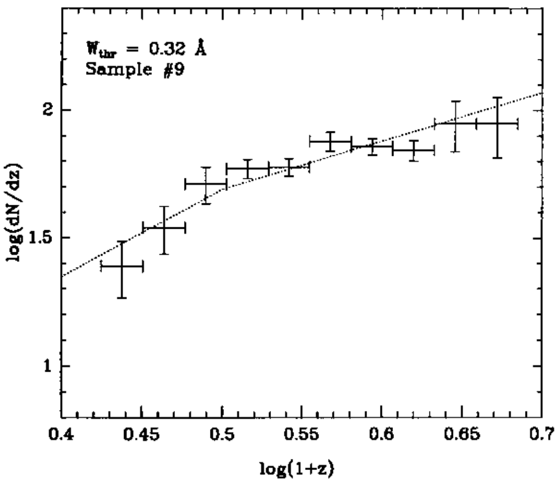

FIG. 3*a*

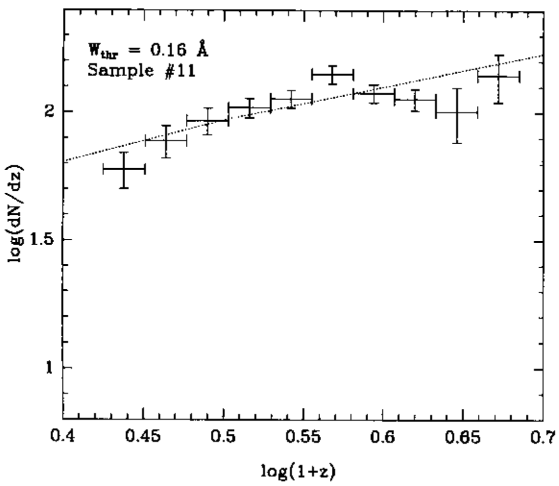

FIG. 3*b*

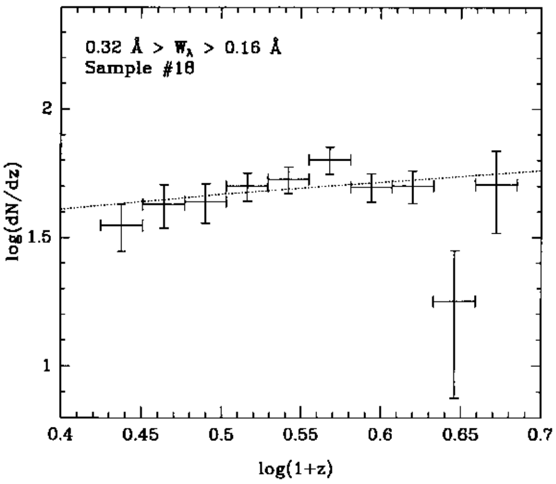

FIG. 3*c*

FIG. 3.—(*a*) log (dN/dz) vs. log ($1 + z$) for sample 9, that is, $W_{\rm thr}$ = 0.32 Å. *Dotted line* shows best fit of eq. (2) with $\gamma = 1.89$. (*b*) log (dN/dz) vs. log ($1 + z$) for sample 11, that is, $W_{\rm thr}$ = 0.16 Å. *Dotted line* shows best fit of eq. (2) with $\gamma = 1.32$. (*c*) log (dN/dz) vs. log ($1 + z$) for sample 18, that is, lines with 0.16 Å < W < 0.32 Å. Dotted line shows best fit of eq. (2) with $\gamma = 0.475$.

distribution of the $z < 2.5$ lines. Similarly, for weak lines only (0.16 Å < W_λ < 0.32 Å), $\gamma = -2.05 \pm 0.90$ for lines with $z > 2.5$. For $z < 2.5$, $\gamma = 1.61 \pm 0.94$, and the probability that $\gamma = -2.05$ for $z < 2.5$ is unacceptably small, $P_{\rm KS} = 9.5 \times 10^{-4}$. In all, the data are consistent with no evolution, or an *increase* in dN/dz over the no-evolution rate from $z \approx 4$ to $z \approx 2.5$, and then modest evolution in the other direction from $z \approx 2.5$ to $z \approx 1.6$. Again, any trends in the weak line sample may be due to subtle line blending and not some physical process. However, the effects are very significant in the line lists as they stand.

An equivalent way to think of these results is to describe the evolution in terms of a change in the equivalent width distribution with redshift. From Table 4, W^* is different for the high- and low-redshift samples at the 2.5 σ level in the sense that the distribution steepens at lower redshift. These two distributions are plotted in Figure 5. Clearly, it is of interest to search for a more significant effect in a larger sample.

To summarize this section, the best-fit $\gamma = 1.89 \pm 0.28$ for lines stronger than 0.32 Å (sample 9), and $\gamma = 1.32 \pm 0.24$ for lines stronger than 0.16 Å (sample 11). There is a significant trend of decreasing γ with decreasing equivalent width limit, or in other words, a change in the equivalent width distribution with redshift. There is no significant curvature in the log dN/dz versus log ($1 + z$) relation for the strong lines, but some steepening of γ at $\sim z = 2.5$ for the weak ones.

3.3. *Comparison with Previous Results*

The most striking result of the previous section is that the evolutionary parameter γ is smaller than that reported by BDO or LWT, and in fact for $W_{\rm thr}$ = 0.16 Å, γ is consistent with the *no evolutionary* value. By contrast, for $W_{\rm thr}$ = 0.36 Å, BDO found $\gamma = 2.36 \pm 0.40$ and LWT found $\gamma = 2.75 \pm 0.29$, whereas for the same criterion, I find $\gamma = 1.85 \pm 0.27$ (sample 13 in Table 4). More recently, Rauch et al. (1992) found $\gamma = 1.68 \pm 0.80$ for a high-resolution echelle sample (for $W_{\rm thr}$ = 0.36 Å), which is completely independent from the sample here. My result is consistent with the echelle sample (although the error in γ for the echelle sample is large), but does not appear to be consistent with the steep value of γ found by LWT. Figure 6 shows the K-S distribution of my data (sample 13, $W_{\rm thr}$ = 0.36 Å). The predicted distributions for the best-fit $\gamma = 1.85$ and LWT's $\gamma = 2.75$ are shown. The LWT $\gamma = 2.75$ is strongly ruled out, with $P_{\rm KS} = 5.9 \times 10^{-5}$. Note that the "no evolution" value of $\gamma = 1$ yields $P_{\rm KS} = 0.013$ and is in fact *not* ruled out. The origin of the descrepancy with the LWT results is not clear, but given the larger, more homogeneous sample on which Table 4 is based, the smaller value of γ may be more reliable. In light of the discussion in the previous section, it could be that γ is a function of redshift, and since the sample here includes a larger number of objects at $z \approx 3$, the best-fit γ to all redshifts comes out smaller. In fact, the LWT sample by itself gives a value of $\gamma = 1.64 \pm 0.37$ for lines with $z > 2.1$, and $\gamma = 1.97 \pm 0.52$ for $z > 2.5$.

One implication of a small value of γ is that more clouds are expected at $z = 0$ than previously thought. First results from

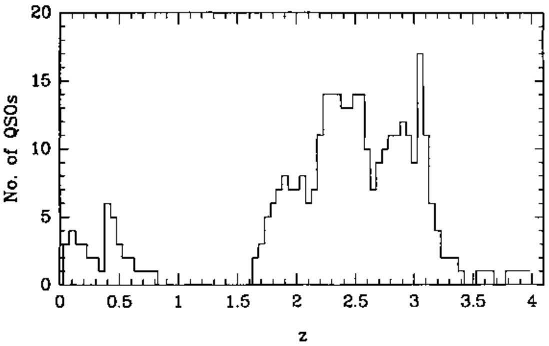

FIG. 4a

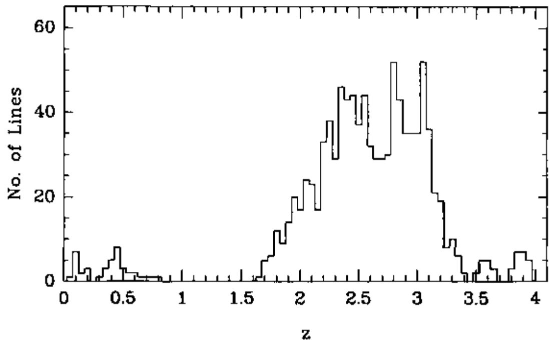

FIG. 4b

FIG. 4.—(*a*) Histogram of number of QSOs contributing lines to sample 9 (W_{thr} = 0.32 Å) as a function of absorption-line redshift. (*b*) Histogram of the number of lines included in sample 9 as a function of absorption-line redshift.

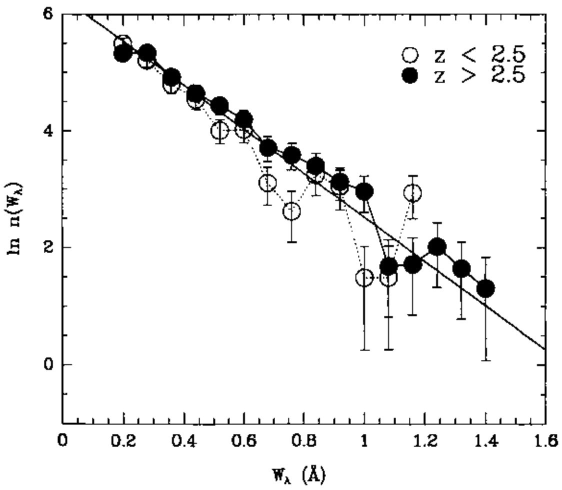

FIG. 5.—Distribution of equivalent widths, as in Fig. 2. Open circles: $z < 2.5$; *solid circles:* $z > 2.5$. Solid line shows maximum likelihood fit from Fig. 2.

the *Hubble Space Telescope* revealed unidentified absorption lines in the far UV spectrum of 3C 273 (z_{em} = 0.158), apparently implying the existence of Lyα forest clouds at $z \approx 0$ (Bahcall et al. 1991; Morris et al. 1991). These authors have noted how the extrapolation of the ground-based data to $z \approx 0$ underestimates the number of lines seen. However, for W_{thr} = 0.36 Å, there are very few lines in the published *HST* spectra and so these authors have adopted γ derived from the W_{thr} = 0.36 Å samples, and assumed a form for the equivalent width distribution, in order to predict the number of lines expected with smaller equivalent widths. If instead $\gamma \approx 1$, especially for small equivalent widths, then this approach would underestimate the predicted numbers of lines.

It is interesting to compare the ground-based results with the data from the larger sample *HST* Quasar Absorption Line Key Project (Bahcall et al. 1993; Schneider et al. 1993). They have published FOS spectra of 11 QSOs with comparable spectra resolution and signal-to-noise to the data in this sample. The *HST* sample contains 43 lines with $W_\lambda > 0.32$ Å, and $z_{em}-z_{abs} > 0.15$. The redshift coverage (z_{abs} = 0 to 1) is shown in Figure 4. Figure 7 shows a plot of log (dN/dz) versus log (1 +

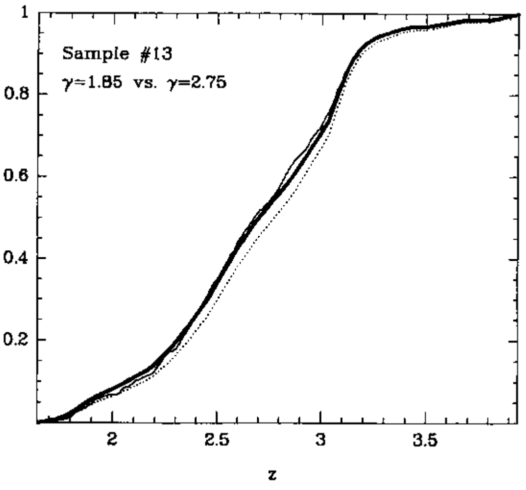

FIG. 6.—K-S distribution, for lines in sample No. 13. Bold line shows predicted distribution, solid line shows results for γ = 1.85, and dotted line shows results for γ = 2.75.

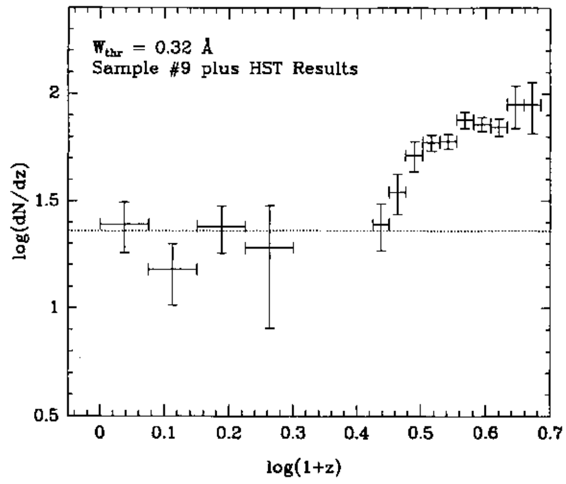

FIG. 7.—log (dN/dz) vs. log (1 + z) for sample No. 9 and results from *HST* reported by Bahcall et al. 1993. *Dashed line* shows γ = 1.89 fit to sample No. 9 only; *dotted line* shows LWT's fit with γ = 2.75.

z) for the *HST* sample and sample 9. The best fit to the *HST* data alone is $\gamma = 0.0 \pm 1.0$ and is shown in Figure 7 as a dotted line. The values of dN/dz for the high-redshift clouds do not fall on this line, which suggests some sort of fundamental change in the nature of the clouds at $z \approx 1.5$ (see speculations in Weymann 1993). Formally, however, a single power law fits all the data adequately with $\gamma = 1.29 \pm 0.14$ (and $A_0 = 12.23$) and a K-S probability $P_{KS} = 0.31$. This is not all that different from the "no evolution" value of $\gamma = 1$, and in fact $\gamma = 1$ is a marginally acceptable fit, with $P_{KS} = 0.014$.

Of course, in even the simplest models for the clouds, γ is not expected to be constant with redshift (e.g., Bechtold et al. 1987; Ikeuchi & Turner 1991; Charlton, Salpeter, & Hogan 1993), but is expected to decrease at lower z. Any interesting constraint on theoretical models from this sort of analysis awaits a larger sample at all redshifts, including the high redshifts studied with the ground-based data.

4. Lyα FOREST STATISTICS FOR $z_{abs} \approx z_{em}$

4.1. *Spectrophotometry of the Total Sample*

In order to model the proximity effect as enhanced photoionization of the clouds by the QSO's EUV photons, it is necessary to have an estimate of the QSO continuum flux at the Lyman limit, f_ν. Many of the objects in the absorption-line sample have spectophotometry available. In Table 5, I list two estimates for f_ν. First, for 35 of the QSOs in the sample, the observed flux at the Lyman limit in the QSO's rest frame has been measured directly; I list this as f_ν(obs) in column (3). This value serves as a lower limit to the flux a cloud near the QSO could see, since in virtually all cases, f_ν(obs) is depressed by line blanketing of absorption lines from intervening material and may also be depressed by reddening by dust contained in material along the line of sight (Pei et al. 1991).

A second estimate of f_ν was made from extrapolating a power law from the measured continuum flux at a rest wavelength of $\lambda 1450$ (which is relatively absorption free) to the Lyman limit. Table 5 lists the apparent magnitude of each QSO continuum at $\lambda 1450$ in the rest frame (converted from f_λ, assuming that the star α Lyra has $f_\lambda = 4.645 \times 10^{-9}$ ergs s^{-1} cm^{-2} Å^{-1}), and the observed spectral index, α. The spectral index was derived from a fit to the continuum between Lyα and C IV emission lines, or in some cases, included the continuum redward of C IV. In any event, α was measured for the continuum redward of the Lyα emission line in order to avoid line blanketing by the Lyα forest. Then f_ν was derived from extrapolating $m(\lambda 1450)$ to the Lyman limit. When a measurement for α was not available, I adopted $\alpha = 0.66$, a typical value (Sargent, Steidel, & Boksenberg 1989; Pei et al. 1991). In cases where $m(\lambda 1450)$ had not been measured, an extrapolation from the V-magnitude listed in Table 1 was made, assuming $\alpha = 0.66$.

Finally, the value of f_ν was corrected for Galactic reddening, using the values of $N_{\rm H\,I}$ listed in Table 5 and assuming that

$$\frac{N_{\rm H\,I}}{E(B-V)} = 4.8 \times 10^{21} \quad \text{atoms cm}^{-2}\ \text{magnitude}^{-1} \quad (3)$$

from Bohlin (1978), and adopting the reddening curve of Seaton (1979). Corrections for reddening were typically small, but neglecting them could in principle introduce a systematic effect with redshift, which would be unfortunate. The resulting dereddened f_ν is listed in Table 5, column f.

In previous work (e.g., LWT), an empirical K-correction given by Evans & Hart (1977) & Tytler (1987) was used to convert visual magnitudes as listed in Hewitt & Burbidge (1987, 1989) to f_ν. Unfortunately, the expressions for the K-corrections given by Evans & Hart (1977) do not extend beyond $z = 2.5$, and the magnitudes listed in Hewitt & Burbidge are not always reliable. Figure 8 shows the flux estimated from spectrophotometry as described above (Table 5, col. f), compared to the flux computed from the K-corrections of Evans & Hart. The dotted lines enclose the region for which the difference between the two estimates would be 40%, the uncertainty claimed by Tytler (1987) and LWT. Clearly, many of the points lay outside this range, and the flux estimated in this way differs substantially from the flux derived here. A plot of f_ν(obs) versus the flux derived from the K-corrections shows a similar scatter.

Figure 9 shows the distribution with redshift of Lyman continuum luminosity for the QSOs in my sample, where the luminosity, L_ν, is defined as

$$L_\nu = 4\pi d_L^2 \frac{f_\nu}{(1 + z_{em})} \quad (4)$$

and d_L is the luminosity distance

$$d_L = \frac{c\{q_0 z + (q_0 - 1)[(1 + 2q_0 z)^{1/2} - 1]\}}{q_0^2 H_0} \quad (5a)$$

for $q_0 > 0$ and

$$d_L = \frac{c}{H_0} z(1 + z/2) \quad (5b)$$

for $q_0 = 0$. In Figure 9 and the rest of this paper, I assume $H_0 = 75$ km s^{-1} Mpc^{-1} and $q_0 = \frac{1}{2}$. The QSOs in LWT are denoted by crosses, and the rest of the QSOs listed in Table 5 are shown

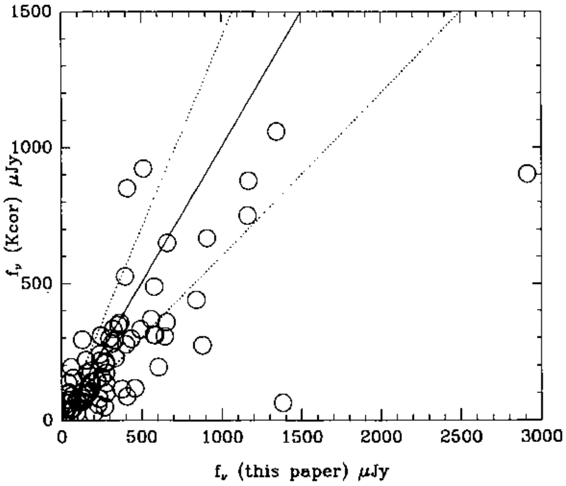

FIG. 8.—Comparison of f_ν as tabulated in Table 5 with f_ν computed from the K-corrections of Evans & Hart (1977). Solid line represents equality of two values; dotted lines represent the envelope of 40% uncertainties.

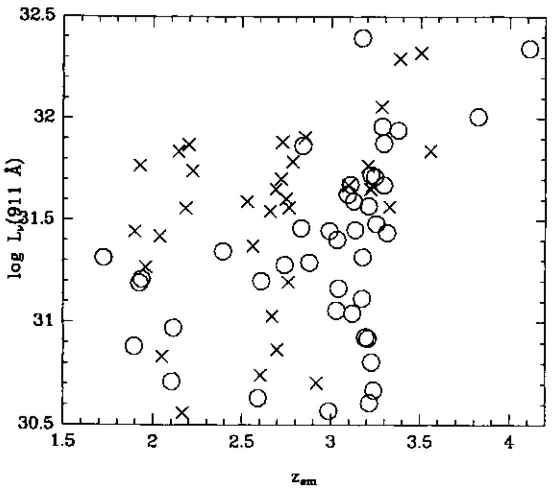

FIG. 9.—Luminosity at the Lyman limit vs. (for $H_0 = 75$ km s^{-1} Mpc^{-1} and $q_0 = \frac{1}{2}$) vs. redshift. Crosses represent QSOs from literature; *open circles* represent QSOs in this paper.

as open circles. While it is still unfortunately the case that the highest redshift QSOs have the largest luminosities, this work has filled in the region between $z = 2.9$ and 3.4 with relatively "low" luminosity objects.

In Table 5, I also list the radio loudness, RL, of each object, defined as

$$\mathrm{RL} = \log\,[S(5\ \mathrm{GHz})/S(\lambda 1450)]\,, \qquad (6)$$

where S(5 GHz) is the radio flux at an observed frequency of 5 GHz, and $S(\lambda\ 1450)$ is the flux at 1450 Å in the rest frame. When 5 GHz radio measurements were not available, the radio flux was extrapolated from other radio measurements, assuming a power law of spectral index $\alpha = -0.3$.

4.2. *Number of Lines with* $z_{abs} \approx z_{em}$

In this section, I compare the number of lines observed with $z_{abs} \approx z_{em}$ with the number of lines expected from the fits described in § 3. I consider only the QSOs listed in Table 3 which have no metal-line system within 8 Mpc of the QSO redshift. I restrict the sample to the QSOs with resolution class "M," i.e., better than 100 km s^{-1} FWHM. This is because, even though the inclusion of the lower resolution data did not seem to effect the global value of γ, the proximity effect may be more sensitive to spectral resolution, since it depends on the presence or lack of only a few lines per QSO.

The resulting sample contains 47 QSOs with redshifts between 1.9 and 3.8. Of these, 15 are from the literature, and 32 newly observed in this paper. There are 22 QSOs with radio information, of which 16 are radio loud, i.e., have RL > 1.

First, it is of interest to show that in this new sample there actually is evidence for a proximity effect, i.e., a deficit of lines near the QSO redshift. The simplest way to do this is to compare the predicted number of lines, N_{pred}, stronger than some equivalent width limit threshold, W_{thr}, obtained by integrating equation (1) over W and z, with the observed number of lines, N_{obs}. In Figure 10 I plot $\Delta N/N_{pred}$ versus ΔR, where

$$\Delta N = N_{pred} - N_{obs}\,, \qquad (7)$$

and ΔR is the luminosity distance from the QSO, defined by

$$\Delta R = \frac{\Delta z}{(1 + z_{em})^{5/2}} \frac{2250}{h_0}\ \mathrm{Mpc}\,, \qquad (8)$$

where $h_0 = H_0/75$ km s^{-1} Mpc^{-1}. Figure 10*a* shows the results for $W_{thr} = 0.32$ Å (with $\gamma = 1.89$ and $A_0 = 5.62$) and Figure 10*b* shows the results for $W_{thr} = 0.16$ Å (with $\gamma = 1.32$, $A_0 = 20.23$). Note that only 33 QSOs had $W_{thr} \leq 0.16$ Å. The vertical error bars on each point are $(N_{obs})^{1/2}/N_{pred}$; the values of the data points are listed in Table 6.

Both Figures 10*a* and 10*b* show that there is a significant deficit of lines, particularly at $\Delta R < 3$ Mpc. The $\Delta R = 0$–3 Mpc point in Figure 10*a*, for example, is 7.6 σ different from zero, the value expected for $\Delta N/N_{pred}$, if there were no proximity effect. The same bin in Figure 10*b* is 5.3 σ different from zero.

While the difference between the deficit for the $W_{thr} = 0.32$ Å sample and the $W_{thr} = 0.16$ Å sample is not great in the ΔR = 0 to 3 Mpc bin, it is suggestive that the inclusion of the weaker lines made the deficit weaker, albeit at the 2 σ level. In Figure 10*c*, $\Delta N/N_{pred}$ versus ΔR is plotted for lines with rest equivalent width W_λ, which have 0.32 Å > W_λ > 0.16 Å. The percentage deficit in the first bin is 0.208 ± 0.149 compared to 0.57 ± 0.073, a 2.4 σ difference. It would be interesting to look for this effect in a larger data set. The lack of as strong a proximity effect for the weak lines as seen for the strong lines is expected in the photoionization model, especially when curve of growth effects are taken into account. For example, Dobrzycki & Bechtold (1991a) show simulations of the effect of a QSO on the Lyα forest, as the intrinsic QSO luminosity is increased (their Fig. 2). First, the weak lines, which presumably are at or near the linear part of the curve of growth, disappear, and the strong, highly saturated lines become weak, but are still detectable (see Fig. 11). Finally, when the QSO influence is very strong, all lines disappear.

The lack of a strong proximity effect for the weak lines is not merely a consequence of the flat value of γ for the weak lines; if blending is severe, the true γ of the underlying distribution may be larger. If one assumes that the strong line $\gamma = 1.89$ applies to the weak lines the effect on Figure 10*c* is to translate all points up by ~0.1. The values of $(N_{pred}-N_{obs})/N_{pred}$ for the first two bins (ΔR = 0–6 Mpc) are then 2 σ different from 0. Note, however, that $\gamma = 1.89$ is a very poor fit to the line distribution even after A_0 is adjusted to fit the total number of lines. For $\gamma = 1.89$ for the weak line sample, $A_0 = 4.42$, but $P_{KS} = 1.5 \times 10^{-5}$. Clearly, higher resolution data for a large sample is necessary to properly sort out what is going on for the weak lines.

Next, I ask whether the deficit depends on QSO redshift, radio loudness, or Lyman limit luminosity. Figure 12*a* shows $\Delta N/N_{pred}$ versus ΔR for QSOs with $z_{em} \geq 3$ and $z_{em} < 3$ separately and $W_{thr} = 0.32$ Å; Figure 12*b* is the same, except for $W_{thr} = 0.16$ Å, and Figure 12*c* shows the result for lines with 0.16 Å < W_λ < 0.32 Å. In all plots, it is evident that the proximity deficit is present at levels consistent with the results of the whole sample, for both $z_{em} \geq 3$ and $z_{em} < 3$.

Next, in Figure 13 I plot $\Delta N/N_{pred}$ versus ΔR for the radio-loud QSOs only (*solid circles*), which I define as those objects in Table 5 which have radio loudness RL > 1. Again Figure 13*a* shows the result for $W_{thr} = 0.32$ Å, Figure 13*b* shows the

TABLE 5

SPECTROPHOTOMETRIC PROPERTIES OF QSOs IN ABSORPTION-LINE SAMPLE

QSO (a)	N_{HI} (b)	f_ν(obs) (c)	m(1450Å) (d)	α (e)	f_ν (f)	RL (g)	Refn. (h)
0000-263*	1.60	60	17.45	1.09	586	quiet	1,2
0001+087	5.36	65	18.48	0.29	270		1
0002+051	3.87	325	16.27	1.01	663	2.00	3,4
0002-422	1.00		17.68		301	<0.87	5,6,7
0014+813*	14.23	(200)	(16.69)	1.60	909	2.55	1,8
0029+073*	3.82	100	17.67	1.07	377		1
0058+019	3.05		16.86	0.80	405	<0.18	9,4
0100+130	4.27		17.4	0.84	401	<0.69	10,4
0114-089	4.27	80	18.00	0.75	317		1
0119-046*	4.35				435	2.81	11,12
0122-380	1.81		16.63		582	<0.76	7,13
0142-100	2.70		16.88		658	<-0.6	14,15
0207-003	2.44	290	17.09	0.57	607		1
0216+080	6.77	60	18.62	0.70	184		1
0237-233	2.23	370	16.53	0.17	844	2.51	3,16
0256-000	5.26	100	17.95	0.58	408		1
0301-005	5.90	100	18.16	0.89	280		1
0302-003*	6.03	110	17.79	0.63	459		1
0334-204	3.02	40	18.30	0.65	227		1
0347-383	1.76	141	18.14	0.75	248	<0.90	5,7,13,17
0421+019	10.57		18.48	0.85	131	2.93	18,19
0424-131*	3.95		18.78	1.5	59	2.72	12,20
0449-135*	6.69	(30)	(18.16)	1.49	279		1
0453-423	1.00		17.53		323	<0.81	7,13
0636+680	5.73	(390)	(16.46)	1.20	1382	3.52	1,21
0731+653	4.22	65	18.68	0.66	160	2.58	1,22
0831+128	3.94		18.5	0.66	161		10
0836+113	4.15				97		23
0837+109	4.44				178		24
0848+163*	3.01				108	<1.20	4,25
0854+191	2.98				144	1.88	4,25
0905+151	3.74				72		23
0913+072	3.84				495		23
0938+119	3.04	17.8	20.23	0.32	46	3.06	12,26
1017+280	2.66	582	15.57		1344		27
1033+137	3.38				253	loud	28
1054-034	3.84		18.04		165	<0.18	29
1101-264	5.53	602	16.01		1164	0.07	29,30,31
1115+080*	3.61	483	16.07	1.04	648	<-0.6	32,33
1151+068	1.60		18.5	0.90	130		10
1159+124*	2.29		17.20	0.22	881		24
1206+119	2.13				279		23
1208+101	1.71		17.85	1.26	333		24
1213+093	1.58				436		34
1215+33	1.30		18.5	0.32	154	2.32	10,35
1225-017	2.44				221		36
1225+317	1.23	862	15.88	0.62	1169	2.20	12,37,38,39
1228+076	1.62				275	<0.76	4,40
1247+267	1.04	550	16.56	0.80	513	-0.6	32,33
1315+472	1.18		19.7		43		41
1334-005	2.06				560		36
1337+113	1.95		19.7	1.51	36		10
1347+112*	2.05		19.2	0.96	65		10
1400+114	1.82				115		23
1402+044	2.19	10	20.01	0.74	45	3.40	26,42
1410+096	1.90				134		23
1442+101	1.72	126	18.36	0.38	278	3.38	26,43,44
1451+123	1.77				157		23
1510+115*	2.66				92		24
1511+091*	2.43				143		24
1512+132	2.75				64		23
1548+092	3.44				336		23
1601+182*	3.38		20.41		34		45
1602+178*	3.38	8.4	20.08	1.22	32		24
1607+183	3.50				163	2.82	28,46
1614+051	4.76	16	20.95		22	3.93	47,48
1623+268	3.53				54		40
1623+269*	3.53		17.5	0.31	413		10
1700+642	1.00	3684	15.26	0.55	2913		49
1738+350	2.81	8	20.76	0.66	25	3.09	1,4
2126-158	4.85	105	17.08	1.43	577	3.22	1,50
2204-408	1.00	68	18.01	1.0	239	1.72	7,13,17
2206-199	2.40		17.8	0.81	240		10
2233+131	4.92	65	18.37	0.82	235		1
2233+136	4.86	45	18.64	0.54	199		1
2311-036	4.01	40	19.27	0.68	92		1
2348-011	3.53	18	19.23	1.21	72		1

[a] QSO name; as in Table 3, an asterisk indicates a metal-line system within 8 Mpc of the emission-line redshift.

[b] Galactic $N_{H\,I}$, in units of 10^{20} cm^{-2}, from Stark et al. 1989 except for 0002+051, 0237−233 and 2126−158 which are taken from Elvis, Lockman, & Wilkes 1989.

[c] Observed flux at the Lyman limit in the QSO rest frame, in microjanskies. Values in parentheses have been corrected for Galactic reddening by authors listed in footnote h.

[d] Observed apparent magnitude at 1450 Å in the QSO rest frame. Values in parentheses have been corrected for Galactic reddening by authors listed in footnote h.

[e] Observed spectral index between C IV and Lyα emission lines, when available; otherwise, the spectral index derived in the vicinity of λ1450. All values have *not* been corrected for Galactic reddening.

[f] Extrapolated flux at the Lyman limit in the QSO rest frame in microjanskies, corrected for Galactic reddening. Derived from m(1450 Å) and α given in footnotes d and e where possible; when no α measured, assumed α = 0.66; when no m_ν(1450 Å) available, used V-magnitude given in Table 1.

[g] Radio loudness, defined as the log [S(5 GHz)/S(λ1450 Å)]. See text.

[h] REFERENCES.—(1) Sargent, Steidel, & Boksenberg 1989; (2) McMahon 1991; (3) Bechtold et al. 1984; (4) Sramek & Weedman 1980; (5) Osmer 1980; (6) Smith et al. 1981; (7) Smith & Wright 1980; (8) Kuhr et al. 1991; (9) Oke, Neugebauer, & Becklin 1970; (10) Pei, Fall, & Bechtold 1991; (11) Adam 1985; (12) Barthel et al. 1988; (13) Osmer & Smith 1980; (14) MacAlpine & Feldman 1982; (15) Surdej et al. 1988; (16) Wills 1975; (17) Osmer 1979; (18) Richstone & Schmidt 1980; (19) Pauliny-Toth et al. 1972; (20) Baldwin & Netzer 1978; (21) Pauliny-Toth et al. 1978; (22) Barthel 1984; (23) Hazard et al. 1986; (24) this paper; (25) Pica & Smith 1983; (26) Oke & Korycansky 1982; (27) Bechtold 1994; (28) Wills, Wills, & Douglas 1987 as reported in Hewitt & Burbidge 1987; (29) Osmer & Smith 1977; (30) Boksenberg & Snijders 1981; (31) Abraham, deMedeiros, & Kaufmann 1984; (32) Green et al. 1980; (33) Kellerman et al. 1989; (34) Foltz et al. 1987; (35) Veron et al. 1981; (36) MacAlpine & Williams 1981; (37) Snijders, Pettini, & Boksenberg 1981; (38) Wilkerson et al. 1978; (39) Battistini, Bracessi, & Formiggini 1974; (40) Sramek & Weedman 1978; (41) Schmidt, Schneider, & Gunn 1986; (42) Feigelson, Isobe, & Kembhavi 1984; (43) Oke 1974; (44) Gearhart et al. 1974; (45) Burbidge et al. 1985; (46) Bennett et al. 1986; (47) Wilkes et al. 1983; (48) Shimmins, Bolton, & Wall 1975; (49) Reimers et al. 1989; (50) Bolton et al. 1975.

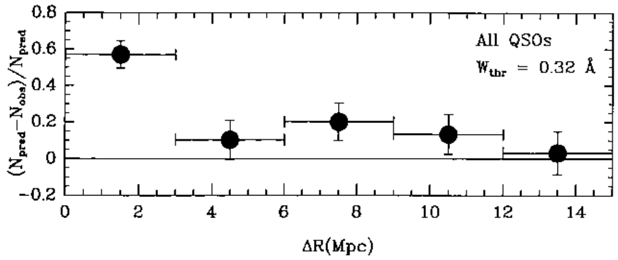

FIG. 10a

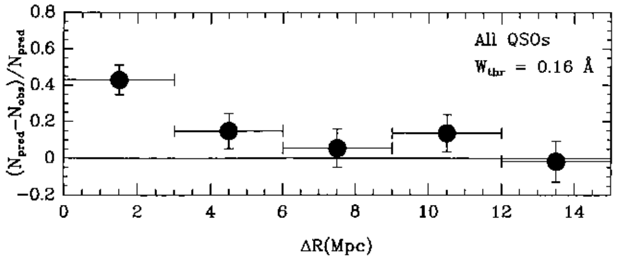

FIG. 10b

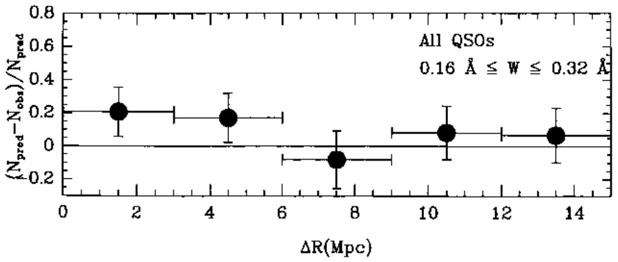

FIG. 10c

FIG. 10.—$(N_{pred}-N_{obs})/N_{pred}$ vs. ΔR(Mpc) h_{75} for all QSOs in sample. (a) $W_{thr} = 0.32$ Å. (b) $W_{thr} = 0.16$ Å. (c) Only lines with $0.16 \le W \le 0.32$ Å.

TABLE 6

N_{obs} VERSUS N_{pred} NEAR THE QSOs

ΔR (Mpc)	N_{obs}	N_{pred}	$(N_{pred}-N_{obs})/N_{pred}$
$W_{thr} = 0.32$ Å, $\gamma = 1.89$, $A_0 = 5.62$; 46 QSOs			
0.0–3.0	33	76.8	0.57 ± 0.075
3.0–6.0	71	79.2	0.10 ± 0.10
6.0–9.0	61	76.4	0.20 ± 0.10
9.0–12.0	64	73.9	0.13 ± 0.11
12.0–15.0	70	72.3	0.032 ± 0.12
$W_{thr} = 0.16$ Å, $\gamma = 1.32$, $A_0 = 20.23$; 33 QSOs			
0.0–3.0	49	85.9	0.43 ± 0.081
3.0–6.0	77	90.5	0.15 ± 0.097
6.0–9.0	82	86.7	0.054 ± 0.10
9.0–12.0	72	83.4	0.13 ± 0.10
12.0–15.0	83	81.6	−0.017 ± 0.11

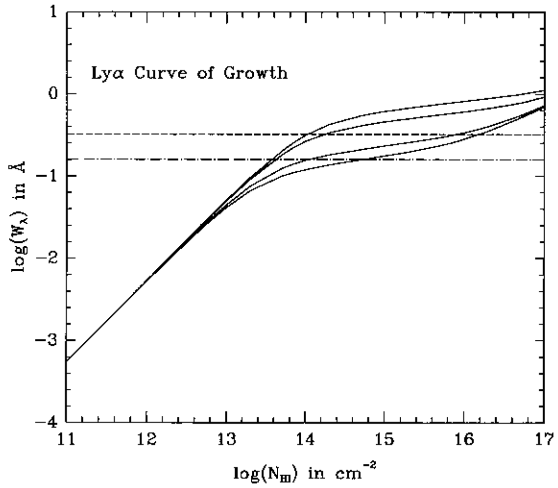

FIG. 11.—Lyα curve of growth. Rest equivalent width of H I Lyα in angstroms as a function of column density, N_{HI} in cm^{-2}. From uppermost to lowest curves, T = 100,000 K, 50,000 K, 10,000 K, and 5000 K. *Dashed line* corresponds to $W_\lambda = 0.32$ Å; dot-dashed line corresponds to $W_\lambda = 0.16$ Å.

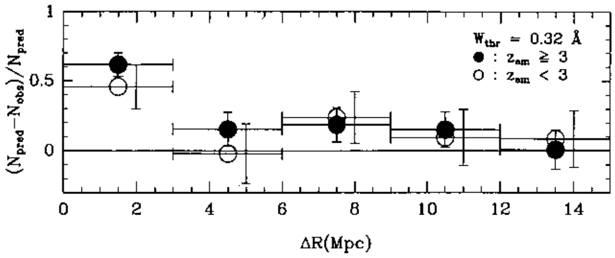

FIG. 12a

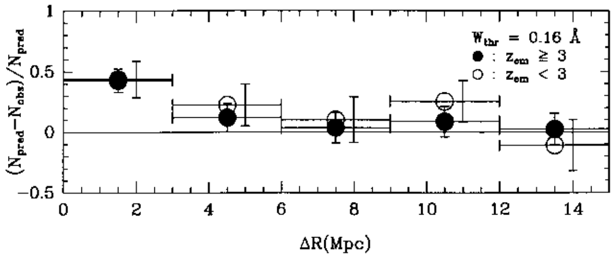

FIG. 12b

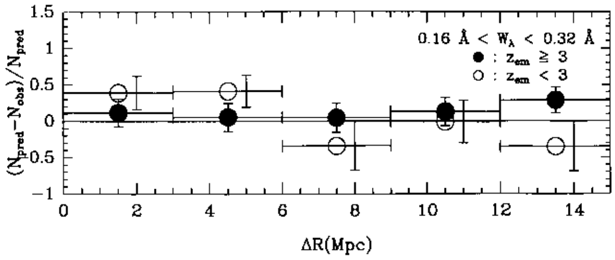

FIG. 12c

FIG. 12.—Dependence of $(N_{pred}-N_{obs})/N_{pred}$ on QSO redshift, z_{em}. *Solid circles:* QSOs with $z_{em} \ge 3$; *open circles:* QSOs with $z_{em} < 3$. Vertical error bars are displaced horizontally for presentation only. (a) $W_{thr} = 0.32$ Å. (b) $W_{thr} = 0.16$ Å. (c) Lines with $0.16 \text{ Å} < W_\lambda < 0.32$ Å.

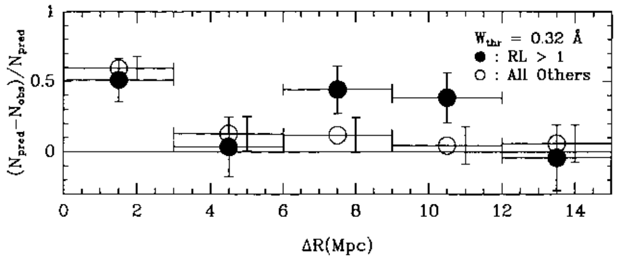

FIG. 13*a*

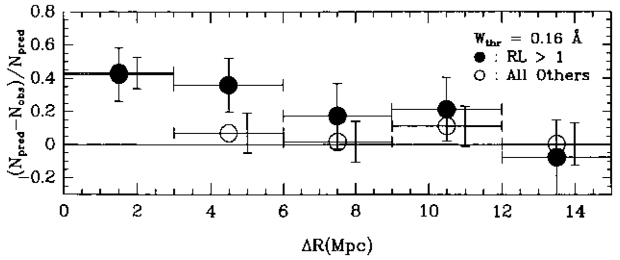

FIG. 13*b*

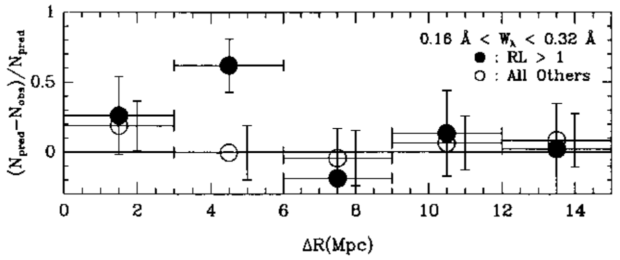

FIG. 13*c*

FIG. 13.—Dependence of $(N_{\rm pred}-N_{\rm obs})/N_{\rm pred}$ on radio loudness. *Solid circles:* QSOs known to be radio loud, i.e., RL > 1; *open circles:* all others. Vertical error bars displaced for presentation only. (*a*) $W_{\rm thr} = 0.32$ Å. (*b*) $W_{\rm thr} = 0.16$ Å. (*c*) 0.16 Å $< W_\lambda <$ 0.32 Å.

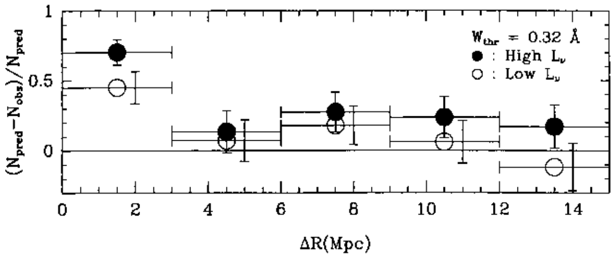

FIG. 14*a*

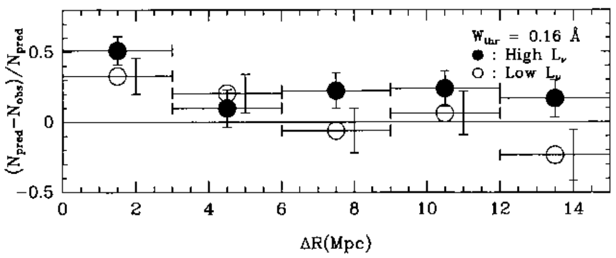

FIG. 14*b*

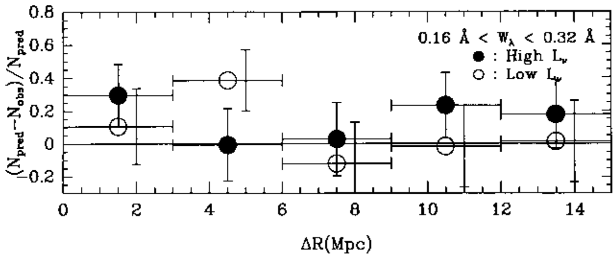

FIG. 14*c*

FIG. 14.—Dependence of $(N_{\rm pred}-N_{\rm obs})/N_{\rm pred}$ on QSO Lyman limit luminosity. *Solid circles:* QSOs with log $(L_\nu) >$ 31.6 ergs s^{-1} Hz^{-1}; *open circles:* QSOs with log $(L_\nu) <$ 31.6 ergs s^{-1} Hz^{-1}. Vertical error bars for the low-luminosity QSOs are displaced horizontally for presentation only. (*a*) $W_{\rm thr} = 0.32$ Å. (*b*) $W_{\rm thr} = 0.16$ Å. (*c*) 0.16 Å $< W_\lambda <$ 0.32 Å.

result for $W_{\rm thr} = 0.16$ Å, and Figure 13*c* shows the result for lines with 0.16 Å $< W_\lambda <$ 0.32 Å. For comparison, all other QSOs are shown as open circles. This includes objects which are known to have RL < 1 and others for which no radio measurements are available. The plots show that the radio-loud objects show a proximity effect at a level consistent with the other QSOs, within large errors. In any event, they do not contribute all of the proximity deficit. Unfortunately, the number of QSOs known to be radio loud is small: only 15 in the $W_{\rm thr} = 0.32$ Å sample and 11 in the $W_{\rm thr} = 0.16$ Å sample.

Finally, if the proximity effect is caused by enhanced photoionization of the clouds by the QSO itself, then one expects that the strength of the deficit should depend on the QSO's Lyman limit luminosity at a fixed distance ΔR from the QSO, all other things being equal. The elegant way devised by BDO to do this is discussed below; here we crudely divide the total sample into a high- and low-luminosity sample and compare the resulting $\Delta N/N_{\rm pred}$ versus ΔR plots. Figure 14 shows the result. In Figure 14*a* I take $W_{\rm thr} = 0.32$ Å, in Figure 14*b*, $W_{\rm thr} = 0.16$ Å, and in Figure 14*c*, lines with 0.16 Å $< W_\lambda <$ 0.32 Å. Solid circles show the result for QSOs with log $(L_\nu) >$ 31.6 ergs s^{-1} Hz^{-1} and open circles shows QSOs with log $(L_\nu) <$ 31.6 ergs s^{-1} Hz^{-1}. This value of log (L_ν) was chosen to give approximately equal numbers of QSOs in the high- and low-luminosity samples. For the $W_{\rm thr} = 0.32$ Å sample, the low-luminosity QSOs show a less-pronounced deficit for $\Delta R < 3$ Mpc than the high-luminosity QSOs, although the difference is only significant at the 2 σ level ($\Delta N/N = 0.703 \pm 0.089$ for high L_ν versus 0.450 ± 0.115 for low L_ν). The same plot including the weak lines (Fig. 14*b*) shows less of an effect. In a gross way then, these plots support the photoionization model for the proximity effect, where at least qualitatively, one expects an increasing effect with luminosity at a fixed distance.

Previously, BDO and LWT had looked for a dependence of ΔN on luminosity by considering ΔN for individual QSOs as a function of log (L_ν). In order to compare the results here with their work, Figures 15 and 16 show such plots for lines with $\Delta z < 0.15$ with respect to $z_{\rm em}$, for $W_{\rm thr} = 0.32$ Å and 0.16 Å, respectively. Also plotted is the dependence of ΔN on $z_{\rm em}$. Note that at $z = 3$, $\Delta z = 0.15$ corresponds to $\Delta R \approx 10$ Mpc. LWT used an intermediate cutoff of $\Delta R = 8$ Mpc. The disadvantage of plotting individual points for each QSO is that only a few lines per QSO are expected anyway, even in the absence of the proximity effect, so there is a lot of scatter just because of the small numbers. The plots of $\Delta N/N_{\rm pred}$ versus the same quantities are very similar and are not shown.

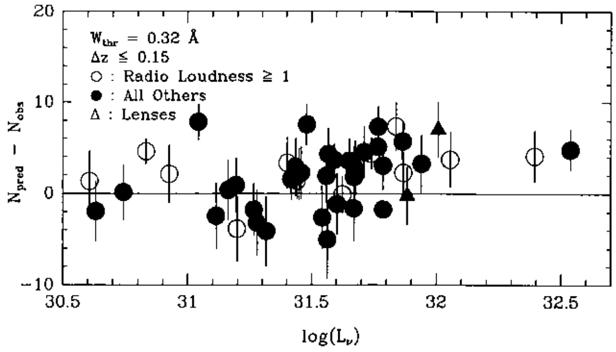

FIG. 15*a*

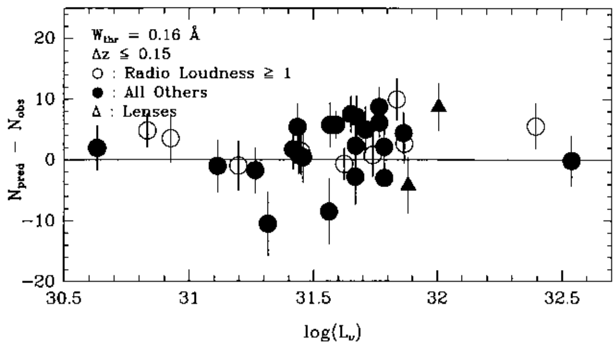

FIG. 16*a*

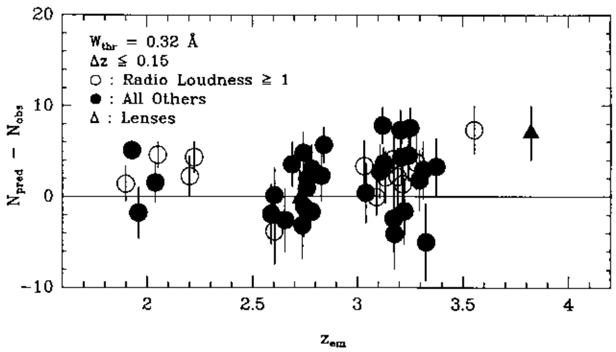

FIG. 15*b*

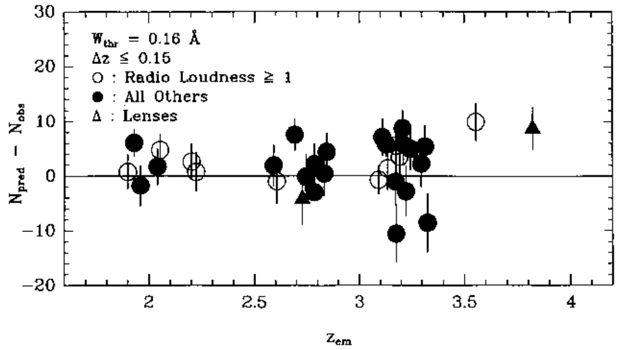

FIG. 16*b*

FIG. 15.—$\Delta N = N_{pred} - N_{obs}$ for lines within $\Delta z = 0.15$ of z_{em}, for $W_{thr} = 0.32$ Å. Points with no error bars have $N_{obs} = 0$. *Open circles:* known radio loud QSOs; *filled circles:* all others, except two radio-quiet gravitational lenses, which are shown as *filled triangles*. (*a*) ΔN vs. Lyman limit luminosity. (*b*) ΔN vs. z_{em}.

FIG. 16.—$\Delta N = N_{pred} - N_{obs}$ for lines within $\Delta z = 0.15$ of z_{em}, for $W_{thr} = 0.16$ Å. Points with no error bars have $N_{obs} = 0$. Symbols same as Fig. 15. (*a*) ΔN vs. Lyman limit luminosity. (*b*) ΔN vs. z_{em}.

Figures 15 and 16 show that there is a significant proximity effect at all redshifts, in that most of the points have $N_{pred} - N_{obs} > 0$, indicating a systematic deficit of lines. To see if the deficit correlates with QSO luminosity or redshift, the nonparametric Spearman rank-order correlation coefficient was computed for the data shown (e.g., Press et al. 1986, p. 489). Results are presented in Table 7, where I list the probability that the data deviate from the null hypothesis that there is *no* correlation. Small numbers indicate the presence of a significant correlation. Apparently, there is little correlation between L_ν and z_{em} for this sample. There is however a significant correlation of ΔN or $\Delta N/N_{pred}$ with L_ν for the strong lines. There is no significant correlation of ΔN with z for any sample. Again, these results are in qualitative agreement with the expectations of the photoionization model. The lack of a correlation between L_ν and ΔN in the LWT sample might have resulted from the way they estimated L_ν (see Fig. 8), and the smaller range of L_ν represented in their sample (see Fig. 9).

Several authors have noted that γ of equation (1) decreases as lines closer and closer to the QSO are included (e.g., LWT, their Fig. 3). No such trend is found to be significant in this data set. For the lines with $W_\lambda > 0.32$ Å, the lines within $\Delta z = 0.15$ of z_{em} have $P_{KS} = 0.12$ for being described by $\gamma = 1.89$ (the fit for $z_{abs} \ll z_{em}$), an acceptable fit. For $W_\lambda > 0.16$ Å, $P_{KS} = 0.013$ for the lines within $\Delta z = 0.15$ of z_{em} to be described by $\gamma = 1.32$, a marginally acceptable fit. For the weak lines only (0.16 Å $< W_\lambda < 0.32$ Å), the analogous K-S probability, $P_{KS} = 0.28$. In all cases, redshift dependence of the number of lines of the form $(1 + z)^\gamma$ is an acceptable description of the lines with $z_{abs} \approx z_{em}$.

Finally, the equivalent width distribution of the lines within $\Delta R = 3$ Mpc, normalized to $z = 2.44$, is shown in Figure 17. The solid line shows the best fit from Figure 2. The distribution for $z_{abs} \approx z_{em}$ does not differ dramatically from this line.

It is by now obvious that many of the results of this and the previous section might benefit from a more detailed, nonparametric treatment of the unbinned data. However, the purpose here was to look for the most obvious trends and postpone such a treatment for a subsequent paper.

To summarize this section, there is clear evidence for a deficit of Lyα forest lines near the QSOs for the sample presented here. Within $\Delta R = 3$ Mpc, the number of lines observed with rest equivalent width $W_\lambda \geq 0.32$ Å differs by at least 7 σ from the number of lines expected from fits to the lines with $z_{abs} \ll z_{em}$. Radio-loud objects show a deficit no stronger nor weaker than other QSOs. The deficit depends on L_ν (at least in the crude treatment presented here) and not on redshift. This last result supports a view that the proximity effect has something

TABLE 7

SPEARMAN RANK COEFFICIENT TEST PROBABILITIES

Sample	L_ν vs. z_{em}	L_ν vs. ΔN	L_ν vs. $\Delta N/N_{pred}$	z_{em} vs. ΔN	z_{em} vs. $\Delta N/N_{pred}$
W_{thr} = 0.32 Å	0.11	0.0015	0.0039	0.11	0.67
W_{thr} = 0.16 Å	0.35	0.065	0.15	0.16	0.72

to do with enhanced photoionization rather than some property of the QSO which evolves with redshift. There is no evidence for a change in the equivalent width distribution of the lines with $z_{abs} \approx z_{em}$, whose total numbers are depleted. I now discuss the photoionization model of BDO in more detail.

4.3. *Simple Photoionization Model*

BDO presented a photoionization model for the proximity effect and showed that, under various simplifying but reasonable assumptions, it fitted the available data well. In this section, I repeat their approach to the analysis with the enlarged sample, and show that their simple model again gives an acceptable fit to the data. In the next section, I discuss how some of the the conclusions reached here depend on the nature of the model assumptions.

4.3.1. *Dependence on z, L_ν, and Equivalent Width*

Following BDO, I consider the number of lines per comoving redshift interval, X_γ, where

$$X_\gamma = \int (1 + z)^\gamma dz\,. \tag{9}$$

If there were no proximity effect, then equation (2) would become

$$dN/dX\gamma = A_0\,. \tag{10}$$

However, assume that each cloud with H I column density N_0

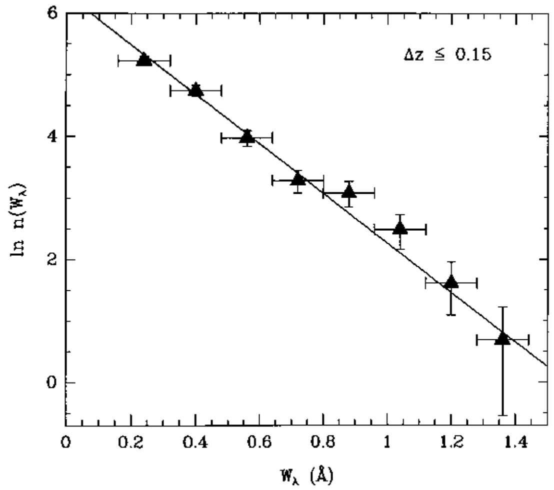

FIG. 17.—Distribution of equivalent widths for lines within $\Delta z = 0.15$ of the QSOs, normalized to $z = 2.44$. Maximum-likelihood best fit from Fig. 2 is shown as solid line.

in the absence of the QSO, instead has an H I column density $N_{\rm H\,I}$ given by

$$N_{\rm H\,I} = N_0(1 + \omega)^{-1}\,, \tag{11}$$

where

$$\omega = \frac{F_\nu^Q}{4\pi J_\nu}\,. \tag{12}$$

$J_\nu(z)$ is the diffuse background radiation at the Lyman limit at redshift z (in units of ergs cm^{-2} s^{-1} Hz^{-1} sr^{-1}) with which the clouds are in photoionization equilibrium, and

$$F_\nu^Q = \frac{L_\nu}{4\pi r_L^2} \tag{13}$$

is the local Lyman limit flux density (in units of ergs cm^{-2} s^{-1} Hz^{-1}) due to the QSO. The luminosity distance of the cloud from the QSO is r_L, and has already been given in equation (8).

Implicit in equations (11)–(13) are several assumptions. First, the clouds are assumed to be highly ionized, so that equation (11) is valid (Bechtold & Wolfe 1994). Also, the frequency dependence of J_ν for frequencies greater than the Lyman limit is assumed to be the same as that for the QSOs so that the ratio of ionization rates equals the ratio of the Lyman limit flux densities. This is not strictly true even if the background is predominantly comprised of the integrated background from QSOs (Bechtold et al. 1987) and is certainly not true if the background originates from hot stars in young galaxies (Miralda-Escude & Ostriker 1990; Songaila et al. 1990). These points will be discussed in § 4.4.3.

Equation (11) describes what happens to an individual cloud with initial column density N_0. If the distribution of H I column densities for the ensemble of clouds is a power law with index β, such that

$$\frac{dN}{dN_{\rm H\,I}} \propto N_{\rm H\,I}^{-\beta} \tag{14}$$

then the number above some column density limit, N_{thr}, is

$$N(N_{\rm H\,I} \geq N_{thr}) \propto N_{thr}^{-\beta+1} \tag{15}$$

The value of β has been found from high-resolution studies to be ~ 1.7 (Carswell et al. 1984; Atwood et al. 1985; Rauch et al. 1992). Barcons & Webb (1991) and Jenkins, Bajtlik, & Dobrzycki (1994) have drawn attention to the fact that $\beta \approx 1.7$ derived from column density limited samples is inconsistent with the value of $W^* \approx 0.28$ Å derived from equivalent width limited samples. This point is discussed further below.

In any event, equation (11) becomes

$$\frac{dN}{dX_\gamma} = A_0[1 + \omega(z)]^{-0.7}, \qquad (16)$$

where

$$\omega(z) = \frac{f_\nu}{4\pi J_\nu(z)} \frac{4z_Q^2(1 + z_Q/2)^2(1 + z)^6}{(1 + z_Q)[(1 + z_Q)^2 - (1 + z)^2]^2}, \qquad (17)$$

for $q_0 = 0$, and

$$\omega(z) = \frac{f_\nu}{4\pi J_\nu(z)} \frac{(1 + z)^5}{(1 + z_Q)} \left[\frac{(1 + z_Q)^{1/2} - 1}{(1 + z_Q)^{1/2} - (1 + z)^{1/2}}\right]^2 \qquad (18)$$

for $q_0 = 0.5$ (see BDO). In these equations, $J_\nu(z)$ and $\omega(z)$ are independent of H_0.

Thus, a plot of dN/dX_γ versus $\log(\omega)$ is a plot of line density versus distance from the QSO scaled according to the ratio of the Lyman limit flux of the QSO at that distance to J_ν at that redshift. The advantage of such a plot over plots such as Figure 10 is that the proximity effect should be the most evident. The disadvantage is that a model for $J_\nu(z)$ needs to be assumed to plot the data.

In the remainder of this section, I assume an EUV background, $J_\nu(z)$, consistent with the best-fit form of BDO and LWT, and consider the behavior of dN/dX_γ as other factors are varied. In the next section, I examine what limits on $J_\nu(z)$ are implied by the new data.

For $J_\nu(z)$, I take the form of BDO, their equation (20), (c.f. Ikeuchi & Ostriker 1986)

$$J_\nu = j_\nu(1 + z)^{3.5}[(1 + Z_{\rm on})^{1.2} - (1 + z)^{1.2}] \qquad (19)$$

with all quasars "turning on" at redshift $Z_{\rm on} = 4.0$ and $j_\nu = 8.17 \times 10^{-24}$ ergs cm^{-2} s^{-1} Hz^{-1} sr^{-1}. Of course, recently dozens of QSOs with $z > 4$ have been found, but in the redshift range relevant to the lines here, this $J_\nu(z)$ is a slowly varying function of z.

Figure 18 shows dN/dX_γ as a function of log (ω) for the QSOs in the total sample. Figure 18*a* is for lines with rest equivalent width threshold $W_{\rm thr} = 0.32$ Å; Figure 18*b* is for $W_{\rm thr} = 0.16$ Å. The Lyman limit flux for each QSO was taken from Table 5, column 6; i.e., it is the power-law extrapolation from redward of the Lyman limit. First of all, the data points in Figure 18*a* clearly are not consistent with the constant value $dN/dX_\gamma = 5.62$, which is expected if there were no proximity effect (eq. [10]). The χ^2 of the data compared to the constant value is 93.0 for seven points; in other words, the data have only a 3×10^{-15}% probability of being consistent with a constant value. For $W_{\rm thr} = 0.16$ Å, the χ^2 is 42.3 giving a 4.5×10^{-7}% probability of showing no proximity effect. The solid line in Figure 18 is the predicted curve from the photoionization model, equation (16). For Figure 18*a*, this is an entirely acceptable fit to the data, with $\chi^2 = 10.7$ for seven points. Including the weaker lines, however, in Figure 18*b*, results in $\chi^2 = 22.3$ for seven points, which is *not* a good fit. Figure 18*c* shows only those lines with rest equivalent width 0.16 Å $< W <$ 0.32 Å. For this subset of the data, $\chi^2 = 8.8$ for the no-proximity effect model, whereas $\chi^2 = 20.3$ for the ionization model. Thus, it appears that the proximity effect is strong for the strong lines, but weak lines show little proximity effect—at least for this J_ν model. A summary of the values for χ^2 for these and subsequent plots is given in Table 8. Also listed is the probability Q_χ that the value of χ^2 would be exceeded by chance if the model is correct (e.g., Press et al. 1986, p. 165). Small values of Q_χ indicate a bad fit.

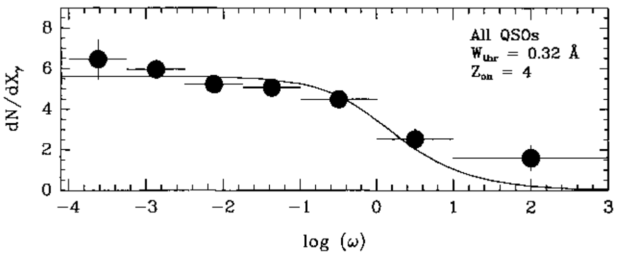

FIG. 18*a*

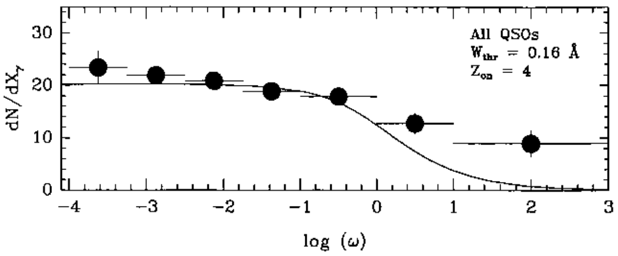

FIG. 18*b*

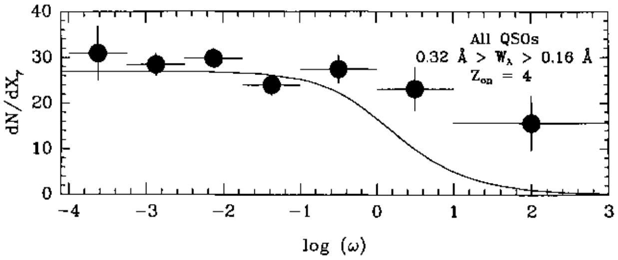

FIG. 18*c*

FIG. 18.—dN/dX_γ as a function of log ω, for all the QSOs in the sample. $J_\nu(z)$ is given by eq. (20) with $Z_{\rm on} = 4$; the flux at the Lyman limit for each QSO is the extrapolated value given in Table 5, col. f. The solid line is the predictions of the photoionization model, eq. (17). (*a*) $W_{\rm thr} = 0.32$ Å. (*b*) $W_{\rm thr} = 0.16$ Å. (*c*) 0.16 Å $< W < 0.32$ Å.

Next, I consider the dependence of the proximity effect on redshift. Figures 19 and 20 compare QSOs at $z_{\rm em} \geq 3$ with QSOs at $z_{\rm em} < 3$, for $W_{\rm thr} = 0.32$ Å and 0.16 Å respectively. The proximity effect is present at both low and high redshifts, and is consistent with the photoionization model. For the weak lines in the high-redshift QSOs (Fig. 20*a*), the fit is not great but still acceptable, with $Q_\chi = 0.018$.

Next, I consider the dependence of dN/dX_γ on intrinsic QSO luminosity. Figures 21 and 22 show dN/dX_γ versus log (ω) for high L_ν and low L_ν QSOs as defined in the previous section, for $W_{\rm thr} = 0.32$ Å, 0.16 Å, and lines with 0.16 Å $<$ $W_\lambda < 0.32$ Å. The plots for the strong lines are well fitted by the

TABLE 8

dN/dX_γ VERSUS ω FITS

Figure (a)	N_{points} (b)	χ^2(const) (c)	Q_χ(const) (d)	χ^2(ioniz) (e)	Q_χ(ioniz) (f)	Sample (g)
18.a	7	93.0	2.9E-17	10.7	0.15	All QSOs, W > 0.32 Å
18.b	7	42.3	4.5E-7	22.3	2.2E-3	All QSOs, W > 0.16 Å
18.c	7	8.8	0.27	20.3	5.0E-3	All QSOs, 0.32 Å > W > Å
19.a	7	79.7	1.6E-14	6.24	0.51	$z_{em} \geq 3$, W > 0.32 Å
19.b	7	27.1	3.2E-4	13.6	0.059	$z_{em} \geq 3$, W > 0.16 Å
19.c	7	9.5	0.22	16.9	0.018	$z_{em} \geq 3$, 0.32 Å > W > Å
20.a	7	22.1	2.4E-3	6.7	0.46	$z_{em} < 3$, W > 0.32 Å
20.b	7	16.9	0.018	9.9	0.20	$z_{em} < 3$, W > 0.16 Å
20.c	7	6.6	0.47	8.7	0.27	$z_{em} < 3$, 0.32 Å > W > 0.16 Å
21.a	6	79.8	4.0E-15	8.6	0.20	High L_ν, W > 0.32 Å
21.b	6	35.8	3.0E-6	18.9	4.3E-3	High L_ν, W > 0.16 Å
21.c	6	7.0	0.32	18.4	5.3E-3	High L_ν, 0.32 Å > W > 0.16 Å
22.a	7	40.3	1.1E-6	12.5	0.087	Low L_ν, W > 0.32 Å
22.b	7	14.0	0.051	9.2	0.24	Low L_ν, W > 0.16 Å
22.c	7	3.9	0.79	2.9	0.89	Low L_ν, 0.32 Å > W > 0.16 Å
23.a	7	90.3	1.1E-16	8.8	0.26	f_ν(obs), W > 0.32 Å
23.b	6	190.5	2.0E-38	4.4	0.62	f_ν(extrap), W > 0.32 Å
24.a	7	35.6	8.7E-6	2.8	0.91	Radio Loud, W > 0.32 Å
24.b	7	30.4	8.0E-5	4.8	0.69	Radio Loud, W > 0.16 Å
24.c	7	14.1	0.049	3.8	0.80	Radio Loud, 0.32 Å > W > 0.16 Å

[a] Figure in which sample appears.
[b] Number of bins used to compute χ^2.
[c] χ^2 with respect to the no proximity effect model (eq. [10]).
[d] Q_χ probability for χ^2(const). Small value indicates poor fit.
[e] χ^2 with respect to photoionization model (eq. [16]).
[f] Q_χ probability for χ^2(ionization). Small value indicates poor fit.
[g] Description of data included in fit. All entries have Ikeuchi-Ostriker models for J_ν with $Z_{on} = 4.0$. See text.

photoionization model, for both low- and high-luminosity subsamples. However, there are too many weak lines near the QSO in the high-luminosity objects (see Table 8). The origin of this is not clear, but it seems that the deviation of weak lines from the photoionization model depends on luminosity of the QSO rather than redshift (Fig. 21 and 22 vs. 19 and 20).

As shown above in Figure 8, the estimate of the QSO Lyman limit flux, f_ν, used here is somewhat different from that of previous authors, particularly LWT. Already from Figures 18–22, it is clear that this does not effect the results too much, since the photoionization model fits the data with the same J_ν model used by BDO and LWT. To make this point further, in Figure 23, I plot dN/dX_γ versus log (ω) for the 22 QSOs for which f_ν at the Lyman limit has been observed directly using f_ν(obs) (Table 5, col. c), and the same plot for the same QSOs, using instead the extrapolated value of f_ν (Table 5, col. f). These two estimates for f_ν should bracket the flux a cloud "sees," at least in the absence of amplification by gravitational lensing. There is no significant difference in the goodness of fit for these two estimates (see Table 8), suggesting that these models are not very sensitive to f_ν.

Finally, in Figure 24, I plot dN/dX_γ for the radio loud QSOs, those with RL > 1. As in Figure 13, the radio-loud QSOs show a strong proximity effect and are well fitted by the photoionization model, for all equivalent widths.

To summarize this section, the simple photoionization model of BDO is a good description of the strong lines ($W_\lambda >$ 0.32 Å) independent of QSO luminosity, redshift, or radio loudness. The weaker lines (0.32 Å > W_λ > 0.16 Å) deviate from the simple model for the high-luminosity QSOs, in that there are more than there should be. In all plots in this section, $J_\nu(z)$ was assumed to be of the form of Ikeuchi & Ostriker (1986) with a quasar turn-on redshift $Z_{on} = 4$ (see eq. [20]). In the next section, I investigate what constraints on $J_\nu(z)$ are implied by the data.

4.3.2. *Limits on $J_\nu(z)$*

As pointed out by Atwood et al. 1985, BDO and others, the simple photoionization model for the proximity effect described above can be used to place semi-empirical limits on J_ν as a function of redshift. In this section, I rederive such limits in the context of the simple model, for 4 forms of J_ν as function of z. The approach is to limit J_ν empirically, for several easy to parameterize forms, rather than to adopt a particular model for, say, the contribution of QSOs to J_ν. Then, as more refined estimates of the redshift dependence of the QSO luminosity function for $z > 3$ become available, computed values of J_ν can be compared to the parameterizations described here.

First, I made the simplest assumption, that J_ν is a constant with redshift, for z = 1.6–4. The plots of dN/dX_γ versus log (ω) were made, as described above, for W_{thr} = 0.32 Å and 0.16 Å, and various values of this constant. The χ^2 of the points (binned as in Fig. 18) was computed as a function of J_ν; the result is shown in Figure 25. The minimum χ^2 occurs at about the same J_ν for both samples; writing $J_\nu = J_{-21} \times 10^{-21}$

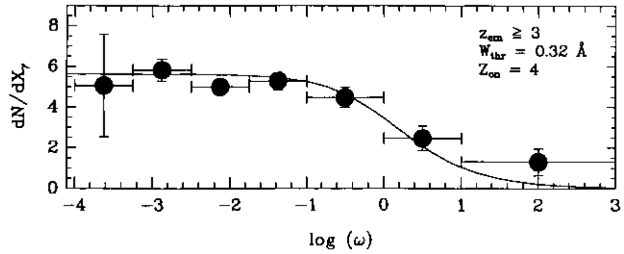

FIG. 19*a*

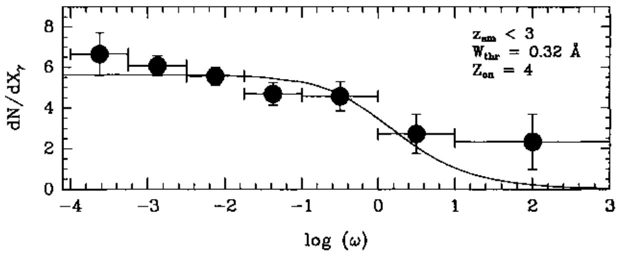

FIG. 20*a*

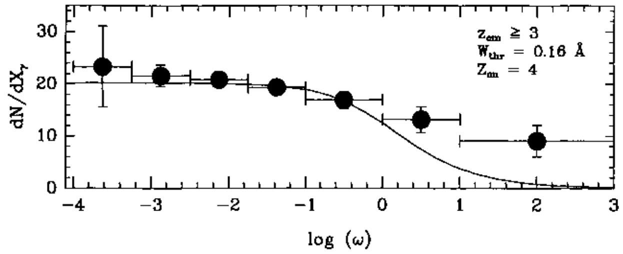

FIG. 19*b*

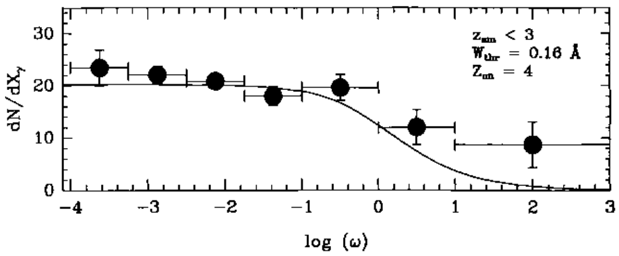

FIG. 20*b*

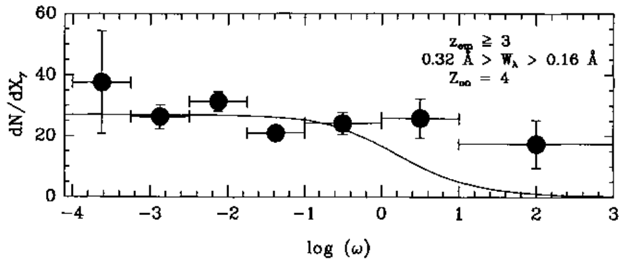

FIG. 19*c*

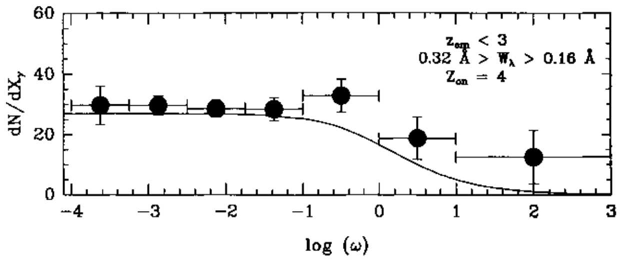

FIG. 20*c*

FIG. 19.—dN/dX_γ as a function of log (ω) for QSOs with $z_{em} \geq 3$. Otherwise, same as Fig. 18. (*a*) W_{thr} = 0.32 Å. (*b*) W_{thr} = 0.16 Å. (*c*) Lines with 0.16 Å < W_λ < 0.32 Å.

FIG. 20.—dN/dX_γ as a function of log (ω) for QSOs with $z_{em} < 3$. Otherwise, same as Fig. 18. (*a*) W_{thr} = 0.32 Å. (*b*) W_{thr} = 0.16 Å. (*c*) Lines with 0.16 Å < W_λ < 0.32 Å.

ergs cm^{-2} s^{-1} Hz^{-1} sr^{-1}, then the best-fit results if $J_{-21} = 3$. Figure 25 shows the uncertainty in J_{-21} to be about a factor of 3. Figure 26 shows dN/dX_γ versus log (ω) for the best-fit value. The value of χ^2 for these and other plots described in this section is given in Table 9. Note that the photoionization model for this J_ν gives an acceptable fit to the W_{thr} = 0.16 Å sample shown in Figure 26*b*.

Second, I took the form described by Ikeuchi & Ostriker (1986), and BDO, in which the QSOs "turn on" at redshift Z_{on}, and then undergo pure luminosity evolution. These models give a form for J_ν very close to more complicated treatments (e.g., Bechtold et al. 1987), and are simpler to parameterize (eq. [19]). The dependence of J_ν on redshift for these models and Z_{on} = 4, 5, 6, and 10 are shown in Figure 27*a*. For the redshifts relevant to this sample, all are slowly varying functions. The fits of the ionization model to the data are summarized in Table 9; representative plots are shown in Figure 28. For W_{thr} = 0.32 Å, Z_{on} = 5 gives the best fit, with Z_{on} = 4 and 6 giving acceptable fits, and Z_{on} = 10 giving a poor fit. For W_{thr} = 0.16 Å, Z_{on} = 6 gives the best fit, with Z_{on} = 4 excluded, and Z_{on} = 5 and 10 marginally acceptable. Thus, the models with $Z_{on} \approx 5$ to 6 give an acceptable fit to the data. Note that these models are slowly varying functions of z in the redshift range probed here, and are similar to the best-fit constant J_ν model described above (see Fig. 27*a*).

Third, I take four forms for J_ν which decline with redshift for high redshift. They are shown in Figure 27*b*. Models 1 and 2 are equal to the Ikeuchi & Ostriker (1986) models with Z_{on} = 4, for $z < 3$; at $z = 4$, they are 10 times and 100 times smaller, respectively. A smooth function was drawn between $z = 3$ and $z = 4$. Models 3 and 4 equal the Z_{on} = 4 models for $z < 2.5$; they are 100 times and 1000 times smaller at $z = 4$, respectively. For these, a smooth function was drawn between $z = 2.5$ and $z = 4$.

The fits to dN/dX_γ versus ω for the different $J_\nu(z)$ assumptions are summarized in Table 9. Representative plots are shown in Figures 29 and 30. For the strong lines (W_{thr} = 0.32 Å), none of the models fit the data very well, and model 4, which has the fastest cutoff, is strongly excluded. The weaker lines (W_{thr} = 0.16 Å) exclude all four models.

Finally, I try the following form for $J_\nu(z)$,

$$J_\nu(z) = J_{\nu 0}(1 + z)^j , \qquad (20)$$

since this is the form used in some analytical models for the clouds (Ikeuchi & Turner 1991; Charlton et al. 1993). For

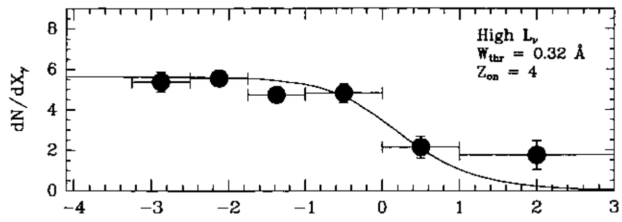

FIG. 21a

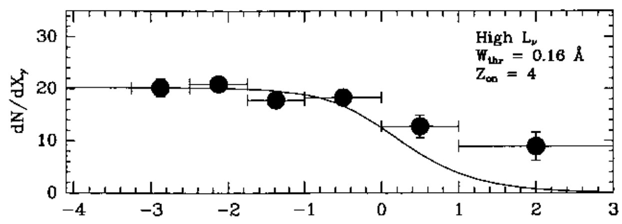

FIG. 21b

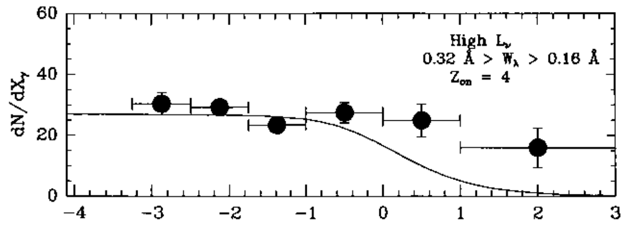

FIG. 21c

FIG. 21.—dN/dX_γ as a function of log (ω) for QSOs with Lyman limit luminosity, log (L_ν) > 31.6 ergs s^{-1} Hz^{-1}. Otherwise, same as Fig. 18. (a) W_{thr} = 0.32 Å. (b) W_{thr} = 0.16 Å. (c) Lines with 0.16 Å < W_λ < 0.32 Å.

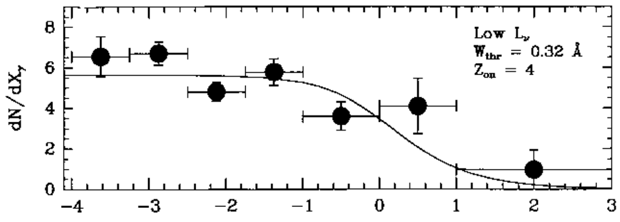

FIG. 22a

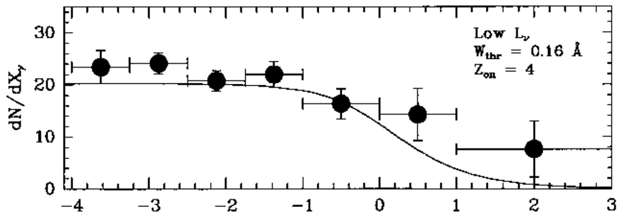

FIG. 22b

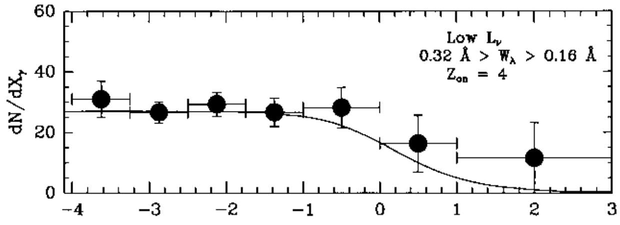

FIG. 22c

FIG. 22.—dN/dX_γ as a function of log (ω) for QSOs with Lyman limit luminosity, log (L_ν) < 31.6 ergs s^{-1} Hz^{-1}. Otherwise, same as Fig. 18. (a) W_{thr} = 0.32 Å. (b) W_{thr} = 0.16 Å. (c) Lines with 0.16 Å < W_λ < 0.32 Å.

various (integral) values of j, $J_{\nu 0}$ was varied to minimize χ^2 as above. For the W_{thr} = 0.32 Å sample, acceptable fits were obtained for $-7 < j < 4$. In Figure 27c, $J_\nu(z)$ is plotted for the extreme cases ($j = -7$ and log $J_{\nu 0} = -16.5$, and $j = 4$ and log $J_{\nu 0} = -23.0$). Not surprisingly, J_ν is fairly well constrained at $z \approx 3$, but the data do not constrain J_ν at $z \approx 2$ very well. A larger sample of absorption-line spectra at $z \approx 2$ would be of interest. Plots of log dN/dX_γ versus log ω are shown in Figure 31 for the best-fit $j = 4$ and $j = -7$ models.

How do these limits compare with previous results? Using the same method of analysis on different samples, both BDO and LWT found $J_{-21} \approx 1$ at $z \approx 3$. The best-fit value here is consistent with these results, although about a factor of 3 larger. Dobrzycki & Bechtold (1991b) derived $J_{-21} \approx 0.1$ at $z = 3.17$, based on a void in the Lyα forest, possibly induced by an intervening QSO. This value is uncertain, however, since the foreground QSO's emission may be anisotropic, or the void may be induced by some other QSO which has not yet been identified. Zuo (1992a,b) related theoretical models for the fluctuations in J_ν to observed fluctuations in $1/W_\lambda$ for the Lyα forest clouds and also found $J_{-21} \approx 0.1$. As Miralda-Escude & Ostriker 1990 have emphasized, these estimates of J_ν are lower bounds, given that other effects, such as quasar winds or inho-

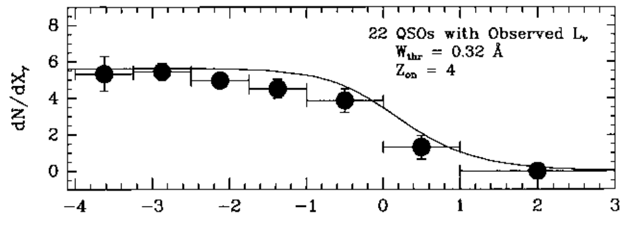

FIG. 23a

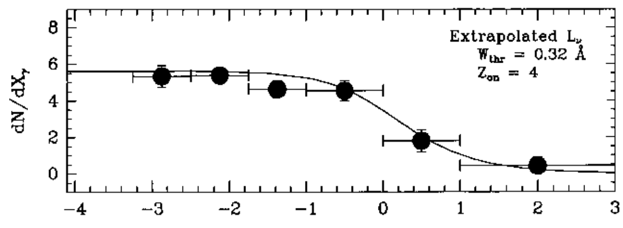

FIG. 23b

FIG. 23.—dN/dX_γ as a function of log (ω) for two estimates of the Lyman limit luminosity and W_{thr} = 0.32 Å. Otherwise, same as Fig. 18. (a) The 22 QSOs with observed L_ν available (Table 5, col. c). (b) The same 22 QSOs, however adopting the extrapolated value of L_ν (Table 5, col. f).

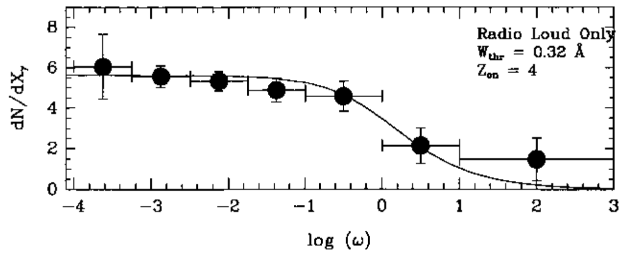

FIG. 24*a*

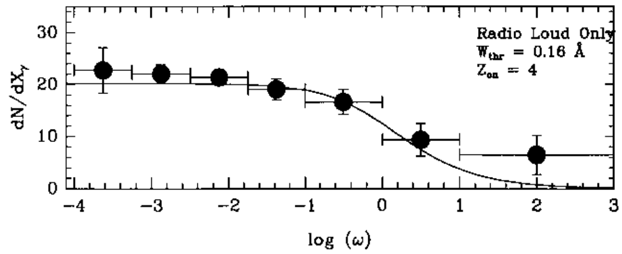

FIG. 24*b*

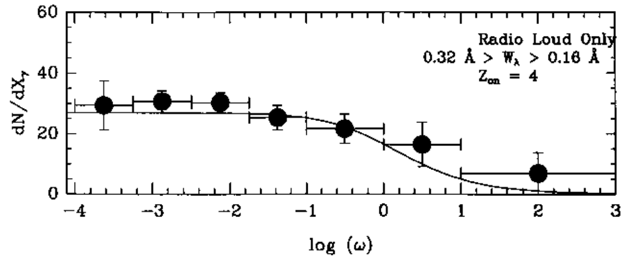

FIG. 24*c*

FIG. 24.—dN/dX_γ as a function of log (ω) for radio-loud QSOs only, i.e., RL > 1. Otherwise, same as Fig. 18. (*a*) W_{thr} = 0.32 Å. (*b*) W_{thr} = 0.16 Å. (*c*) Lines with 0.16 Å < W < 0.32 Å.

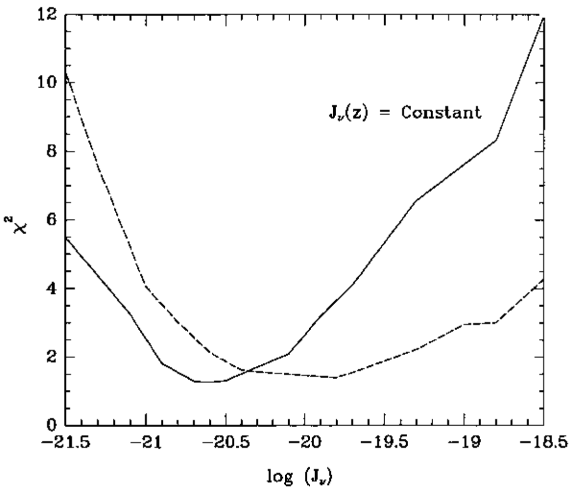

FIG. 25.—Reduced χ^2 for fits of dN/dX_γ vs. ω assuming log J_ν is constant with redshift, vs. the value of that constant, in units of ergs cm^{-2} s^{-1} Hz^{-1} sr^{-1}. *Solid line* is for W_{thr} = 0.32 Å sample, and *dashed line* is for W_{thr} = 0.16 Å.

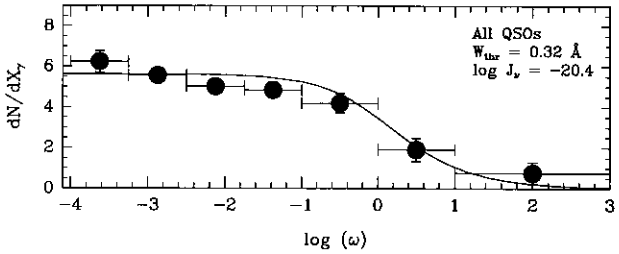

FIG. 26*a*

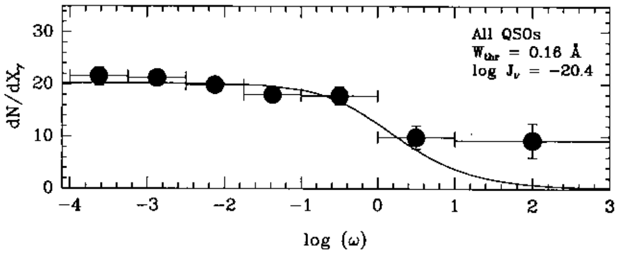

FIG. 26*b*

FIG. 26.—dN/dX_γ for all QSOs, and J_{-21} = 3, constant with redshift. Otherwise, same as Fig. 18. (*a*) W_{thr} = 0.32 Å. (*b*) W_{thr} = 0.16 Å.

mogeneities in the IGM near QSOs could compete with photoionization as a cause for any observed proximity effect.

Several authors have computed the contribution of likely ionizing sources to J_ν, which can then be compared to the estimates given above. Bechtold et al. (1987) found that J_ν decreases sharply at $z > 2.5$, and that $J_{-21} \approx 10^{-2}$ at $z = 3$. However, these calculations were done at a time when little was known about the high-redshift behavior of the QSO luminosity function, except that there was some sort of decline at $z > 2.5$; in fact, no QSOs were known at that time with $z > 3.8$. More recent calculations by Madau (1992) based on the luminosity functions of Boyle (1991), Irwin et al. (1991), and Schmidt, Schneider, & Gunn (1991) show that the decline is more gradual for redshifts $2 < z < 4$, with $J_{-21} \approx 0.1$ at $z = 3$. However, Fall & Pei (1993) emphasize that the contribution from QSOs computed by Madau (1992) and others is a lower limit since the contribution from intrinsically faint QSOs is poorly known and may be large. If high-redshift QSOs are obscured by dust, then both Miralda-Escude & Ostriker (1990) and Fall & Pei (1993) find that J_{-21} could easily be as high as 1 at $z \approx 3$, given plausible assumptions for the dust content of galaxies.

Young galaxies may emit enough EUV radiation from massive stars to be a significant contributor to J_ν as well (Bechtold 1987; Miralda-Escude & Ostriker 1990; Songaila et al. 1990). Miralda-Escude & Ostriker (1990) have contructed the most detailed models for the contribution from young galaxies to J_ν. They find that young galaxies can plausibly provide a background flux comparable to that from QSOs.

Clearly, limits on J_ν from the proximity effect at lower redshifts will be of interest, since the contribution from QSOs and young galaxies are in principle better understood at $z < 2$ than at higher redshifts.

TABLE 9

dN/dX_γ VERSUS ω FITS: DEPENDENCE ON J_ν

Figure (a)	N_{points} (b)	χ^2 (c)	Q_χ (d)	J_ν (e)	Sample (f)
26.a	7	9.6	0.21	Constant (-20.4)	W > 0.32 Å
26.b	7	11.4	0.12	Constant (-20.4)	W > 0.16 Å
18.a	7	10.7	0.15	$Z_{on} = 4$	W > 0.32 Å
28.a	7	11.7	0.11	$Z_{on} = 5$	"
28.b	7	14.7	0.040	$Z_{on} = 6$	"
28.c	7	25.0	7.7E-4	$Z_{on} = 10$	"
18.b	7	22.3	2.2E-3	$Z_{on} = 4$	W > 0.16 Å
	7	16.0	0.025	$Z_{on} = 5$	"
	7	12.7	0.080	$Z_{on} = 6$	"
	7	12.7	0.079	$Z_{on} = 10$	"
	7	14.8	0.039	Model #1	W > 0.32 Å
30.a	7	14.5	0.042	Model #2	"
	7	14.7	0.041	Model #3	"
29.a	7	27.4	2.8E-4	Model #4	"
	7	18.8	8.7E-3	Model #1	W > 0.16 Å
30.b	7	21.3	3.3E-3	Model #2	"
	7	30.3	8.3E-5	Model #3	"
29.b	7	47.6	4.2E-8	Model #4	"

[a] Figure in which sample appears.
[b] Number of bins used to compute χ^2.
[c] χ^2 with respect to photoionization model (eq. [16]).
[d] Q_χ probability for χ^2. Small value indicates poor fit.
[e] Adopted J_ν dependence of Z. Z_{on} = 4, 5, 6, and 10 are models described in Ikeuchi & Ostriker 1986, eq. (19) and Fig. 27*a*. Models 1, 2, 3, and 4 are empirical models shown in Fig. 27*b*. See text.
[f] Description of data included in fit.

4.4. *Additions to the Simple Model*

As mentioned above, in constructing the photoionization model of BDO, several simplifying assumptions were made. In this section I discuss how these assumptions and other factors may effect the limits on J_ν derived in the previous section. Where possible, I have tried to estimate quantitatively the relative magnitude of each effect.

4.4.1. *What Are the Systemic Redshifts of the QSOs?*

Detailed studies of QSO emission line profiles have shown that there are systematic velocity differences between the lines of high-ionization and low-ionization species (Gaskell 1982; Wilkes 1984). If the Balmer lines and Mg II λ2798 measure the true systemic redshift of the QSO, then the peak of the Lyα, C IV λ1549 and C III] λ1909 emission lines are shifted 1000 to 2000 km s^{-1} to the blue (Espey et al. 1989; Corbin 1990; Carswell et al. 1991b). The redshifts of the objects listed in Table 3 are mostly derived from Lyα, C IV and C III] which are seen in the optical, since the Balmer lines and the narrow forbidden lines such as [O III] λ5007 are shifted into the infrared. Hence, the redshifts used in the above analysis may be systematically low. For comparison, at $z = 3$, $\Delta z = 0.05$ corresponds to ΔR = 3.5 Mpc, and Δv = 3800 km s^{-1}. Thus, this is not a negligible consideration.

The fact that the redshift derived from the Lyα emission line is *lower* than the systemic redshift means that the proximity deficit discussed above is a *lower* limit to the actual deficit. If the shifts had been the other way, i.e., if the Lyα emission line redshifts were systematically too high, then one could imagine that a false proximity effect could have been induced. In fact, there are unidentified lines just redward of the peak of Lyα emission in some objects (see Table 2), which may be Lyα.

The value of J_ν derived from the photoionization model is affected. If the QSO systemic redshift is higher, then the clouds are farther away from the QSO, and J_ν is *lower* than estimated above. Quantitatively, if the redshifts are all actually 1500 km s^{-1} higher than the redshifts listed in Table 3, and if J_ν is a constant with redshift, then the best fit is obtained for $J_{-21} = 1$ for the W_{thr} = 0.32 Å sample. Interestingly, for this fit, $\chi^2 = 5.3$ for seven points ($Q_\chi = 0.62$), which is a better fit than any fit listed in Table 9. The plot of dN/dX_γ versus log (ω) is shown in Figure 32.

In summary, if the true QSO redshift has been underestimated, the likely effect is to decrease the estimate of J_ν from the proximity effect by about a factor of 3.

4.4.2. *Is $\beta = 1.7$?*

The power-law index for the neutral hydrogen column density, β, in equation (15) is measured by Voigt profile fitting of the Lyman series in echelle data. These studies find $\beta \approx 1.7$ (see Rauch et al. 1992 and references therein). However, the observed equivalent width distribution is not consistent with this result, assuming a plausible distribution of b-values (Barcons & Webb 1991; Jenkins et al. 1994). Possible explanations include either that the N(H I) distribution is flatter than β = 1.7 at low column densities, or that there is significant cluster-

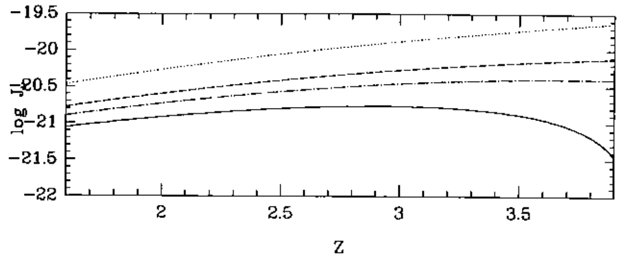

FIG. 27*a*

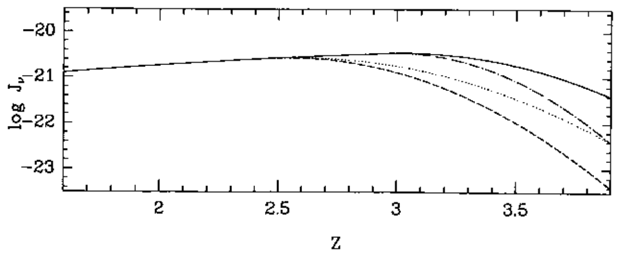

FIG. 27*b*

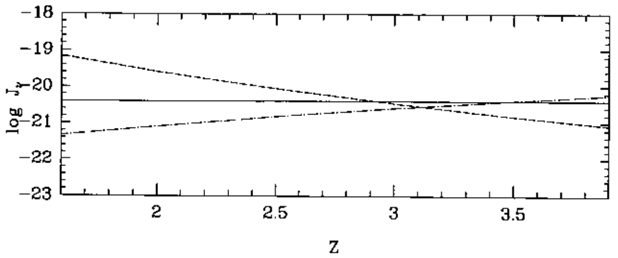

FIG. 27*c*

FIG. 27.—log J_ν (ergs cm^{-2} s^{-1} Hz^{-1} sr^{-1}) at the Lyman limit as a function of redshift. (*a*) Ikeuchi & Ostriker 1986 models for Z_{on} = 10 (*dotted line*), 6 (*dashed line*), 5 (*dot-dashed line*), and 4 (*solid line*). See eq. (19) in text. (*b*) Models No. 1 (*solid line*), No. 2 (*dot-dashed line*), No. 3 (*dotted line*), and No. 4 (*dashed line*). (*c*) $J_\nu(z) = J_{\nu 0}(1+z)^j$ for best fit to W_{thr} = 0.32 Å sample. Solid line shows $j = 0$ model [log ($J_{\nu 0}$) = −20.5], *dotted line* shows $j = -7$ model [log ($J_{\nu 0}$) = −16.5] and j = 4 model [log ($J_{\nu 0}$) = −23.0].

ing of lines on small velocity scales. Webb et al. (1992) also suggested that β might be as low as 1.3, in order to explain the spectrum of the z = 4.11 QSO 0000−263, if the Gunn-Peterson opacity at that redshift is zero.

To illustrate the possible effect on J_ν estimates, I constructed photoionization models identical to those of BDO described above, except taking β = 1.5 and β = 1.3. The value of β is unlikely to be smaller than 1.3. The result is plotted in Figure 33. Assuming that J_ν is constant with redshift, if β = 1.3, the best-fit J_ν for the W_{thr} = 0.32 Å sample turns out to be about a factor of 3 smaller than the β = 1.7 models. So if β = 1.3, then J_{-21} = 1.

4.4.3. *Spectrum of J_ν*

Implicit in equation (12) is the assumption that the spectrum of the ambient background, J_ν, is the same as the spectrum of the QSOs, so that the ratio of the ionization rates equals the ratio of the flux densities at the Lyman limit. Obviously, little is known directly about the intrinsic EUV spec-

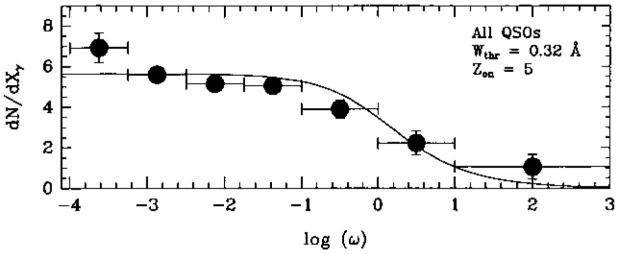

FIG. 28*a*

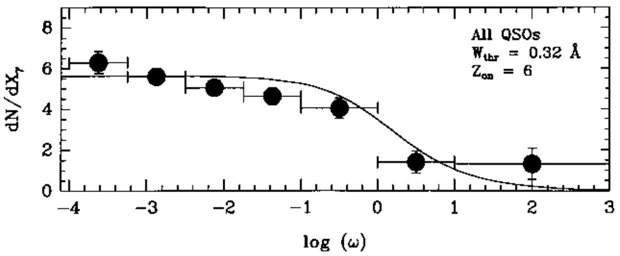

FIG. 28*b*

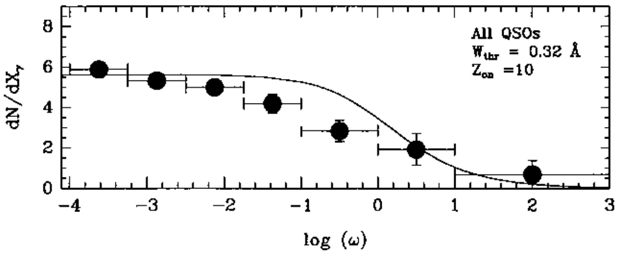

FIG. 28*c*

FIG. 28.—dN/dX_γ for all QSOs, and W_{thr} = 0.32 Å. J_ν is given by eq. (19), for different values of the quasar "turn-on" redshift, Z_{on}. Otherwise, same as Fig. 18. (*a*) Z_{on} = 5. (*b*) Z_{on} = 6. (*c*) Z_{on} = 10.

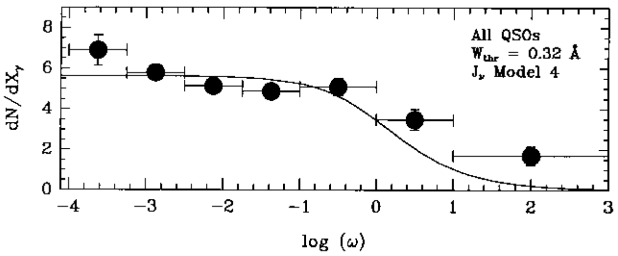

FIG. 29*a*

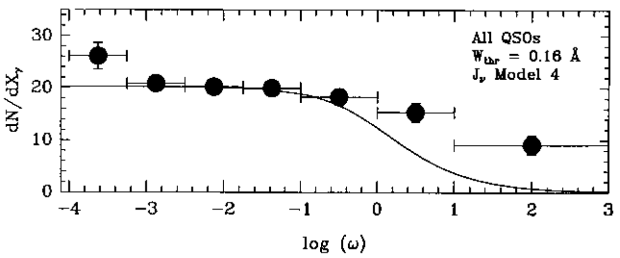

FIG. 29*b*

FIG. 29.—dN/dX_γ for all QSOs and J_ν given by model No. 4 of Fig. 27*b*. Otherwise, same as Fig. 18. (*a*) W_{thr} = 0.32 Å. (*b*) W_{thr} = 0.16 Å.

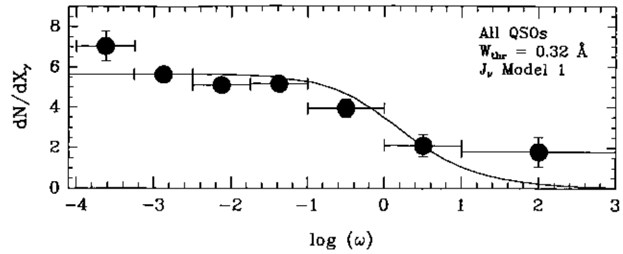

FIG. 30*a*

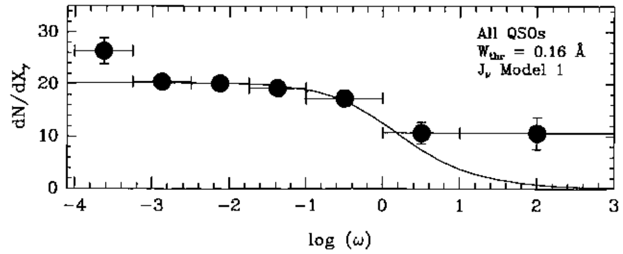

FIG. 30*b*

FIG. 30.—dN/dX_γ for all QSOs and J_ν given by model No. 1 of Fig. 27*b*. Otherwise, same as Fig. 18. (*a*) $W_{thr} = 0.32$ Å. (*b*) $W_{thr} = 0.16$ Å.

trum of QSOs below the Lyman limit, and one expects some diversity in their properties. Moreover, even if one could identify QSOs or young galaxies as the main contributors to the background, the spectrum of J_ν is not identical to that of the individual objects.

One reasonably expects these effects to be small, since the hydrogen neutral fraction depends on the ionization rate, Γ, which is given by

$$\Gamma = \int_{\nu_{LL}}^{+\infty} \frac{J_\nu(\mathrm{tot})}{h\nu} \sigma(\nu) d\nu , \qquad (21)$$

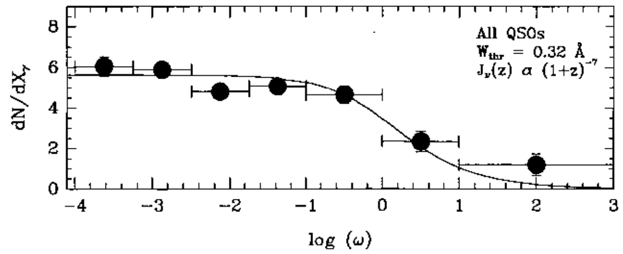

FIG. 31*a*

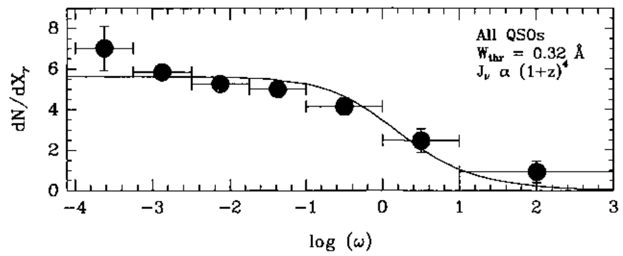

FIG. 31*b*

FIG. 31.—dN/dX_γ for all QSOs and $W_{thr} = 0.32$ Å, and $J_\nu(z)$ shown in Fig. 27*c*. Otherwise, same as Fig. 18. (*a*) $j = -7$ (*b*) $j = 4$.

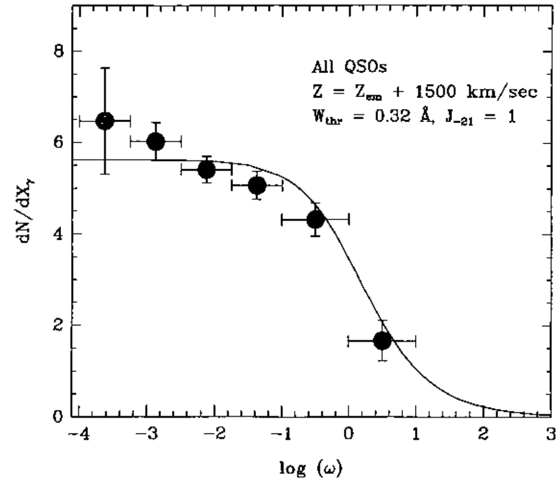

FIG. 32.—dN/dX_γ for all QSOs and $W_{thr} = 0.32$ Å, assuming the emission-line redshifts of Table 3 are 1500 km sec^{-1} lower than the true systemic redshift of the QSO. $J_{-21} = 1.0$, constant with redshift. Otherwise, same as Fig. 18.

where the cross section for absorption $\sigma(\nu) \propto \nu^{-3}$, ν_{LL} is the frequency of the Lyman limit, and $J_\nu(\mathrm{tot})$ is the total flux density, that is, J_ν plus F_ν^Q, where F_ν^Q is defined in equation 13.

The factor of ν^{-4} in the integral for Γ suggests that the effect of the spectral differences should be small. However, extreme assumptions for the spectrum of J_ν could effectively multiply the right side of equation (12) by an arbitrarily large or small factor. To illustrate more realistic situations, I compared the ionization rate due to the Miralde-Escude & Ostriker's (1990) model 11 (which has J_ν as the sum of QSOs and young galaxies; see their Fig. 17*h*) to the ionization rate due to a QSO, assuming the QSO has a power-law spectrum below the Lyman limit. At the point in space where $F_\nu^Q = J_\nu$ at the Lyman limit, the ratio of ionization rates can be larger or smaller than unity by ~25%, depending on the QSO power-law index, α,

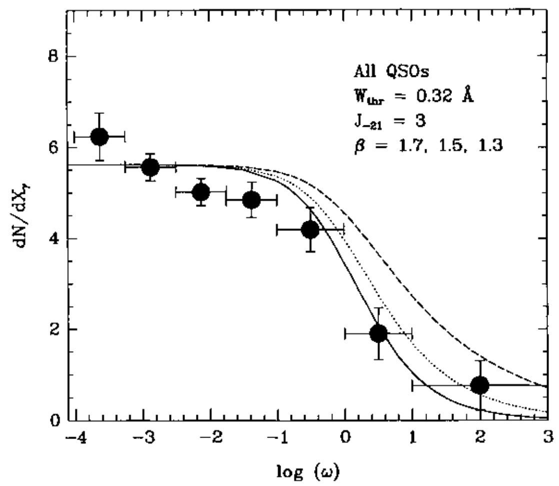

FIG. 33.—The effect of uncertainty in neutral hydrogen column density distribution index β. dN/dX_γ for all QSOs for $W_{thr} = 0.32$ Å, and $J_{-21} = 3$. *Solid line:* $\beta = 1.7$; *dotted line:* $\beta = 1.5$; *dashed line:* $\beta = 1.3$. Otherwise, same as Fig. 18.

for $0.5 < \alpha < 2$. Thus, the uncertainty in J_ν derived from the proximity effect resulting from spectral differences between J_ν and the QSOs is probably quite small.

4.4.4. *QSO Variability*

The timescale for the clouds to equilibrate after changes in ionizing flux is $\sim 10^4$ years (e.g., BDO). Thus the observed proximity effect reflects the luminosity variations of the QSO on timescales of about this length. BDO made a simple model to describe possible QSO variations and found that the absorption-line data were better fitted with a model where the QSO varied randomly by a factor of about 10 in the relevant timescales than a model with no variability. If true, this would be unique evidence for long-term QSO variability. One also might worry about the effect of QSO variability on the estimate of J_ν. Qualitatively, if a QSO was brighter in the past, then J_ν is overestimated; if the QSO was fainter, then J_ν is underestimated. However, if on average the QSO was not systematically brighter or fainter in the past, then the best-fit J_ν should not be affected.

BDO showed that if the observed QSO magnitude, M_0, is drawn from a Gaussian distribution of width σ in magnitudes, then equation (16) becomes

$$\frac{dN}{dX_\gamma} = \frac{A_0}{2\sigma(\pi)^{1/2}} \int_{-\infty}^{+\infty} e^{-(y/4\sigma^2)} (1 + \omega \times 10^{-0.4y})^{-0.7} dy\,. \quad (22)$$

For the $W_{\rm thr} = 0.32$ Å sample, $\sigma = 2.5$ gives a better fit than $\sigma = 0$, with $J_{-21} = 3$, constant with redshift ($\chi^2 = 2.2$ for 7 points). The plot is shown in Figure 34. Thus this new sample is consistent with the suggestion of BDO that QSOs vary on long timescales. Given the other sources of uncertainty discussed in this section the evidence for variability is not conclusive, however.

4.4.5. *Gravitational Lensing*

Although the fraction of high-redshift QSOs that are lensed may be small (e.g., Maoz et al. 1992a and references therein),

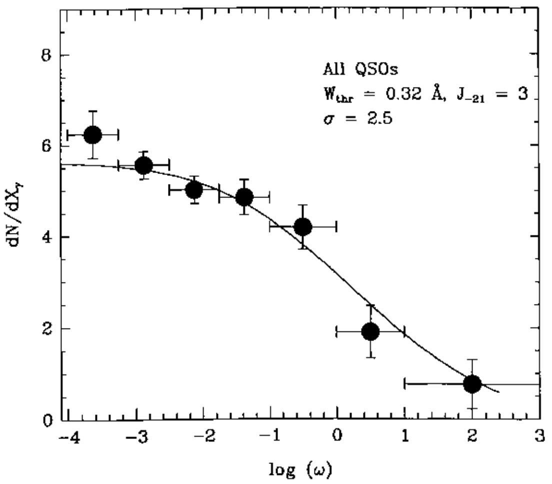

FIG. 34.—dN/dX_γ vs. log (ω) for $W_{\rm thr} = 0.32$ Å sample, $J_{-21} = 3$, and BDO variability model with $\sigma = 2.5$. See eq. (22). Otherwise, same as Fig. 18.

one might expect a significant selection effect in an absorption line sample for preferentially including QSOs whose continuum is amplified by lensing. York et al. (1991) found evidence that suggests that lensing is an important bias in a heterogeneous absorption line sample drawn from the literature, whereas Lanzetta et al. (1991) argued that there was no evidence for having preferentially used lenses in their study of the statistics of damped Lyα systems.

If lensing has brightened the QSO continuum in the absorption-line sample used here, then the QSOs are intrinsically fainter then they appear, and J_ν has been overestimated (BDO). The fact that $\Delta N/N_{\rm pred}$ is correlated with luminosity but not redshift argues that lensing is not an important factor. However, comparison of the proximity effect in a sample of lensed QSOs with unlensed objects would be an interesting test of the photoionization model (BDO).

There are two known lenses in the absorption-line sample of Table 3, 1115+080 (Weymann et al. 1980) and UM 673 = 0142−100 (Surdej et al. 1987), and one lens candidate, 1208+101 (Magain et al. 1992; Maoz et al. 1992b). Q1115+080 was excluded from the proximity effect analysis because it has a metal-line system with $z_{\rm abs} \approx z_{\rm em}$. The other two were included. They are shown in Figure 15 and 16 as filled triangles. Apparently, there is enough scatter in the plots of ΔN versus L_ν that neither QSO stands out as having too weak a proximity effect for its apparent luminosity. A larger sample of high-redshift lenses, or better limits on the possibility of lensing for the objects in this sample, would be of interest. Fifteen QSOs in this absorption-line sample have already been the subject of searches for multiple images, with negative results (Crampton et al. 1989; Bahcall et al. 1992; Maoz et al. 1992a).

4.4.6. *The Neutral Fraction of the Clouds*

For some time, the available evidence suggested that the Lyα forest clouds were highly ionized, with neutral fraction $N_{\rm HI}/N_{\rm H} \approx 10^{-4}$ or less (see Sargent et al. 1980 or Chaffee et al. 1986 for a discussion). However, observations at very high resolution sometimes reveal clouds with very narrow widths, and hence quite cool temperatures, $T < 10{,}000$ K (Chaffee et al. 1983; Pettini et al. 1990). These temperatures are difficult to achieve in the standard models for the clouds, where the clouds are low density, low metallicity, and photoionized. The implication is that the clouds are instead nearly neutral. However, if this is the case, the observations of common absorption in gravitationally lensed images implies a peculiar geometry for the clouds (e.g., Smette et al. 1992). The observational question of what fraction of the clouds are really cold remains open (e.g., Carswell et al. 1991).

If the neutral fraction of the clouds is high, then J_ν derived from the photoionization model above is *overestimated* since to see a given proximity effect requires that the QSO flux dominates J_ν by larger factors than the case where the clouds are highly ionized (e.g., Pettini et al. 1990; their Fig. 7). A quantitative discussion is given in Bechtold & Wolfe (1994). They find, for example, that if the neutral fraction is $N_{\rm HI}/N_{\rm H} = 0.95$, then $J_{-21} = 0.01$ for the $W_{\rm thr} = 0.32$ Å sample presented here. This value for J_ν is an order of magnitude *smaller* than Madau's (1992) calculation of the contribution of QSOs. It is difficult to imagine circumstances where the ambient flux a cloud sees is very much smaller than the contribution from observed QSOs. Thus, the proximity effect could be taken as evidence that the clouds are in fact not neutral, in general, if the effect is the result of photoionization. In any event, the assumption that the clouds are highly ionized has a very large effect on the derived value of J_ν.

5. SUMMARY

A new sample of QSO absorption-line spectra has been used to investigate the statistics of the Lyα forest lines at high redshift. For $z_{abs} \ll z_{em}$, the number of lines per unit redshift are well described by the $(1 + z)^\gamma$ form, with $\gamma = 1.89 \pm 0.28$ for $W_{thr} = 0.32$ Å, and $\gamma = 1.32 \pm 0.24$ for $W_{thr} = 0.16$ Å. For $z_{abs} \approx z_{em}$, the number of lines is significantly depleted, with the strength of the deficit correlated with quasar Lyman limit luminosity but not quasar redshift. Applying the simple photoionization model of BDO, limits on $J_\nu(z)$ can be estimated. With J_ν assumed to be a constant with redshift over the observed redshift range, the data are best fitted with $\log J_\nu \approx -20.5$ ergs cm^{-2} s^{-1} Hz^{-1} sr^{-1}. However, if $J_\nu(z) \propto (1 + z)^j$, acceptable fits are obtained for $-7 < j < 4$. A number of effects plausibly cause the derived J_ν to be uncertain by large factors. The most likely effect results from the fact that the QSO redshifts have been underestimated because they are derived from emission lines that are shifted by 1000–2000 km s^{-1} from the true systemic redshift. This decrease J_ν by a factor of ~ 3, which then brings it into rough agreement with the expected contribution of QSOs.

What conclusions can be drawn from these results? Ikeuchi & Turner (1991) and Charlton et al. (1993) have derived analytical forms for γ as a function of $J_\nu(z)$ for simple cloud models. In principle, if one knows j and γ at a particular redshift, one can distinguish between models where the clouds are confined by a hot IGM and models where the clouds are gravitationally bound. Unfortunately, the limits on j are so poor, that neither model is excluded (see Fig. 4*b* in Charlton et al. 1993). Constraining j by modeling the proximity effect, and measuring γ at $z \approx 2$ and $z > 4$ will be useful for investigating the nature and evolution of the Lyα forest clouds.

It is a pleasure to thank the staffs of the Multiple Mirror Telescope Observatory, Steward Observatory, and Palomar Observatory for their assistance. I thank C. Price and S. Shectman for setting up the 2D FRUTTI Photon Counter at the 5 m and providing advice on its use. I thank P. A. Strittmatter for providing partial funds for the purchase of the echellette grating used at the MMT Red Spectrograph, and computer equipment. I am grateful to the director of the MMT, and the MMT Visitors Program which provided telescope time for this project. E. Paley reduced the spectrum of Q1206+119, and B. Frye organized the previously published line lists from the literature. A. Dobrzycki and S. Shectman wrote software used here. J. P. Ostriker and the Princeton Astronomy Department provided a quiet atmosphere and computer services during which some of this paper was written. Much of the analysis was done while the author was a visitor at CTIO; the hospitality of the Director and staff there is appreciated. Helpful conversations with J. Ostriker, J. Charlton, A. Dobrzycki, M. Fall, A. Wolfe, S. Shectman, and J. Lowenthal are appreciated. The anonymous referee read the manuscript very carefully, and significantly improved the presentation. This work was supported by RII-8800660 and AST-9058510 of the National Science Foundation, and a gift from Sun Microsystems.

REFERENCES

Abraham, Z., deMedeiros, J. R., & Kaufmann, P. 1984, AJ, 89, 200
Adam, G. 1985, A&AS, 61, 225
Anderson, S. F., Weymann, R. J., Foltz, C. B., & Chaffee, F. H. 1987, AJ, 94, 278
Atwood, B., Baldwin, J. A., & Carswell, R. F. 1985, ApJ, 292, 58
Bahcall, J. N., et al. 1993, ApJS, 87, 1
Bahcall, J. N., Jannuzi, B. T., Schneider, D. P., Hartig, G. F., Bohlin, R., & Junkkarinen, V. 1991, ApJ, 377, L5
Bahcall, J. N., Maoz, D., Doxsey, R., Schneider, D. P., Bahcall, N. A., Lahav, O., & Yanny, B. 1992, ApJ, 387, 56
Bajtlik, S., Duncan, R. C., & Ostriker, J. P. 1988, ApJ, 327, 570 (BDO)
Baldwin, J. A., & Netzer, H. 1978, ApJ, 226, 1
Barcons, X., & Webb, J. K. 1991, MNRAS, 253, 207
Barthel, P. 1984 Ph.D. thesis, Sterrewacht Leiden
Barthel, P. D., Miley, G. K., Schilizzi, R. T., & Lonsdale, C. J. 1988, A&AS, 73, 515
Battistini, P., Braccesi, A., & Formiggini, L. 1974, A&A, 35, 93
Bechtold, J. 1987, in *Proc. 3d IAP Workshop on High Redshift and Primeval Galaxies*, ed. J. Bergeron, D. Kunth, B. Rocca-Volmerange, & J. Tran Thanh Van (Paris: Editions Frontières), 397
Bechtold, J., Green, R. F., Weymann, R. J., Schmidt, M., Estabrook, F., Sherman, R., Wahlquist, D., & Heckman, T. 1984, ApJ, 281, 76
Bechtold, J., Weymann, R. J., Lin, Z., & Malkan, M. A. 1987, ApJ, 315, 180
Bechtold, J., & Wolfe, A. M. 1994, in preparation
Bennett, C. L., Lawrence, C. R., Burke, B. F., Hewitt, J. N., & Mahoney, J. 1986, ApJS, 61, 1
Bohlin, R. 1978, ApJ, 224, 132
Boksenberg, A., & Snijders, M. A. J. 1981, MNRAS, 194, 353
Bolton, J. G., Shimmins, A. J., Wall, J. V., & Butler, P. W. 1975, Australian J. Phys., Astrophys. Suppl., No. 34, 1
Boyle, B. J. 1991, in Proc. 1990 Texas/ESO-CERN Symp. on *Relativistic Astrophysics*, Cosmology, and Fundamental Physics, ed. J. D. Barrow, L. Mestel, P. A. Thomas (New York: Academy of Sciences), 14
Burbidge, E. M., Smith, H. E., Junkkarinen, V. T., & Hoag, A. A. 1985, ApJ, 288, 82
Carswell, R. F., Morton, D. C., Smith, M. G., Stockton, A. N., Turnshek, D. A., & Weymann, R. J. 1984, ApJ, 278, 486
Carswell, R. F., Lanzetta, K. M., Parnell, H. C., & Webb, J. K. 1991a, ApJ, 371, 36
Carswell, R. F., Webb, J. K., Baldwin, J. A., & Atwood, B. 1987, ApJ, 319, 709
Carswell, R. F., Whelan, J. A. J., Smith, M. G., Boksenberg, A., & Tytler, D. 1982, MNRAS, 198, 91
Carswell, R. F., et al. 1991b, ApJ, 381, L5
Cen, R., & Ostriker, J. P. 1993, ApJ, 417, 404
Chaffee, F. H., Foltz, C. B., Bechtold, J., & Weymann, R. J. 1986, ApJ, 301, 116
Chaffee, F. H., & Latham, D. W. 1982, PASP, 94, 386
Chaffee, F. H., Weymann, R. J., Latham, D. W., & Strittmatter, P. A. 1983, ApJ, 267, 12
Charlton, J., Salpeter, E., & Hogan, C. 1993, ApJ, 402, 493
Corbin, M. R. 1990, ApJ, 357, 346
Crampton, D., McClure, R. D., Fletcher, J. M., Hutchings, J. B. 1989, AJ, 98, 1188
Dobrzycki, A., & Bechtold, J. 1991a, in *Space Distribution of Quasars*, ed. D. Crampton (San Francisco: ASP), 272
———. 1991b, ApJ, 377, L69

Dobrzycki, A., & Bechtold, J. 1994, in preparation
Elvis, M., Lockman, F. J., & Wilkes, B. J. 1989, ApJ, 97, 777
Espey, B. R., Carswell, R. F., Bailey, J. A., Smith, M. G., & Ward, M. J. 1989, ApJ, 342, 666
Evans, A., & Hart, D. 1977, A&A, 58, 241
Fall, M., & Pei, Y. C., 1993, ApJ, 402, 479
Feigelson, E. D., Isobe, T., & Kembahvi, A. 1984, AJ, 89, 1464
Foltz, C. B., Chaffee, F. H., Hewitt, P. C., MacAlpine, G. M., Turnshek, D. A., & Weymann, R. J. 1987, AJ, 94, 1423
Frye, B., Bechtold, J., Dobrzycki, A., & Moustakas, L. 1993, MNRAS, in press 263, 575
Gaskell, C. M. 1982, ApJ, 263, 483
Gearhart, M. R., et al. 1974, Nature, 249, 743
Giallongo, E. 1991, MNRAS, 251, 541
Green, R. F., Pier, J., Schmidt, M., Estabrook, F., Lane, A., & Wahlquist, H. 1980, ApJ, 239, 483
Hazard, C., Morton, D. C., McMahon, R., Sargent, W. L. W., & Terlevich, R. 1986, MNRAS, 223, 87
Hewitt, A., & Burbidge, G. 1987, ApJS, 63, 1
———. 1989, ApJS, 69, 1
Ikeuchi, S., & Ostriker, J. P. 1986, ApJ, 301, 522
Ikeuchi, S., & Turner, E. L. 1991, ApJ, 381, L1
Irwin, M., McMahon, R. G., & Hazard, C. 1991, in *Space Distribution of Quasars,* ed. D. Crampton (San Francisco: ASP), 117
Jenkins, E., Bajtlik, S., & Dobrzycki, A. 1994, in preparation
Kellerman, K. I., Sramek, R., Schmidt, M., Shaffer, D. B., & Green, R. F. 1989, AJ, 98, 1195
Kuhr, H., Pauliny-Toth, I. I. K., Witzel, A., & Schmidt, J. 1981, AJ, 86, 854
Lanzetta, K. M., Wolfe, A. M., Turnshek, D. A., Lu, L., McMahon, R. G., & Hazard, C. 1991, ApJS, 77, 1
Latham, D. W. 1982, in IAU Colloq. 67, Instrumentation for Astronomy with Large Optical Telescopes, ed. C. M. Humphries (Dordrecht: Reidel), 245
Lu, L., Wolfe, A. M., & Turnshek, D. A. 1991, ApJ, 367, 19 (LWT)
MacAlpine, G. M., & Feldman, F. R. 1982, ApJ, 261, 412
MacAlpine, G. M., & Williams, G. A. 1981, ApJS, 45, 113
Madau, P. 1992, ApJ, 389, L1
Magain, P., Surdej, J., Vanderriest, C., Pirenne, B., & Hutsemekers, D. 1992, A&A, 253, L13
Maoz, D., Bahcall, J. N., Doxsey, R., Schneider, D. P., Bahcall, N. A., Lahav, O., & Yanny, B. 1992a, ApJ, 394, 51
Maoz, D., et al. 1992b, ApJ, 386, L1
McMahon, R. 1991, private communication
Meiksin, A., & Madau, P. 1993, preprint
Miralde-Escude, J., & Ostriker, J. P. 1990, ApJ, 350, 1
Morris, S. L., Weymann, R. J., Savage, B. D., & Gilliland, R. L. 1991, ApJ, 377, L21
Morton, D. C., York, D. G., & Jenkins, E. G. 1988, ApJS, 68, 449
Murdoch, H. S., Hunstead, R. W., Pettini, M., & Blades, J. C. 1986, ApJ, 309, 19
Oke, J. B. 1974, ApJ, 189, L47
Oke, J. B., & Gunn, J. E. 1982, PASP, 94, 586
Oke, J. B., & Korycansky, D. G. 1982, ApJ, 255, 11
Oke, J. B., Neugebauer, G., & Becklin, E. E. 1970, ApJ, 159, 341
Osmer, P. S. 1979, ApJ, 227, 18
———. 1980, ApJS, 42, 523
Osmer, P. S., & Smith, M. G. 1977, ApJ, 213, 607
———. 1980, ApJS, 42, 333
Parnell, H. C., & Carswell, R. F. 1988, MNRAS, 230, 491
Pauliny-Toth, I. I. K., Kellerman, K. I., Davis, M. M., Fomalont, E. B., & Shaffer, D. B. 1972, AJ, 77, 265
Pauliny-Toth, I. I. K., Witzel, A. Preuss, E., Kuhr, H., Kellerman, K. I., & Fomalont, E. 1978, AJ, 83, 451
Pei, Y. C., Fall, S. M., & Bechtold, J. 1991, ApJ, 378, 6
Pettini, M., Hunstead, R. W., Smith, L., & Mar, D. P. 1990, MNRAS, 246, 545
Pica, A. J., & Smith, A. G. 1983, ApJ, 272, 11
Press, W. H., Flannery, B. P., Teukolsky, S. A., & Vetterling, W. T. 1986, *Numerical Recipes* (New York: Cambridge Univ. Press)
Rauch, M., Carswell, R. F., Chaffee, F. H., Foltz, C. B., Webb, J. K., Weymann, R. J., Bechtold, J., & Green, R. F. 1992, ApJ, 390, 387
Reimers, D., et al. 1989, A&A, 218, 71
Richstone, D., & Schmidt, M. 1980, ApJ, 235, 361
Robertson, J. G., & Shaver, P. A. 1983, MNRAS, 204, 69P
Sargent, W. L. W., Boksenberg, A., & Steidel, C. C. 1988, ApJS, 68, 539
Sargent, W. L. W., Steidel, C. C., & Boksenberg, A. 1989, ApJS, 69, 703
Sargent, W. L. W., Young, P. J., & Boksenberg, A. 1982a, ApJ, 252, 54
Sargent, W. L. W., Young, P. J., Boksenberg, A., Carswell, R. F., & Whelan, J. A. J. 1979, ApJ, 230, 49
Sargent, W. L. W., Young, P. J., Boksenberg, A., & Tytler, D. 1980, ApJS, 42, 41
Sargent, W. L. W., Young, P. J., & Schneider, D. 1982b, ApJ, 256, 374
Schmidt, M., Schneider, D. P., & Gunn, J. E. 1986, ApJ, 310, 518
———. 1991, in *Space Distribution of Quasars,* ed. D. Crampton (San Francisco: ASP), 109
Schmidt, G. D., Weymann, R. J., & Foltz, C. B. 1989, PASP, 101, 713
Schneider, D., et al. 1993, ApJS, 87, 45
Seaton, M. J. 1979, MNRAS, 187, 73P
Shimmins, A. J., Bolton, J. G., & Wall, J. V. 1975, Australian J. Phys. Astrophys. Suppl., 34, 63
Smette, A., Surdej, J., Shaver, P. A., Foltz, C. B., Chaffee, F. H., Weymann, R. J., Williams, R. E., & Magain, P. 1992, ApJ, 389, 39
Smith, M. G., & Wright, A. E. 1980, MNRAS, 191, 871
Smith, M. G., et al. 1981, MNRAS, 195, 437
Snijders, M. A. J., Pettini, M., & Boksenberg, A. 1981, ApJ, 245, 386
Songaila, A., Cowie, L. L., & Lilly, S. J. 1990, ApJ, 348, 371
Sramek, R. A., & Weedman, D. W. 1978, ApJ, 221, 468
———. 1980, ApJ, 238, 435
Stark, A. A., Gammie, C. F., Wilson, R. W., Bally, J., Linke, R., Heiles, C., & Hurwitz, M. 1989, ApJS, 79, 77
Surdej, J., et al. 1987, Nature, 329, 695
———. 1988, A&A, 198, 49
Trevese, D., Giallongo, E., & Camurani, L. 1992, ApJ, 398, 491
Turnshek, D. A., Wolfe, A. M., Lanzetta, K. M., Briggs, F. H., Cohen, R. D., Foltz, C. B., Smith, H. E., & Wilkes, B. J. 1989, ApJ, 344, 567
Tytler, D. 1987, ApJ, 321, 69
Veron, M. P., Veron, P., Pauliny-Toth, I. I. K., & Witzel, A. 1981, A&AS, 43, 195
Webb, J. K., Barcons, X., Carswell, R. F., & Parnell, H. C. 1992, MNRAS, 255, 319
Weymann, R. J., Carswell, R. F., & Smith, M. G. 1981, ARA&A, 19, 41
Weymann, R. J., Latham, D., Angel, J. R. P., Green, R. F., Liebert, J. W., Turnshek, D. A., Turnshek, D. E., & Tyson, J. A. 1980, Nature, 285, 641
Weymann, R. J. 1993, in Proc. 3d Teton Summer Astrophysics Conf., The Evolution of Galaxies and Their Environment: ed. J. M. Shull & H. Thronson (Dordrecht: Kluwer), in press
Wilkerson, M., Coleman, G., Gilbert, G., Strittmatter, P. A. S., Williams, R., Baldwin, J., Carswell, R., & Grandi, S. 1978, ApJ, 223, 364
Wilkes, B. J. 1984, MNRAS, 207, 73
Wilkes, B. J., Wright, A. E., Jauncey, D. L., & Peterson, B. A. 1983, Proc. Astron. Soc. Australia, 5, 1
Williger, G. M., Carswell, R. F., Webb, J. K., Boksenberg, A., & Smith, M. G. 1989, MNRAS, 237, 635
Wills, B. J. 1975, Australian J. Phys. Suppl., 38, 1
Wolfe, A. M., Turnshek, D. A., Smith, H. E., & Cohen, R. D. 1986, ApJS, 61, 249
Yee, H. K. C., & Green, R. F. 1987, ApJ, 319, 28
York, D. G., Yanny, B., Crotts, A., Carilli, C., Garrison, E., & Matheson, L. 1991, MNRAS, 250, 24
Young, P. J., Sargent, W. L. W., & Boksenberg, A. 1982a, ApJ, 252, 10
———. 1982b, ApJS, 48, 455
Zuo, L. 1992a, MNRAS, 258, 36
———. 1992b, MNRAS, 258, 45